

Quantitative Analysis of Microstructure of Silicate Ceramics and its

Relationship to Thermal Expansion Property

(珪酸塩セラミックスの微構造の定量解析及び熱膨張特性との関係)

2014

Masaki Katayama

Contents

Chapter 1 Introduction

1-1 Silicate ceramics	1
1-2 Cordierite ceramics	2
1-3 Purpose of this study	3
1-4 Course of this study	4

Chapter 2 Quantification of ceramic microstructures with digital images of photomicrograph

2-1 Introduction.....	9
2-2 Experimental procedure.....	9
2-2-1 Quantification of domain structure of cordierite ceramics.....	9
2-2-2 Quantification of primary grains constituting mullite ceramics.....	10
2-3 Result and Discussion.....	10
2-3-1 Quantification of cordierite domain by digital image analysis	10
2-3-2 Applying digital image analysis for quantification of microstructure of mullite ceramics..	15
2-4 Conclusions.....	19

Chapter 3 Effect of Microstructure on the Thermal Expansion Coefficient of Sintered Cordierite Prepared from Sol Mixtures

3-1 Introduction.....	21
3-2 Experimental Procedures	21
3-2-1 Preparation.....	21
3-2-2 Characterization.....	22
3-3 Results and Discussion	22
3-3-1 Thermal reaction and sintering of sol mixtures.....	22
3-3-2 Thermal expansion properties of dense ceramics.....	27
3-3-3 Microstructure of sintered cordierite	27
3-3-4 Quantification of average domain size and CTE modeling	32
3-4 Conclusions.....	37

Chapter 4
Effect of Particle Size of Tabular Talc Powders on
Crystal Orientation and Sintering of Cordierite Ceramics

4-1 Introduction.....	39
4-2 Experimental procedure.....	40
4-2-1 Materials.....	40
4-2-2 Preparation.....	41
4-2-3 Characterization.....	41
4-3 Results and Discussions.....	42
4-3-1 Crystal orientation of talc powders	42
4-3-2 Effect of the particle orientation of talc powders on crystal orientation of cordierite	48
4-3-3 Effect of particle size of talc powders on densification of cordierite ceramics	52
4-3-4 Anisotropic CTE of sintered cordierite ceramics	52
4-4 Conclusions.....	56

Chapter 5
Crystal orientation of cordierite generated
at the interface between $\text{Al}_2\text{O}_3 \cdot 2\text{SiO}_2$ and $3\text{MgO} \cdot 4\text{SiO}_2$

5-1 Introduction.....	57
5-2 Experimental procedures	57
5-2-1 Materials.....	57
5-2-2 Preparation.....	58
5-2-3 Characterization.....	59
5-3 Results and Discussions.....	59
5-3-1 Phase composition of powders used for compacts and coating layers.....	59
5-3-2 Phase changes of the coated surface of the compact.....	62
5-3-3 Correlation between crystal orientation of cordierite and heat-treatment temperature.....	65
5-4 Conclusions.....	74

Chapter 6
Preparation of Dense Mullite Polycrystals by Reaction Sintering of Kaolin
Materials and Alumina and their Microstructure

6-1 Introduction.....	76
6-2 Experimental Procedure.....	76
6-2-1 Starting Materials	76
6-2-2 Characterization.....	80

6-3 Results and Discussion	80
6-3-1 Thermal changes of kaolin	80
6-3-2 Thermal reaction of the mixtures	85
6-3-3 Densification of the mixtures	88
6-3-4 Microstructure of Mullite	90
6-3-5 Quantification of Microstructure	90
6-4 Conclusion	94

Chapter 7

Conclusions

7-1 Quantification of ceramic microstructures with digital images analysis	95
7-2 Effect of microstructure on CTE of dense cordierite prepared from sol mixtures	95
7-3 Effect of particle size of talc on crystal orientation of cordierite ceramics	95
7-4 Preferred crystal orientation of cordierite by interdiffusion of $\text{Al}_2\text{O}_3 \cdot 2\text{SiO}_2$ and $3\text{MgO} \cdot 4\text{SiO}_2$	96
7-5 Preparation of dense mullite ceramics and their microstructure	96
List of Publications	98
Others	99
Presentations at international conferences and seminars	100
Acknowledgment	101

Chapter 1

Introduction

1-1 Silicate ceramics

Many natural silicate minerals are found in earth crust since chemical composition of earth crust is consisted of a large amount of oxygen, silicon and aluminum.¹ Crystalline or amorphous silicate materials, or their composites dominantly constitute ceramics such as refractories, tiles, potteries and porcelains, since these ceramics can be prepared using the natural silicate minerals (called also as clay minerals) as raw materials. The fundamental structural unit of silicate is SiO_4 -tetrahedrons, and SiO_4 -tetrahedron groups such as SiO_4^{4-} , $\text{Si}_2\text{O}_7^{6-}$, $\text{Si}_3\text{O}_9^{6-}$, $\text{Si}_4\text{O}_{12}^{8-}$, $\text{Si}_6\text{O}_{18}^{12-}$, $(\text{SiO}_3)_n^{2n-}$, $(\text{Si}_4\text{O}_{11})_n^{6n-}$, $(\text{Si}_2\text{O}_5)_n^{2n-}$, and $(\text{SiO}_2)_n$ are formed basing on the connecting style of SiO_4 -tetrahedrons in the framework of crystal structure. Furthermore, the connecting styles of SiO_4 -tetrahedrons are mineralogically classified into six types of structures referred to as neso-, soro-, cycro-, ino-, phyllo- and tecto-silicates. Silicate based ceramics have a rigidity, a thermal stability, corrosion resistance, weather resistance, and electric insulation, and have been applied in many industrial fields depending on their various properties. Particularly, the silicate ceramics such as steatite ($\text{MgO}\cdot\text{SiO}_2$), forsterite ($2\text{MgO}\cdot\text{SiO}_2$), mullite ($3\text{Al}_2\text{O}_3\cdot 2\text{SiO}_2$), zircon ($\text{ZrO}\cdot\text{SiO}_2$) and cordierite ($2\text{MgO}\cdot 2\text{Al}_2\text{O}_3\cdot 5\text{SiO}_2$) have superior properties, and therefore have been applied for industrial use such as structural, electrical, and high-temperature materials.

On the other hand, new types of ceramic materials having advanced properties were needed for fields of science and technology with growing demand for advanced materials, presently.² They are produced from highly purified minerals and pure metal oxides, or from chemically prepared precursors using sol-gel processing,³ atomic layer deposition,⁴ gas-phase synthesis⁵ and liquid-phase synthesis.^{6,7} We have called them advanced ceramics. Using a highly purified or chemically obtained raw materials and regulating a preparation routes can control chemical compositions and microstructures of resultant ceramics. As a result, advanced ceramics have excellent properties and can be applied to various field of modern science and technology as electronic materials, catalyst, fluorescent materials, magnetic materials optical materials, nanomaterials, coatings, superconducting material, structural materials and composites etc. Advanced ceramics can be catabolized into two types depending on the constituent; oxides such as Al_2O_3 , TiO_2 , ZrO_2 , ZnO_2 , ZrW_2O_8 , Al_2TiO_3 , CaTiO_3 , BaTiO_3 , MnFe_2O_4 , LiCoO_2 and $\text{Y}_2\text{Nb}_2\text{O}_7$ etc., and non-oxides such as SiC , Si_3N_4 , AlN , GaN , ZrC , WC and BN etc.

Also on silicate ceramics, highly-purified raw materials can be used, and the preparation techniques are drastically improved owing to appearing advanced ceramics, and the chemical composition and the microstructure can be arbitrarily controlled. As a result, the extremely pure silicate ceramics such as mullite and cordierite, already mentioned above, are expected to serve their superior properties in the fields of modern science and technology, as well as advanced ceramics. Especially, cordierite ceramics have been widely used in many industrial fields and

studied by many researchers for a long time.

1-2 Cordierite ceramics

Cordierite ($2\text{Al}_2\text{O}_3 \cdot 2\text{MgO} \cdot 5\text{SiO}_2$) is categorized mineralogically into cyclosilicate, and has several types of polymorphs, α -cordierite (hexagonal), β -cordierite (orthorombic) and a metastable μ -cordierite, which appear as a metastable phase at a limited temperature and time.⁸ The indialite is the name used for the synthesized α -cordierite, having a pseudohexagonal lattice due to the impurities not eliminated in the synthesis process, and is found in many commercial cordierite ceramics.⁹ Cordierite also has large anisotropic coefficients of thermal expansion (CTEs) of $2.5 \times 10^{-6} \text{ K}^{-1}$ and $-0.9 \times 10^{-6} \text{ K}^{-1}$ along the a and b axes, and c axis, respectively. It is reported that this large anisotropic CTE is attributed to its unique crystal structure.¹⁰ Cordierite crystal is formed by six-membered ring composed of six T_2O_4 -tetrahedrons. Here, T2 sites are occupied by Si or Al. The rings are situated on top of each other as a result of rotation about 30° with the lines connecting the center of the rings parallel to the c axis.¹¹ The T_1O_4 -tetrahedron and MgO_6 octahedron are connected to the six-membered rings.¹¹ Here, T1 sites are occupied by Si or Al.

Sintered cordierite ceramics usually have a low CTE of approximately $1.7 \times 10^{-6} \text{ K}^{-1}$, corresponding to an average value of crystal axes expansion, in the range from room temperature to 900°C . It has long been considered to be difficult to produce dense cordierite ceramics since cordierite incongruently melt near the sintering temperature. In order to prepare dense cordierite ceramics, various preparation methods have been discussed. Mixing of a sintering aid¹² resulted in a decrease of the cordierite crystallization temperature and an increase of the density of the final product. However, addition of the sintering aids degrades the thermal expansion and dielectric properties. Homogeneous and fine cordierite powder that can be sintered without the addition of sintering aids is prepared from glass-ceramic processes¹³ and advanced sol-gel processes.¹⁴⁻¹⁷ The former involves a sintering of quenched glass or glass powder compact in the stoichiometric composition of cordierite. The latter uses metal alkoxides as starting materials and produces cordierite ceramics via sol-gel processes. However, these methods have not reached practical applications because of problems such as complex procedures and expensive raw materials. Sumi et al. reported^{18,19} the preparation method of dense cordierite ceramics using pure kaolin and synthesized fine particles of $\text{Mg}(\text{OH})_2$. However, a slight difference from the chemical composition of cordierite led to the coexistence of a small amount of spinel ($\text{MgO} \cdot \text{Al}_2\text{O}_3$). This spinel increases the CTE of cordierite polycrystals. Although it is difficult to obtain densely sintered body, the most popular technique available is ultimately the solid-state reaction of precursor oxides²⁰⁻²³ such as talc, kaolinite and alumina owing to its cost effectiveness and its adaptability for forming and firing processes.^{24,25}

Porous cordierite ceramics have been prepared by extruding the powder mixtures mainly composed of kaolin and talc, and have been extensively utilized for various applications such as honeycomb structured catalyst carriers in the car exhaust systems²⁶⁻³⁰, a diesel particulate filter

(DPF)²⁶, ceramic gas turbine heat exchangers,³¹ hot gas filters,³¹ and molten metal filters,³² etc. It is well known that the porous cordierite prepared from kaolin and talc exhibits extremely low CTE less than $1.0 \times 10^{-6} \text{ K}^{-1}$ along the direction parallel to extruding direction.²¹ The extremely low CTE is thought to be caused by two factors: (1) occurrence of microcracks and (2) preferable crystal orientation of cordierite.

When the sintered multi-phase ceramics are cooled from high processing temperatures, a spontaneous microcracking occur depending on the difference in thermal expansion properties.³³⁻³⁵ In single-phase polycrystalline ceramics, anisotropic thermal expansion of crystal axes also induces microcracking. According to the many researches already reported,^{33,36,37} the temperature difference to generate microcracks depends on the grain size of polycrystalline bodies and the degree of thermal expansion anisotropy of a crystal. Hamano etc.³⁸⁻⁴¹ studied the relationship between microstructure and thermal expansion properties of aluminum titanate polycrystals, which has a larger thermal expansion anisotropy than that of a cordierite crystal, and reported that polycrystalline aluminum titanate prepared by reaction-sintering had a large secondary grains (hereafter referred to domain) constructed by many primary grains in the same crystal orientation and that the domain size affected the CTE of aluminum titanate polycrystals. Cordierite honeycomb ceramics were also reported⁴²⁻⁴⁵ to possess domain structure, and the domain structure was also considered to affect thermal expansion property of cordierite honeycombs. However, quantification of domain structure was extremely difficult, and the relationship between CTE and domain structure has not yet been clarified.

The *c*-axis of cordierite crystal having negative CTE aligns parallel to the extruding direction during a sintering and thermal reactions,^{20,21} so that the CTE of extruding direction shows a lower value than usual CTE of sintered cordierite without crystal orientation. Lachman^{20,21} reported that *c*-axes of cordierite crystals aligned in vertical to *c*-axes of tabular kaolinite and that talc powder used for precursor mixture react with Al_2O_3 component contained in kaolin and corundum powders to form eutectic liquid. Thereafter, the preferable crystal orientation of cordierite has been believed to be attributed to the preferable orientation of large anisotropic tabular kaolinite used as raw material of cordierite ceramics, induced during extrusion molding. However, factors causing preferred orientation of cordierite crystal are not discussed enough in details.

1-3 Purpose of this study

It has been difficult to characterize the microstructure of cordierite ceramics because of their multiple structures. Generally, primary small cordierite grains observed by scanning electron microscope constitute a large secondary grain. This secondary grain has been called “domain”. However, the domain size has only been roughly estimated by the microcracks using scanning electron microscope. The precise domain size was difficult to evaluate because the microcracks (gap) between many domains were in the size below $>0.1\mu\text{m}$. A cordierite crystal is in hexagonal system and has an optical anisotropy, namely birefringence. In the area of petrographic researches,

optical polarizing microscope is frequently used for an observation of optically anisotropic crystals. The purposes of this study were as follows.

- (1) A quantitative evaluation of microstructure of ceramics could be attained by the digital image analysis of photographs of ceramics using an optical polarizing microscope and a scanning electron microscope.
- (2) The domain structure of cordierite can be quantitatively evaluated by a digital image analysis of photographs and the relationship between the domain size and the thermal expansion properties can be clarified. Especially, an extra-low thermal expansion property can be explained by quantitative evaluation of microcracks.
- (3) Conventionally, a preferred crystal orientation of cordierite ceramics prepared from the mixture of kaolin, talc and alumina by extrusion molding has been reported to depend on the prior orientation of anisotropically shaped raw material particles, especially tabular kaolinite particles. However, the effect of the anisotropic shape of talc particles has been ignored in many researches. The purpose of this study was to clarify the effect of orientation property of tabular talc particles on the preferable crystal orientation of cordierite.
- (4) When kaolinite and talc powders are used as a starting mixture for the extrusion of cordierite-based ceramics, the c-axis of the cordierite crystals is aligned vertically to the c-axis of the kaolinite crystals during heat-treatment. Lachman et al. reported that this preferred orientation of cordierite was attributable to the crystal structure and orientation of kaolinite similarly to mullite crystals topotactically generated from kaolinite. However, many crystalline phases such as mullite, enstatite, sapphirine, spinel, and cristobalite are transiently generated during heat-treatment of a starting mixture containing silicates. The purpose of this study was to investigate the thermal reaction mechanism of preferable orientation of cordierite crystals between the interface of $\text{Al}_2\text{O}_3\text{-SiO}_2$ mixtures and MgO-SiO_2 mixtures.
- (5) Mullite ceramics are also valuable in a variety of industry, such as refractories, ceramic packages of electro circuits and so on. The purpose of this study was to clarify the effect of preparation process of raw materials on the sintering and densification of mullite ceramics and to evaluate quantitatively the resultant microstructures.

1-4 Course of this study

- (1) The digital image analysis with the aid of optical polarization microscopy was introduced to quantify domain structures of cordierite ceramics prepared by reaction sintering. Digital image analysis was also available for quantification of microstructure of mullite ceramics using the aid of SEM. Using the computer software, microstructures of silicate ceramics can be easily measured from digital images of photomicrograph. (Chapter 2)
- (2) Dense cordierite ceramics were prepared from a sol mixture of alumina, silica, and magnesia, and the relationship between microstructure and thermal expansion was clarified for sinters

with relative density greater than 97%. In the dense cordierite ceramics, submicrometer-sized primary cordierite crystals aligned in the same crystal orientation and constituted the domain structure. We discovered that these domain structures could be easily observed by optical polarizing microscopy and quantified by digital image analysis of the photographs. The occurrence of microcracks between domains larger than 40 μm was induced by the thermal expansion anisotropy of the cordierite crystal axes. As a result, the mean thermal expansion coefficient of the cordierite ceramics decreased to $0.4 \times 10^{-6} \text{ K}^{-1}$ from the average value of the crystal axes of $1.7 \times 10^{-6} \text{ K}^{-1}$. This lower thermal expansion coefficient could be theoretically explained by partial microcracking. (Chapter 3)

- (3) Cordierite ceramics were prepared from several types of kaolin powders and talc powders having various median particle size with nanometer-sized alumina sol. Powder mixtures were uniaxially pressed, followed by cold isostatic pressing to make thin compacts. Crystal orientation of talc particle and resultant cordierite were evaluated using the X-ray diffraction profile measured on the uniaxially pressed surface of calcined compacts and sintered compacts, respectively. Coarser talc powders above $3 \mu\text{m}$ aligned their *c*-axis in vertical to the uniaxially pressed surface of the calcined compact during uniaxially pressing, owing to highly anisotropic tabular shape. The crystal orientation of resultant cordierite increased with an increase in the crystal orientation of talc powders on the pressed surface. This result indicated that the *c*-axis of cordierite crystal preferably oriented vertical to the *c*-axis of talc particle oriented. Using the combination of kaolin powders below $5 \mu\text{m}$ and talc powders having median particle size between $3 \mu\text{m}$ and $5 \mu\text{m}$, densely sintered cordierite, having relative density of 95 % and high crystal orientation of approximately 85 % [$I_{110} / (I_{110} + I_{002})$], could be obtained. (Chapter 4)
- (4) This study examines the thermal reaction, and preferred orientation, of cordierite crystals at the interface between $\text{Al}_2\text{O}_3 \cdot 2\text{SiO}_2$ and $3\text{MgO} \cdot 4\text{SiO}_2$ materials, prepared from fine calcined kaolin and talc, or oxide sol mixtures with an isotropic particle shape. Four types of compacts, coated with a thin layer of a different composition, were prepared and heat-treated at various conditions. In the case of all four combinations, MgO and Al_2O_3 were sufficiently diffused at temperatures above $1300 \text{ }^\circ\text{C}$ to generate cordierite crystals ($\text{MgO} \cdot 2\text{Al}_2\text{O}_3 \cdot 5\text{SiO}_2$) at the interface between $\text{Al}_2\text{O}_3 \cdot 2\text{SiO}_2$ and $3\text{MgO} \cdot 4\text{SiO}_2$. Below $1345 \text{ }^\circ\text{C}$, the *c*-axes of cordierite crystals were preferentially oriented parallel to the interface. It was also found that the contacting interface of $\text{Al}_2\text{O}_3 \cdot 2\text{SiO}_2$ and $3\text{MgO} \cdot 4\text{SiO}_2$ materials provided a trigger for the nucleation and growth of cordierite crystals. Above $1345 \text{ }^\circ\text{C}$, further diffusion of MgO and Al_2O_3 resulted in the appearance of the $\text{MgO} \text{--} \text{Al}_2\text{O}_3 \text{--} \text{SiO}_2$ system eutectic melt, prompting cordierite crystals to align parallel to each other, and at an angle to the interface, by dissolution and recrystallization. (Chapter 5)

- (5) Dense and mono-phase mullite ceramics were prepared by reaction sintering of relatively pure kaolins with several kinds of alumina. Removal of coarse kaolin particles $>1\mu\text{m}$ by sedimentation substantially improved thermal reactivity and sinterability of kaolin and its mixtures with alumina. As for mixtures of refined kaolin and submicron corundum powder having a mullite composition, relative densities of above 98% were accomplished by heat-treatment at 1650°C for 1 h. Effect of alumina particle size on thermal reactivity between alumina and kaolin was investigated, and the difference in thermal reaction sequence between alumina and kaolin was clarified. A combination of sub-micron corundum and elutriated kaolin yielded a monodispersed and fine-grained mullite ceramics. (Chapter 6)

References

- 1 H. Sakai, "Introduction to earth science," Tokai university, (2003)
- 2 Aldrich chemistry, *Material Matters*, Vol.4, No.2, 2(2009)
- 3 Aldrich chemistry, *Material Matters*, Vol.1, No3, 8–9(2006)
- 4 Aldrich chemistry, *Material Matters*, Vol.3, No.2, 28–30(2008)
- 5 Aldrich chemistry, *Material Matters*, Vol.4, No.1, 2–4(2009)
- 6 M. Hirano and E. Kato *J. Amer. Ceram. Soc.* 79 [3] 777–80(1996)
- 7 M. Hirano, C. Nakahara, K. Ota and M. Inagaki, *J. Am. Ceram. Soc.*, 85 [5] 1333–5(2002)
- 8 U. Selvaraj, S. Komarnemi and R. Roy, *J. Am. Ceram. Soc.*, 73 [12] 3663–9(1990)
- 9 J. R. GONZÁLEZ-VELASCO, M. A. GUTIÉRREZ-ORTIZ, R. FERRET, A. ARANZABAL, and J. A. BOTAS, *J. Mat. Sci.*, 34 1999 – 2002(1999)
- 10 M. F. Hochella, Jr., and G. E. Brown, Jr., *J. Am. Ceram. Soc.*, 69 [1] 13–8 (1986)
- 11 H. Ikawa, T. Otagiri, O. Imai, M. Suzuki, K. Urabe and S. Udagawa, *J. Am. Ceram. Soc.*, 69 [6] 492–8 (1986)
- 12 R.W. Dupon, R. L. McConville, D. J. Musolf, A. C. Tanous, and M. S. Thompson, *J. Am. Ceram. Soc.*, 73 335(1990)
- 13 C. Panda, W. M. Mobley and R. Raj, *J. Am. Ceram. Soc.*, 72 [12] 2361–4 (1989)
- 14 H. Suzuki, K. Ota and H. Saito, *J. Ceram. Soc. Jpn.*, 95 [2] 163–9 (1987)
- 15 H. Suzuki, K. Ota and H. Saito, *J. Ceram. Soc. Jpn.*, 95 [2] 170–5 (1987)
- 16 N. Kikuchi, T. Sei, T. Tuchiya, S. Hayashi and K. Hayamizu, *J. Ceram. Soc. Jpn.*, 101 [7] 824–9 (1993)
- 17 J. Rokoh, H. Imai and H. Hirashima, *J. Ceram. Soc. Jpn.*, 105 [1] 43–7 (1997)
- 18 K. Sumi, Y. Kobayashi and E. Kato, *J. Am. Ceram. Soc.*, 81 [4] 1029–32 (1998)
- 19 K. Sumi, Y. Kobayashi and E. Kato, *J. Ceram. Soc. Jpn.*, 106 [7] 693–7 (1998)
- 20 I. M. Lachman and R. M. Lewis, *U.S. Patent* No.3,885,977 (1975)
- 21 I. M. Lachman, R. D. Bagley and R. M. Lewis, *Ceramic Bulletin* Vol. 16, No12 (1981)
- 22 R. Johnson, B. P. Saha, I. Ganesh, V. Mahender, S. Bhattacharjee, Y. R. Mahajan and M. M. K. Khaja, *Trans. Ind. Ceram. Soc.*, 59 [3] 93 (2000)
- 23 B. P. Saha, R. Johnson, I. Ganesh, G. V. N. Rao and Y. R. Mahajan, *Mater. Chem. Phys.*, 67 [1–3] 140 (2001)
- 24 J. Howitt, in "Catalysis and Automobile Emission Control," edited by A. Crucq and Frennet (Elsevier Science and Publisher).
- 25 R. Morrell, *Proc. Brit. Ceram. Soc.*, 28 52 (1979)
- 26 P. M. Then and P. Day, *Interceram.*, 69(1) 20 (2000)
- 27 H. Kainer and H. Reh, *Interceram.*, 40 (2) 99 (1991)
- 28 R. Johnson, B. P. Saha, I. Ganesh, V. Mahender, S. Bhattacharjee, Y. R. Mahajan and M. M. K. Khaja, *Trans. Indian. Ceram., Soc.* 59(3) 93(2000)
- 29 T. M. Gardner, S. E. Lott, S. J. Lockwood and L. I. Mclaughlin, *U.S. Patent* No. 5,830,421

- (1998)
- 30 H. Ray, *Interceram*, 5 54 (1987)
- 31 J. P. Day and D. L. Hickman, *J. Am. Ceram. Soc.*, 52 (1995)
- 32 Y. R. Mahajan and R. Johnson, “Current Scenario and Future Projections,” in *Materials Research* : edited by R. Chidabaram (Materials Research Society of India, 2003)
- 33 J. A. Kuszyk and R. C. Bradt, *J. Am. Ceram. Soc.*, 56 [8] 420–3(1973)
- 34 I. Yamai and T. OOTA, *J. Am. Ceram. Soc.*, 68 [5] 273–8(1985)
- 35 F. J. Parker and R. W. Rice, *J. Am. Ceram. Soc.*, 72 [12] 2364–6(1989)
- 36 J. J. Cleveland and R. C. Bradt, *J. Am. Ceram. Soc.*, 61 [11-12] 478–81(1973)
- 37 A.G. Evans, *Acta. Metall.*, 26 [12] 1845–1853(1978)
- 38 K. Hamano, Y. Ohya, and Z. Nakagawa, *Yogyo-Kyokai-Shi*, 91 [2] 94–101 (1983)
- 39 Y. Ohya, K. Hamano, and Z. Nakagawa, *Yogyo-Kyokai-Shi*, 92 [5] 261–7 (1984)
- 40 D. F. Qian, Y. Ohya, K. Hamano and Z. Nakagawa, *Yogyo-Kyokai-Shi*, 93 [6] 315–21 (1985)
- 41 D. F. Qian, Y. Ohya, Z. Nakagawa and K. Hamano, *J. Ceram. Soc. Jpn*, 103 [10] 1022–6 (1995)
- 42 A. Shyam, E. Lara-Curzio, A. Pandey, T. R. Watkins and K. L. More, *J. Am. Ceram. Soc.*, 95 [5] 1682–91 (2012)
- 43 T. Harada, T. Hamanaka, K. Hamaguch and S. Asami, *Patent US* 4,869,944 (1989)
- 44 G. Bruno, A. M. Efremov, C. P. An, B. R. Wheaton and D. J. Hughes, *J.Mater.Sci.*, 47 3674–89 (2012)
- 45 G. Bruno and S. Vogel, *J. Am. Ceram. Soc.*, 91 [8] 2646–52 (2008)

Chapter 2

Quantification of ceramic microstructures with digital images of photomicrograph

2-1 Introduction

Cordierite ceramics possess domain structure, which consist of submicron-sized primary cordierite crystals aligned in the same crystal orientation.^{1,2} The domain structures were thought to affect CTE, but it have been difficult to quantify the sizes and distributions of domains.

On the other hand, it is well known that the size and the distribution of grains affect various properties of polycrystals,³⁻¹⁵ and several methods have been used to quantify them.^{6-8,15} Major characterization methods are carried out with the aid of microscopy, such as optical polarization microscopy (OPM), scanning electron microscopy (SEM), and transmission electron microscopy (TEM). Ordinarily, a transparent overlay containing one or more test lines of known length is fixed in place over a photomicrograph of microstructure.¹⁶ Counting the number of intercepts between the test line and grain boundaries, and measuring distance between two intercepts closest each other can obtain the size and distribution of grains constituting polycrystalline ceramics.¹⁷ This measurement method are called “Linear intercept method”. Linear intercept method has been the most frequently used for quantification of size and distribution of grains constituting ceramics, since they do not need special devices and tools for measurement. However, linear intercept method also requires great care to obtain grain size distribution. Thus, easy and accurate method to quantify a microstructure of ceramics is strongly needed.

Recently, using the computer software, particle characteristics such as shape and size etc. can be easily measured from digital images of photomicrograph.¹⁸ The aid of the software makes also measurement of ceramics microstructures more easily than before. Here after, this method are referred to as “digital image analysis”. However, there are few reports of the microstructure measurement with the aid of the software using digital images of photomicrographs.

In this chapter, domain structures of cordierite ceramics were quantified with digital image analysis. Furthermore, digital image analysis was adopted also in measuring the microstructure of sintered mullite ceramics.

2-2 Experimental procedure

2-2-1 Quantification of domain structure of cordierite ceramics

Cordierite specimens were prepared by reaction sintering of various raw materials, and then petrographic thin specimens having a thickness of about 30 μm were prepared. The microstructures of the sintered specimens were observed by optical polarizing microscope (BX 53-P, OLYMPUS Corp.co. Ltd).

2-2-2 Quantification of primary grains constituting mullite ceramics

Sintered mullite tablets were prepared by reaction sintering of pure kaolin and alumina, and then their surface was polished and thermally etched at 20 °C lower than sintering temperature for 10 min. The microstructures of the sintered specimens were observed by SEM (JSM-6335FM, JEOL co. Ltd.) at an acceleration voltage of 2.0 kV.

2-3 Result and Discussion

2-3-1 Quantification of cordierite domain by digital image analysis

Cordierite domains are thought to have an optical anisotropy same as the primary crystals since they consist of primary crystal grains aligned in same crystal orientation. Therefore, OPM using transmitted light was used for the domain observation. While turning the sample stage in a crossed Nicol prism, the large area repeated bright and dark as shown in Fig.2-1. These areas were thought to be the large domains composed of many submicron-sized primary grains oriented in the same direction. Thus, the domain structure of cordierite ceramics could be easily observed with the aid of an optical polarizing microscope. In comparison of specimens (A) with (B), the size and distribution of domains seem to be different. These microphotographs were also binarized by digital processing, and the digital images were used for quantification of the size and distribution of domains.

Determining the individual domain areas of $S_1, S_2 \dots S_i$, from the digital image obtained by optical polarizing microscopy, equivalent diameter D_i of a circle having same area as S_i was obtained from

the equation, $D_i = 2 \times \sqrt{\frac{S_i}{\pi}}$. The curves of the cumulative domain number versus the equivalent

diameter, D_i , were shown in Fig.2-2. Here, a corresponding size to 50 number percent of the cumulative domain was defined as the average domain size, D_{50} . The average domain size of specimens (A) and (C) showed 8 and 30 μm , respectively. These quantified domain size did not correspond to visual result shown in OPM images. Therefore, the number-size distribution is unfavorable for quantification of domain size.

Many researchers¹⁹⁻²⁵ have applied Turner's work²⁶ to examine CTEs of anisotropic thermal expansion ceramics and composites. Turner²⁶ investigated the behavior of CTE in composites or polycrystalline solids and found that when the bulk modulus or rigidity of two crystals differs, the CTE of their composite cannot be shown in direct proportion to volume fraction. The average thermal expansion, α_r , could be calculated using the following equation, where K is the bulk modulus, F is the volume fraction, and ρ is the density.

$$\alpha_r = \frac{\sum \alpha_i K_i F_i / \rho_i}{\sum K_i F_i / \rho_i}$$

On the other hand, in cases such as the present research where the bulk modulus, rigidity, and density can be assumed constant, CTE is proportional to the volume fraction of each phase:

$$\alpha_r = \sum \alpha_i F_i$$

Assuming that a polycrystalline solid is composed of monophase anisotropic crystals, the CTE of the solid is proportional to the volume fraction of the domain in that direction, as reported in the literature²³⁻²⁵. Thus, the distribution of domain size, which can be obtained from the digital image analysis, must be considered from the viewpoint of volume, same as that of mullite grain size. The distributions of domain size and domain volume were estimated by the following procedure. The

volumes of the individual domains were calculated using the equation $V_i = \frac{4}{3} \pi \left(\frac{D_i}{2} \right)^3$. From the

curve of cumulative domain volume versus the equivalent diameter, D_i , a corresponding size for 50 volume percent of the cumulative domain was redefined as the average domain size, D_{50} . Fig.2-3 shows domain size distributions and average domain size based on the volume. Specimens (A) and (C) respectively showed average domain size of 15 and 51 μm , and they had narrow domain size distributions. These results were good agreement with the result of OPM observation.

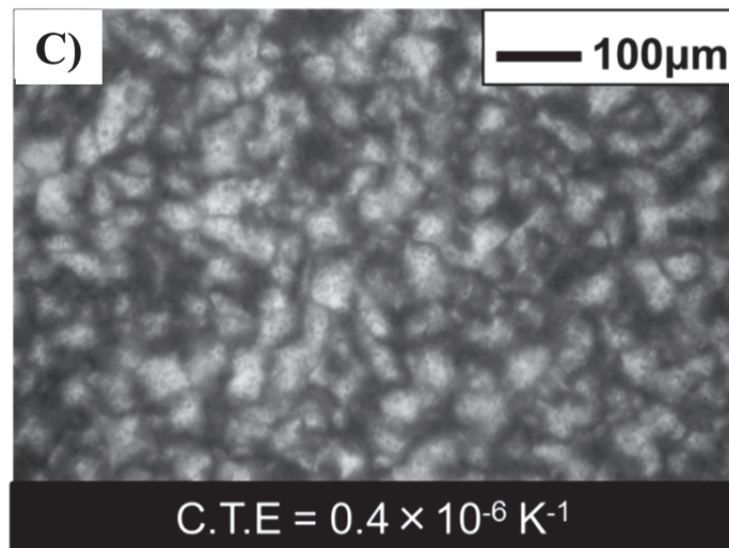
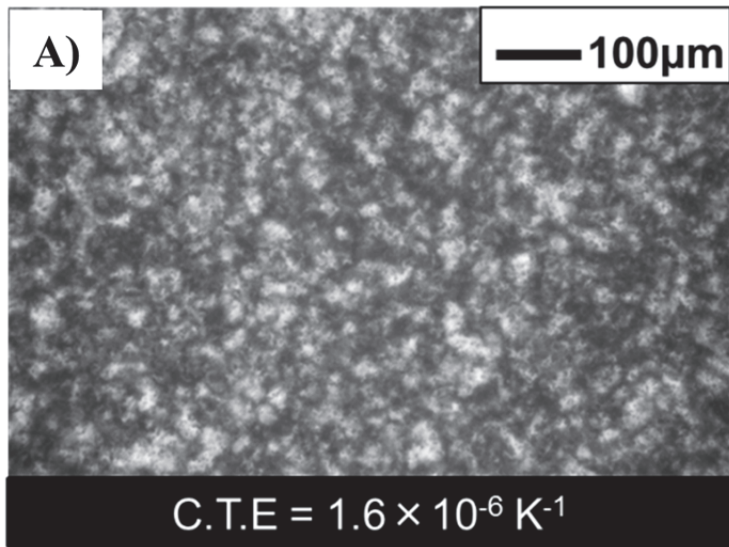


Fig.2-1 OPM images of cordierite ceramics

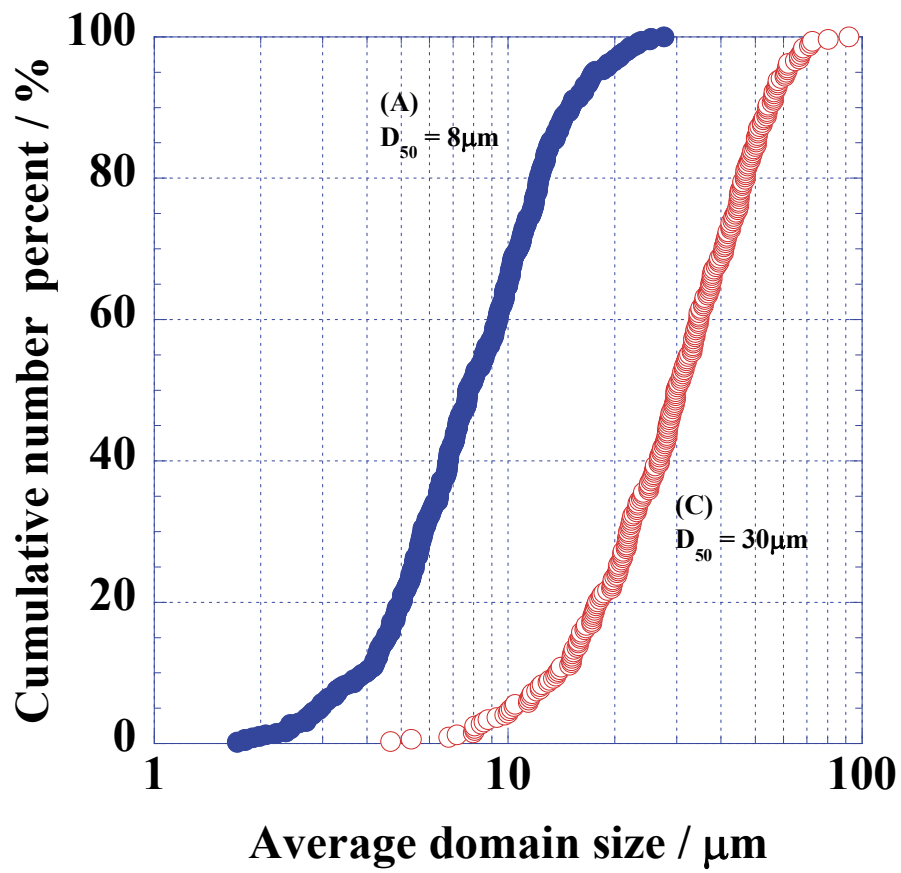


Fig.2-2 Average domain size and domain size distributions of cordierite, based on the domain number

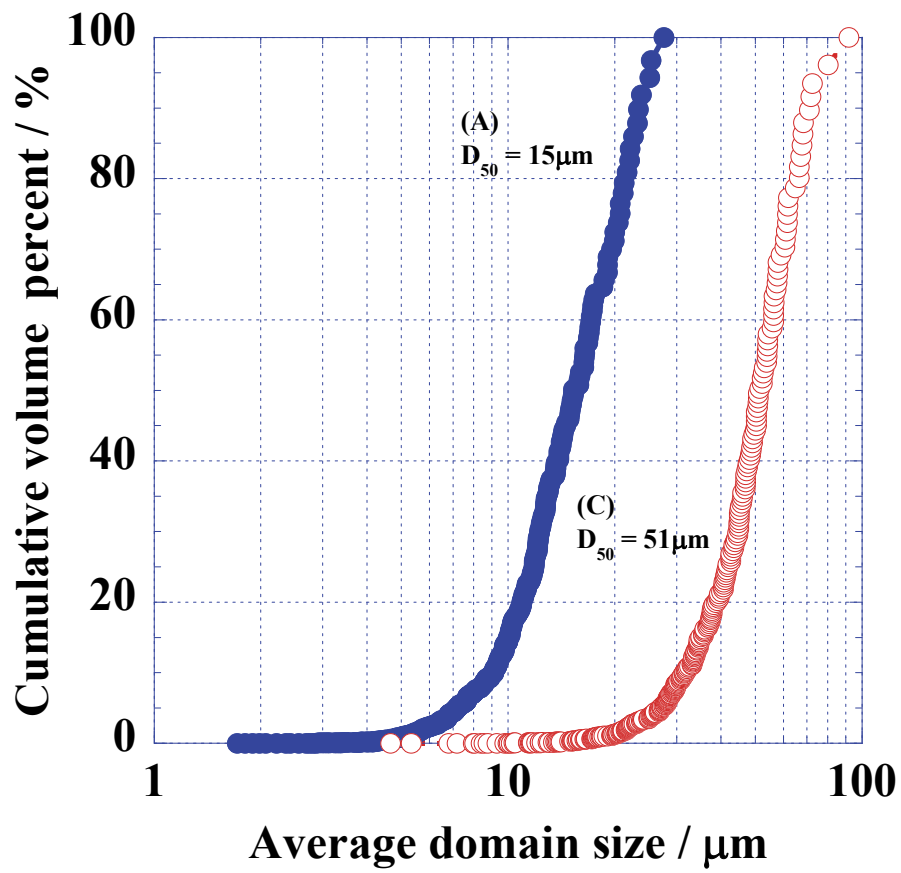


Fig.2-3 Average domain size and domain size distributions of cordierite, based on the domain volume

2-3-2 Applying digital image analysis for quantification of microstructure of mullite ceramics

Fig.2-4 shows SEM images of the three mullite specimens prepared under different conditions. Specimen (A) consisted of submicron grains. On the other hand, for specimens (B) and (C), extremely coarse grains were partially observed, and the number of coarse grain in specimen (C) increased more than that of specimen (B). These microphotograph images were binarized by digital processing, and the digital data were used for quantification of the grain size and distribution.

Determining the individual domain areas of $S_1, S_2 \dots S_i$ from the digital image obtained by SEM, equivalent diameter d_i of a circle having same area as S_i was obtained from the equation, $D_i = 2 \times \sqrt{\frac{S_i}{\pi}}$, similar to quantification of cordierite domains. Fig.2-5 shows grain number-size distributions of mullite ceramics. Average grain size of specimens (A), (B), and (C) showed 0.3, 0.3, and 0.4 μm , respectively. The difference in grain size did not observe, and these results did not correspond to SEM observation. Also in a case of quantification of grain size of ceramics, the number-size distribution is unsuitable for quantification of domain size.

The volumes of the individual grains were calculated using the equation $V_i = \frac{4}{3} \pi \left(\frac{d_i}{2} \right)^3$, where d_i is the equivalent diameter of a circle having the same area as S_i , and is equal to $2 \times \sqrt{\frac{S_i}{\pi}}$. From the curves of cumulative grain volume versus the equivalent diameter d_i , an equivalent size for 50 volume percent of the cumulative grains was defined as the average grain size d_{50} . Fig.2-6 shows the grain size distributions and average grain size of mullite specimens. In order corresponding to specimens (A)-(C), grain size distributions became wider. Average grain size of specimens (A), (B), and (C) respectively showed 0.7, 0.8, and 1.0 μm . These results corresponded well to the result of SEM observation.

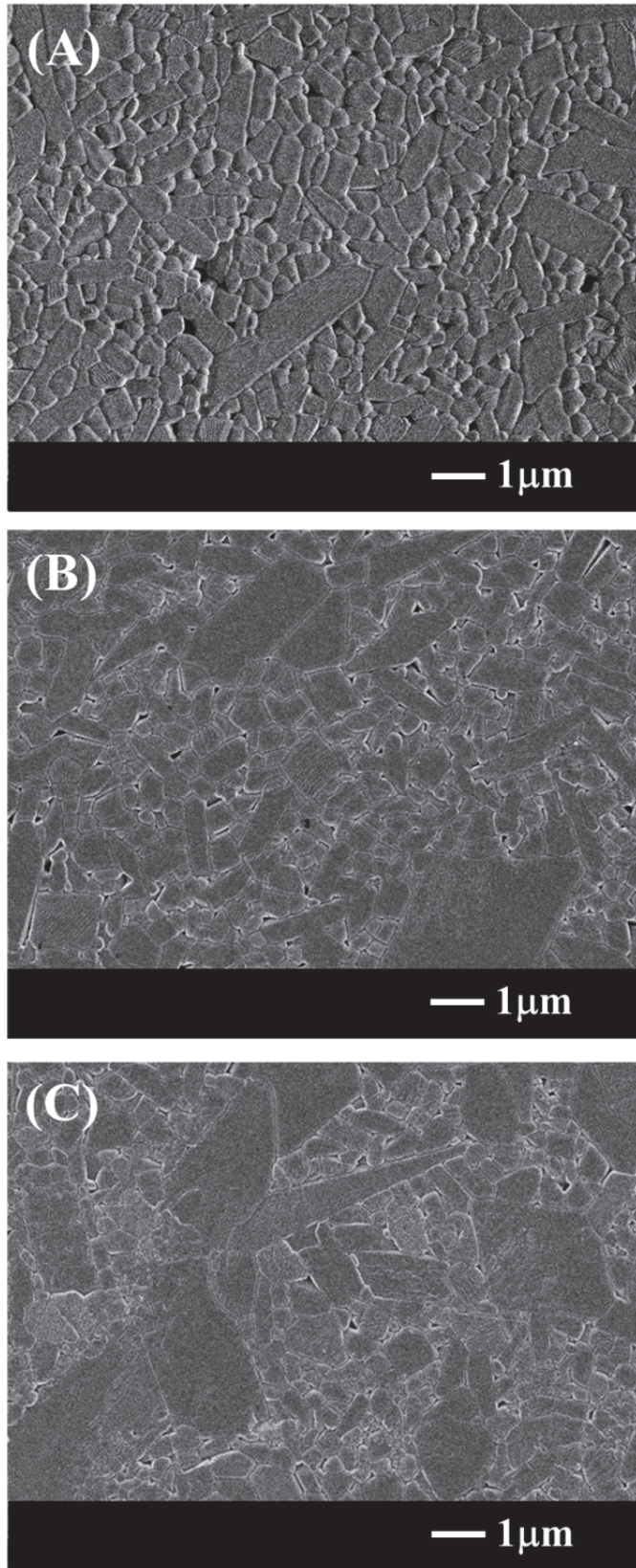


Fig.2-4 SEM images of mullite prepared under various condition

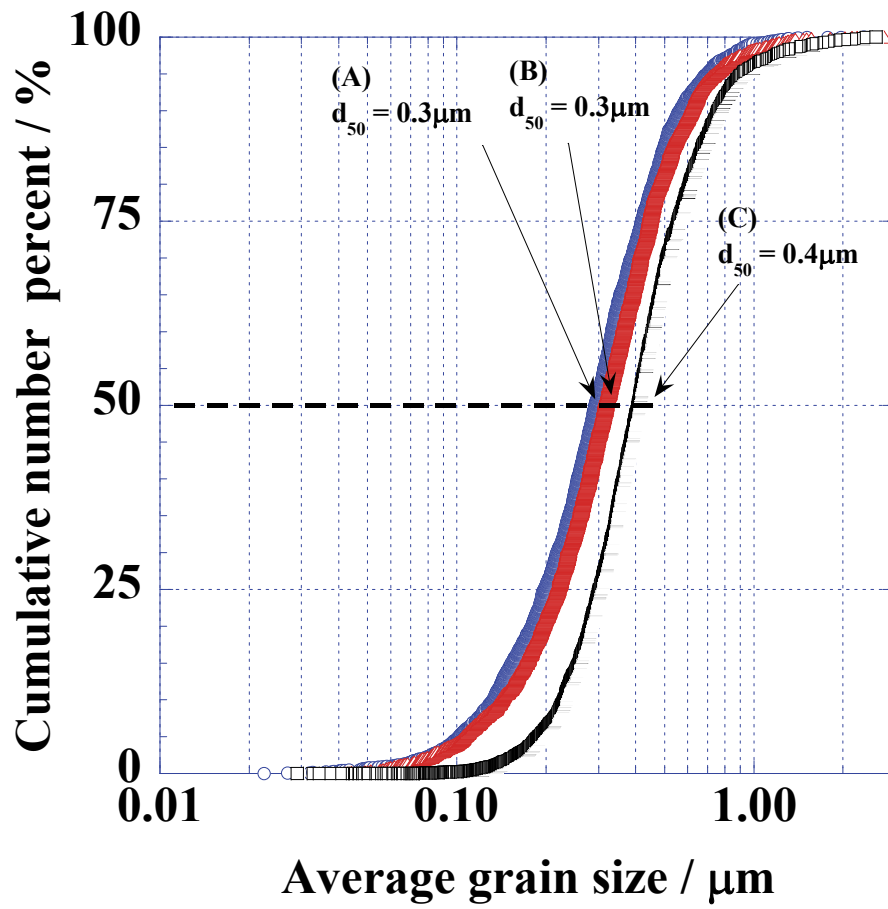


Fig.2-5 Grain number-size distributions of mullite ceramics

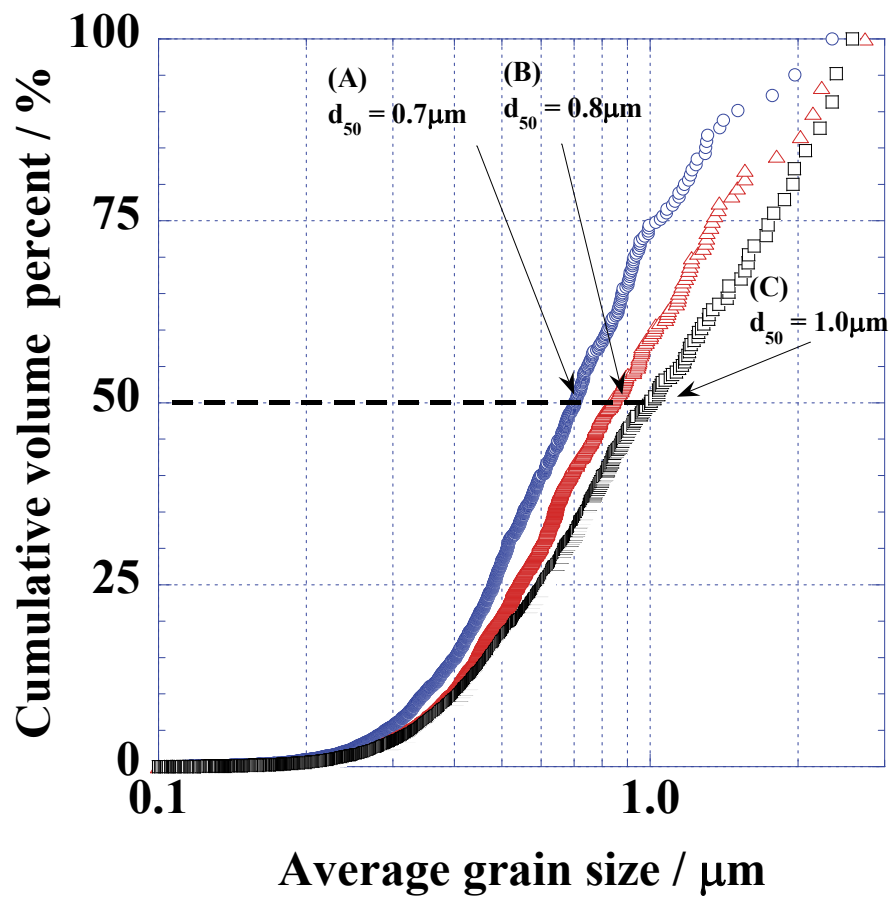


Fig.2-6 Grain volume-size distributions of mullite ceramics

2-4 Conclusions

Microstructure of cordierite ceramics and mullite ceramics respectively were quantified by digital image analysis of binarized photomicrographs, and next conclusions were obtained:

- 1 In sintered cordierite compacts, large domain structure could be observed by optical polarizing microscopy and it was confirmed that the domains were composed of primary submicron grains aligned in the same crystal orientation.
- 2 Also the size and distribution of primary grains of mullite ceramics could be easily quantified with digital image analysis.
- 3 The results of digital image analysis corresponded well to observation by SEM or OPM. Thus, the digital image analysis is available to estimate primary and secondary microstructures of ceramics.

References

- 1 T. Harada, T. Hamanaka, K. Hamaguch and S. Asami, *Patent US 4,869,944* (1989)
- 2 A. Shyam, E. Lara-Curzio, A. Pandey, T. R. Watkins and K. L. More, *J. Am. Ceram. Soc.*, 95 [5] 1682–91 (2012)
- 3 S. G. Lee, Y. W. Kim and M. Mitomo, *J. Am. Ceram. Soc.*, 84 [6] 1347–53 (2001)
- 4 A. de Pablos, M. I. Osendi and P. Miranzo, *J. Am. Ceram. Soc.*, 85 [1] 200–6 (2002)
- 5 H.S. Lee and T. Kimura, *J. Am. Ceram. Soc.*, 81 [12] 3228–36 (1998)
- 6 T. Hotta, K. Nakahira, M. Naito, N. Shinohara, M. Okumiya and K. Uematsu, *J. Mater. Res.*, 14 [7] 2970–9(1999)
- 7 H. Abe, T. Hotta, M. Naito, N. Shinohara and K. Uematsu, *J. Am. Ceram. Soc.*, 86 [6] 1019–21(2003)
- 8 W.E. Lee and W.M. Rainforth, *Ceramic Microstructures–Property Control by Processing*, Chapman and Hall, London, 1994
- 9 P. Chantikul, S.J. Bennison and B.R. Lawn, *J. Am. Ceram. Soc.*, 73 [8] 2419–27 (1990)
- 10 D. Kovar and M.J. Readey, *J. Am. Ceram. Soc.*, 79 [2] 305–12(1996)
- 11 A. Krell and P. Blank, *J. Am. Ceram. Soc.*, 78 [4] 1118–20 (1995)
- 12 F. Xiong, R.R. Manory, L. Ward, M. Terheci and S. Lathabai, *J. Am. Ceram. Soc.*, 80 [5] 1310–2 (1997)
- 13 S.J. Penn, N.McN. Alford, A. Templeton, X. Wang, M. Xu, M. Reece and K. Schrapel, *J. Am. Ceram. Soc.*, 80 [7] 1885–88 (1997)
- 14 J. Seidel, N. Claussen and J. Rodel, *J. Eur. Ceram. Soc.*, 15, 395–404(1995)
- 15 W.D. Kingery, H. K. Bowen and D. R. Uhlmann, *Introduction to Ceramics*, 2nd Ed. Wiley, New York, 1976.
- 16 T. Hotta, J. Tatami, H. Tanaka, N. Shinohara, H. Emoto, M. Hattori, Y. Kishi, H. Abe, M. Naito and K. Uematsu, *American Ceramic Society Bulletin* 83.11 (2004): 9101–5
- 17 J. C. Wurst, J. A. Nelson, *J. Am. Ceram. Soc.*, 55 [2] 109(1972)

- 18 C.F. Moraa, A.K.H. Kwana, H.C. Chan, *Cement and Concrete Research*, 28 [6] 921–32 (1998)
- 19 H. Ikawa, T. Watanabe, K. Urabe, and S. Udagawa, *Yogyo-Kyokai-Shi*, 93 [12] 762–7 (1985)
- 20 N. Chawla, X. Deng, and D. R. M. Schnell, *Mater. Sci. Eng., A*, 426, 314–22 (2006)
- 21 H. Choe, T. Hsieh, and J. Wolfenstine, *Mater. Sci. Eng., A*, 237, 250–5 (1997)
- 22 J. Milhans, S. Ahzi, H. Garmestani, M. A. Khaleel, X. Sun, and B. J. Koeppel, *Mater. Des.*, 30 1667–73(2009)
- 23 A. M. Efremov, *Philos. Mag. A*, 86 [36] 5431–40 (2006)
- 24 G. Bruno, A. M. Efremov, B. R. Wheaton, and J. E. Webb, *Acta Mater.*, 58, 6649–55 (2010)
- 25 G. Bruno, A. M. Efremov, B. Clausen, A. M. Balagurov, V. N. Simkin, B. R. Wheaton, J. E. Webb, and D. W. Brown, *Acta Mater.*, 58, 1994–2003 (2010)
- 26 P. S. Turner, *J. Res. NBS*, 37, 239–50 (1946)

Chapter 3

Effect of Microstructure on the Thermal Expansion Coefficient of Sintered Cordierite Prepared from Sol Mixtures

3-1 Introduction

Cordierite ($2\text{Al}_2\text{O}_3 \cdot 2\text{MgO} \cdot 5\text{SiO}_2$) is in the hexagonal crystal structure and has large anisotropic coefficients of thermal expansion (CTEs) of $2.5 \times 10^{-6} \text{ K}^{-1}$ and $-0.9 \times 10^{-6} \text{ K}^{-1}$ along the a and b axes, and c axis, respectively. Sintered cordierite ceramics have low CTE of approximately $1.7 \times 10^{-6} \text{ K}^{-1}$ in the range from room temperature to 900 °C. Therefore, they have superior thermal shock resistance. For this reason, it has long been utilized as a refractory material, filtering material for molten metals, and honeycomb-structured catalyst carrier in automobile exhaust systems. It can be difficult to produce dense cordierite ceramics using natural raw materials since they incongruently melt near the sintering temperature. Thus, many techniques to prepare dense cordierite ceramics have been proposed. These include glass-ceramic processes¹ and advanced sol-gel processes²⁻⁵. The former involves sintering quenched glass in the stoichiometric composition of cordierite or its glass powder compact. The latter uses metal alkoxides as starting materials and produces cordierite ceramics via gel-sol processes. However, these methods have not reached practical applications because of problems such as complex procedures and expensive raw materials. We have already reported^{6, 7} the preparation of dense cordierite ceramics using kaolinite particles and synthesized fine particles of $\text{Mg}(\text{OH})_2$. However, a slight difference from the chemical composition of cordierite led to the coexistence of a small amount of spinel ($\text{MgO} \cdot \text{Al}_2\text{O}_3$). This spinel increases the CTE.

In this study, we produced sintered cordierite ceramics from $\text{Mg}(\text{OH})_2$ particles, silica sol, and alumina sol with the relative density of at least 97 %. However, these ceramics showed a wide range of CTEs from 0.4×10^{-6} – $1.6 \times 10^{-6} \text{ K}^{-1}$ between room temperature and 900 °C. Observations with a scanning electron microscope (SEM) and optical polarizing microscope revealed that the submicron primary cordierite crystals constructed large domains with sizes of several tens of micrometers in the same crystal orientation. Moreover, digital image analysis of the photographs obtained by optical polarizing microscopy revealed that there was a clear relationship between the quantified domain size and CTE.

3-2 Experimental Procedures

3-2-1 Preparation

Ultrafine particles of $\text{Mg}(\text{OH})_2$ were precipitated from a mixture of magnesium chloride solution and ammonia solution, and separated by centrifugation. The resultant $\text{Mg}(\text{OH})_2$, silica sol (Nissan Chemical Industries, SNOWTEX-O), and alumina sol (Nissan Chemical Industries, ALUMINASOL 520) were ultrasonically dispersed in the stoichiometric composition of cordierite

($2\text{Al}_2\text{O}_3 \cdot 2\text{MgO} \cdot 5\text{SiO}_2$). TiO_2 fine particles (Kishida Chemical, anatase) were used to produce samples with various microstructures. The suspensions were stirred and then dried under an infrared lamp. After calcination for one hour at $800\text{ }^\circ\text{C}$, the samples were milled with an alumina mortar. The sample powders were then uniaxially pressed into a 16-mm-diameter die by a uniaxial press at the pressure of 39.2 MPa followed by a cold isostatic pressing at 196 MPa. The resultant green disk was heated to $1000\text{ }^\circ\text{C}$ in an electric furnace at the rate of $5\text{ }^\circ\text{C}/\text{min}$ and then heated at the rate of $2.5\text{ }^\circ\text{C}/\text{min}$ above $1000\text{ }^\circ\text{C}$. The furnace was maintained at a prescribed temperature for one hour and then it was left to cool.

3-2-2 Characterization

The crystalline phases of the sintered compacts were identified by X-ray diffractometry (Rigaku Corp., RINT 2500) utilizing $\text{Cu K}\alpha$ X-ray radiation and a graphite monochromator. The lattice thermal expansion of the generated cordierite was measured by high-temperature powder X-ray diffractometry. The diffractometer was attached to an electronic furnace that had a window covered with Kapton film on which aluminum was deposited, and 99.999% silicon powder was used as an internal standard and N_2 gas was flowed during the measurement in order to prevent oxidation of the silicon powder. Bulk density and apparent porosity were measured using the Archimedes' immersion method. The CTE of the sintered compact was measured using thermomechanical analysis equipment (TMA 8310, Rigaku Corp.) at a heating and cooling rate of $10\text{ }^\circ\text{C}/\text{min}$ between room temperature and $900\text{ }^\circ\text{C}$. The microstructures of the sintered specimens were observed by SEM (JSM-6335FM, JEOL Ltd.) at an acceleration voltage of 2.0 kV, and an optical polarizing microscope (BX 53-P, Olympus Corp.).

3-3 Results and Discussion

3-3-1 Thermal reaction and sintering of sol mixtures

(A) Thermal reaction of sol mixtures

Figure 3-1 shows the X-ray diffraction patterns of samples that were heat treated between $900\text{ }^\circ\text{C}$ and $1200\text{ }^\circ\text{C}$ for one hour then left to cool. Around $900\text{ }^\circ\text{C}$, decomposed MgO reacted with γ -alumina and silica to form spinel ($\text{MgO} \cdot \text{Al}_2\text{O}_3$). Above $1000\text{ }^\circ\text{C}$, a small amount of enstatite ($\text{MgO} \cdot \text{SiO}_2$) crystallized from amorphous phases. Around $1175\text{ }^\circ\text{C}$, μ -cordierite suddenly appeared from amorphous phases in the composition of the $\text{MgO}-\text{Al}_2\text{O}_3-\text{SiO}_2$ system. Amorphous phases remained until the temperature reached $1175\text{ }^\circ\text{C}$, which was presumed from the broad band at about $2\theta = 22^\circ$.

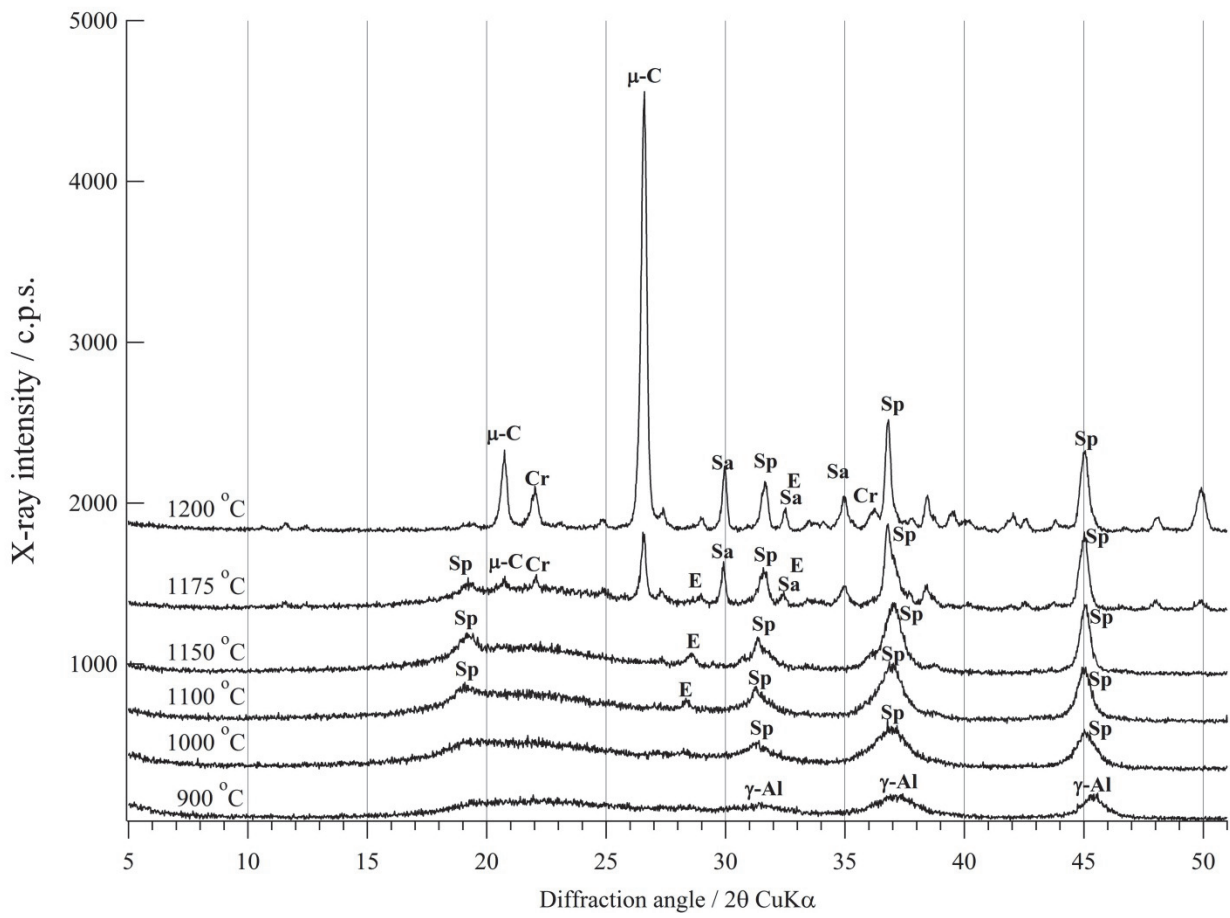


Fig. 3-1 XRD patterns of sol mixtures of alumina, silica, and Mg(OH)₂

Table 3-1 Diffraction data of each crystalline phase used for determination of phase changes of specimens.

Crystals	JCPDS number	Miller index	2 θ / ° CuK α
Cordierite	13-0294	110	10.5
Spinel	21-1152	311	36.8
Sapphirine	44-1430	-231	32.3
Cristobalite	27-0605	220	35.8
Enstatite	19-0768	221	28.3
μ -Cordierite	14-0249	-202	26.4

Figure 3-2 presents the qualitative changes in crystal phases above 1100 °C. The height of a single diffraction peak of each crystalline phase shown in Table 3-1 was used to determine the approximate amount of each crystal phase. These diffraction peaks were selected because they do not overlap. At 1175 °C, both sapphirine (4MgO·5Al₂O₃·2SiO₂) and μ -cordierite, which were crystals in the MgO-Al₂O₃-SiO₂ system, crystallized. At 1200 °C, the broad band around 2 θ = 22° attributed to the amorphous phases almost disappeared while the peaks for μ -cordierite and cristobalite rapidly increased. Above 1200 °C, α -cordierite suddenly started to increase with consumption of μ -cordierite, sapphirine, spinel, and enstatite. At 1300 °C, the sintered compacts had completely transformed into monophase α -cordierite. We concluded that the α -cordierite was generated by transformation of μ -cordierite and solid-state reaction between sapphirine, spinel, cristobalite, and enstatite. It has been reported^{2, 4, 5, 8-10} that α -cordierite directly crystallized without formation of additional intermediate crystalline phases such as spinel or cristobalite when the atomically homogeneous amorphous powder was heat treated. In this research, nanosized sol mixtures were used as starting material to produce cordierite so that intermediate crystals such as spinel, enstatite, and sapphirine appeared during reaction process.

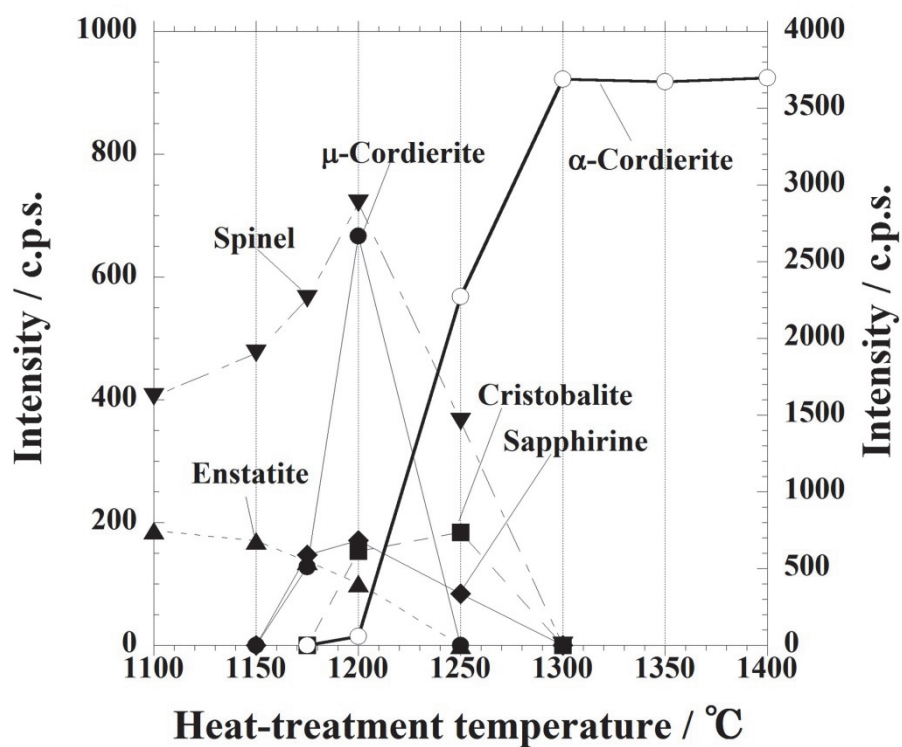


Fig. 3-2 Phase changes of powder mixtures of alumina sol, silica sol, and Mg(OH)₂ having cordierite composition

(B) Sintering characteristics

The bulk density and apparent porosity of the compacts sintered at each prescribed temperature are shown in Fig. 3-3. Here, bulk density and apparent porosity were determined by the Archimedes' immersion method. Bulk density rapidly increased in the range from 1000 °C to 1200 °C and the apparent porosity was almost 0 % at 1200 °C, revealing these powders to be very sinterable. As can be seen in the XRD pattern shown in Fig. 1, the amorphous phase was still present below 1175 °C. Therefore, it was thought that the viscous flow of the amorphous phase promoted sintering and densification of the substance. At 1200 °C, the bulk density had become greater than the value of $2.507 \times 10^3 \text{ kg m}^{-3}$ calculated from the lattice parameters of α -cordierite owing to the presence of μ -cordierite and sapphirine, which have somewhat larger density than α -cordierite. Above 1200 °C, the formation of α -cordierite started to increase and the bulk density started to decrease. Since the compact turned into monophase cordierite above 1300 °C, the bulk density showed a constant value of approximately $2.47 \times 10^3 \text{ kg m}^{-3}$. The relative density of the α -cordierite sample, which could be calculated from the ratio of bulk density to calculated density ($2.507 \times 10^3 \text{ kg m}^{-3}$), was about 98%. Thus, we successfully prepared dense α -cordierite (hereafter referred to as cordierite).

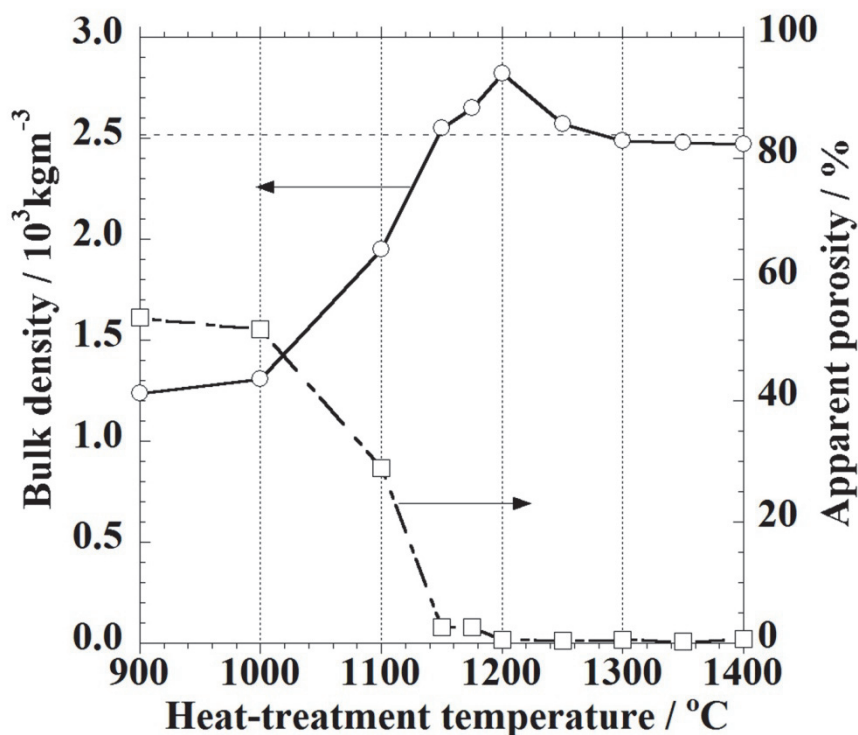


Fig. 3-3 Bulk density and apparent porosity of samples heat treated at various temperatures

3-3-2 Thermal expansion properties of dense ceramics

Figure 3-4 shows the thermal expansion curves of sintered compacts A, B, and C, which contain different amounts of TiO₂. The CTEs of the sintered cordierite ceramics showed various values in the range of 0.4×10^{-6} – $1.6 \times 10^{-6} \text{ K}^{-1}$, largely depending on the preparation conditions. There were more differences between heating and cooling curves in sintered compacts having lower CTE. The occurrence of microcracks was supposed from this result, as suggested for Al₂TiO₅¹¹.

3-3-3 Microstructure of sintered cordierite

The polished surfaces of sintered cordierite compacts A and C were observed by SEM as shown in Fig. 3-5. Microcracks were not found in sintered compact A, which showed a CTE of $1.6 \times 10^{-6} \text{ K}^{-1}$ similar to the average of the crystal axes expansion. On the other hand, numerous microcracks were observed on the polished surface of sintered compact C, which showed lower expansion. In general, stresses arise in sintered compacts composed of crystals with thermal expansion anisotropy. The stresses are proportional to the product of the CTE difference, $\Delta\alpha$, and the difference between the sintering temperature and room temperature, ΔT . Kuszyk and Bradt¹² studied the influence of grain size on the effects of thermal expansion anisotropy in MgTi₂O₅. They clarified that an increase in grain size induced abrupt decrease in CTE and showed that the critical size for microcrack formation depended on the strain energy and fracture surface energy.

The high-resolution SEM image of the polished and thermally etched surface of sintered compact A is shown in Fig. 3-6. Submicron-sized primary grains could be observed in each sintered compact. Since the primary grain size did not differ despite varying preparation conditions, it is difficult to proclaim the intergranular stress between primary grains as the source of microcracks.

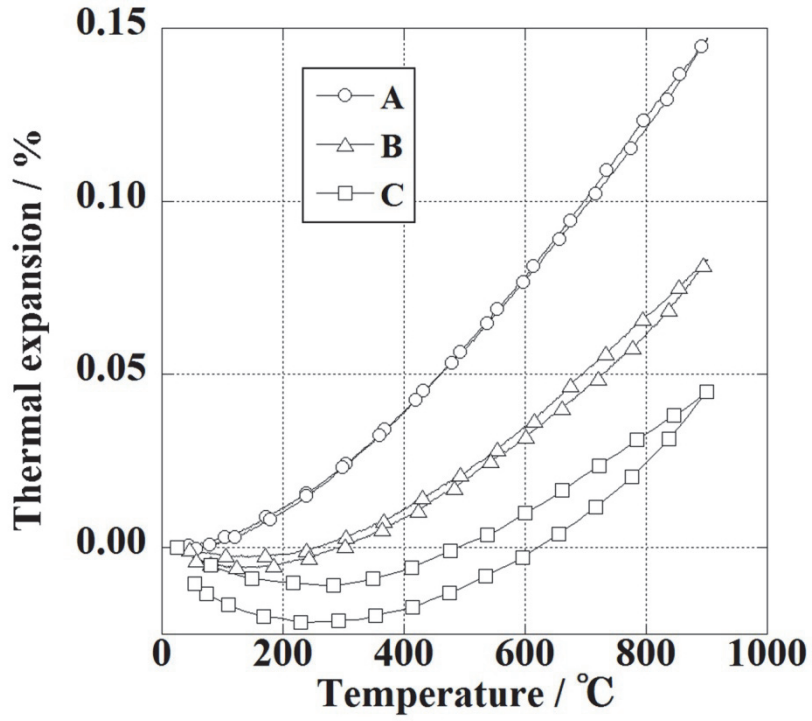


Fig. 3-4 Thermal expansion curves of dense cordierite prepared under various conditions

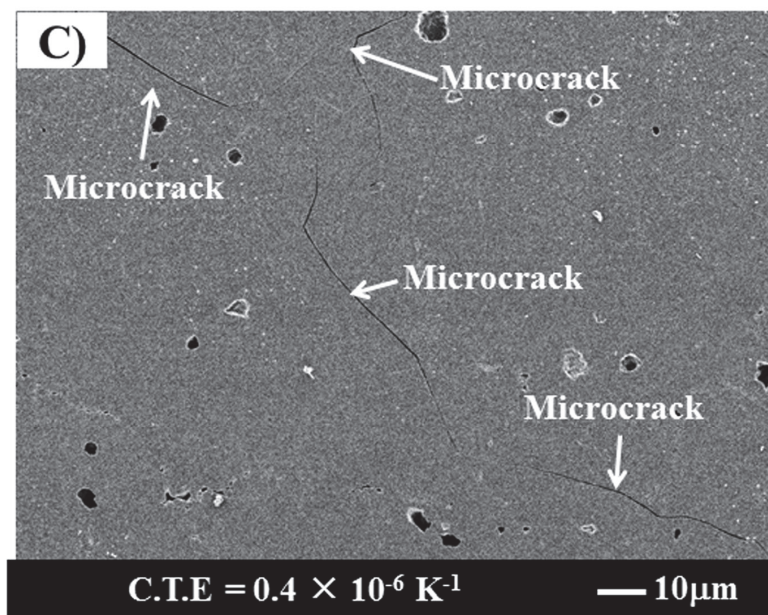
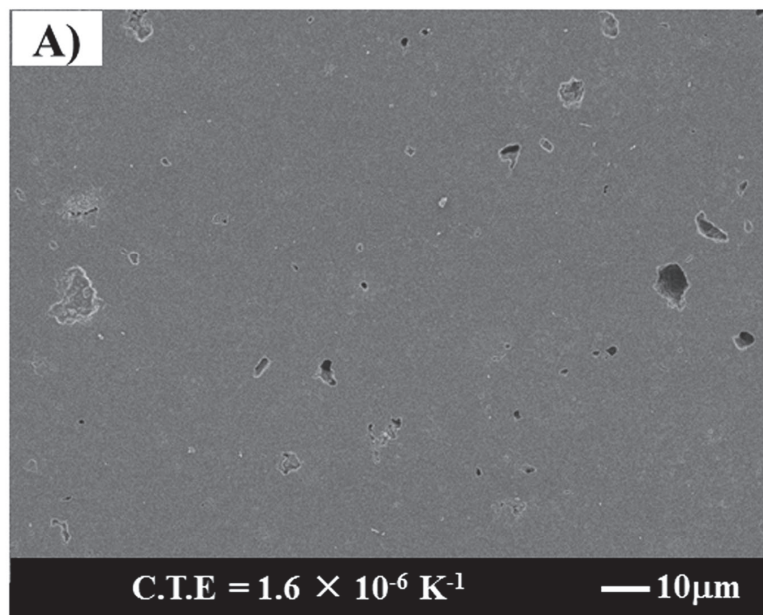


Fig. 3-5 SEM images of polished samples having CTEs of A) $1.6 \times 10^{-6} \text{ K}^{-1}$ and C) $0.4 \times 10^{-6} \text{ K}^{-1}$

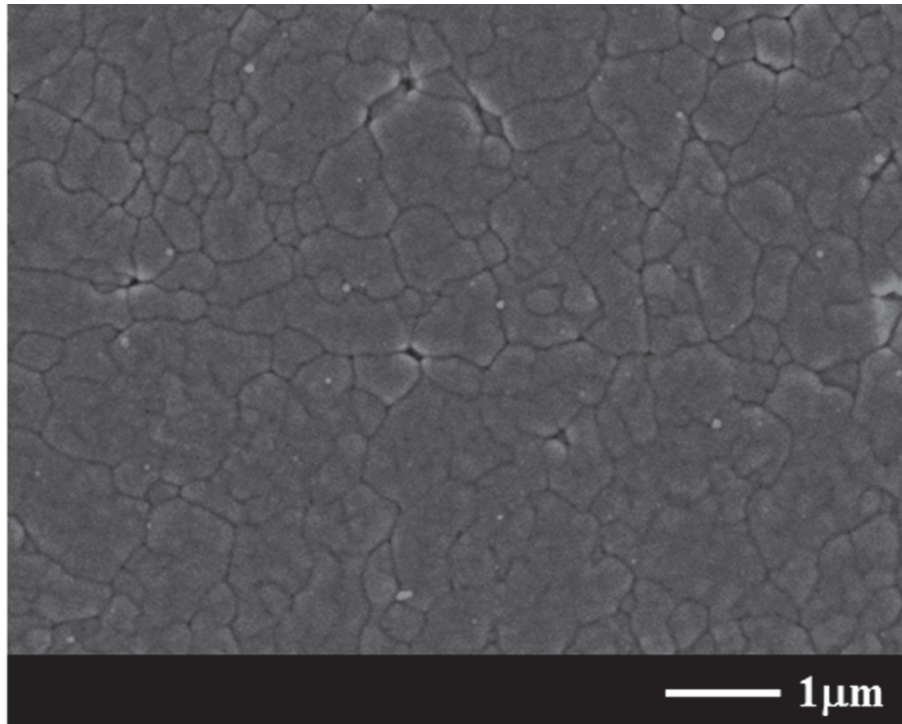


Fig. 3-6 SEM image of dense cordierite ceramics that were polished, then thermally etched

Hamano etc.¹³⁻¹⁶ studied the relationship between microstructure and thermal expansion properties of aluminum titanate, which has larger thermal expansion anisotropy than cordierite. They showed that a large secondary particle was constructed by many primary grains in the same crystal orientation and that the domain structure affected the CTE of aluminum titanate polycrystals.

Cordierite honeycomb ceramics were also reported¹⁷⁻²⁰ to possess domain structure, which affected CTE, on the basis of SEM observations. However, quantitative analysis of the domain size is quite difficult by only SEM observation. Therefore, petrographic thin samples of the cordierite ceramics having a thickness of about 30 μm were observed by optical polarizing microscopy using transmitted light. While turning the sample stage in a crossed Nicol prism, the large area repeated bright and dark as shown in Fig. 3-7. These areas were thought to be the large domains composed of many submicron-sized primary grains oriented in the same direction. Thus, the domain structure of cordierite ceramics could be easily observed with the aid of an optical polarizing microscope. Figure 3-7a shows the domain structure of sintered compact A, which showed an average CTE of $1.6 \times 10^{-6} \text{ K}^{-1}$. Fig. 3-7b shows the domain structure of sintered compact C having a CTE of $0.4 \times 10^{-6} \text{ K}^{-1}$. Comparing these figures, it can be concluded that the larger the domain grows, the smaller the CTE becomes.

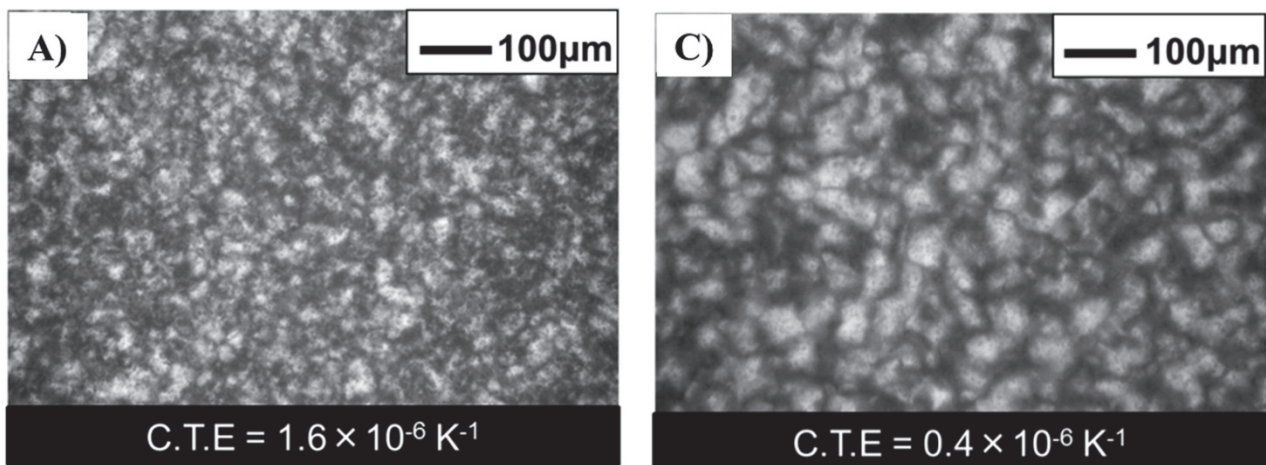


Fig. 3-7 Polarizing microscope images of samples with CTEs of A) $1.6 \times 10^{-6} \text{ K}^{-1}$ and C) $0.4 \times 10^{-6} \text{ K}^{-1}$

3-3-4 Quantification of average domain size and CTE modeling

In order to reveal the quantitative relationship between domain size and CTE, the size and distribution of the domains were quantified from the binarized image obtained by optical polarizing microscopy. Many researchers²¹⁻²⁷ have applied Turner's work²⁸ to examine CTEs of anisotropic thermal expansion ceramics and composites. Turner²⁸ investigated the behavior of CTE in composites or polycrystalline solids and found that when the bulk modulus or rigidity of two crystals differs, the CTE of their composite cannot be shown in direct proportion to volume fraction. The average thermal expansion, α_r , could be calculated using the following equation, where K is the bulk modulus, F is the volume fraction, and ρ is the density.

$$\alpha_r = \frac{\sum \alpha_i K_i F_i / \rho_i}{\sum K_i F_i / \rho_i}$$

On the other hand, in cases such as the present research where the bulk modulus, rigidity, and density can be assumed constant, CTE is proportional to the volume fraction of each phase:

$$\alpha_r = \sum \alpha_i F_i$$

Assuming that a polycrystalline solid is composed of monophase anisotropic crystals, the CTE of the solid is proportional to the volume fraction of the domain in that direction, as reported in the literature²⁵⁻²⁷. Thus, the distribution of domain size, which can be obtained from the image analysis, must be considered from the viewpoint of volume. The distributions of domain size and domain volume were estimated by the following procedure. Determining the individual domain areas of $S_1, S_2 \dots S_i$, from the digital image obtained by optical polarizing microscopy, the volumes of the

individual domains were calculated using the equation $V_i = \frac{4}{3} \pi \left(\frac{D_i}{2} \right)^3$, where D_i is the equivalent

diameter of a circle having the same area as S_i , and is equal to $2 \times \sqrt{\frac{S_i}{\pi}}$. From the curve of cumulative domain volume versus the equivalent diameter, D_i , a corresponding size for 50 volume percent of the cumulative domain was defined as the average domain size, D_{50} .

Figure 3-8 shows the relationship between average domain size D_{50} and the average CTE from room temperature to 900 °C for various sintered cordierite ceramics. Changing the amount of TiO_2 could lead to various CTEs in the sintered compacts. A clear relationship could be seen between the domain size and CTE of the sintered compacts. When the domain size was smaller than 40 μm , CTE was around $1.7 \times 10^{-6} \text{ K}^{-1}$, which coincided with previously reported results.¹⁷ On the other hand, when the domain size exceeded 40 μm , CTE decreased rapidly to around $0.4 \times 10^{-6} \text{ K}^{-1}$. When the amount of TiO_2 was changed, the sintered compacts showed various CTEs, but the detailed trend was not clear. Additional research is needed to clarify the effect of TiO_2 on CTE and

domain size in reaction-sintered cordierite.

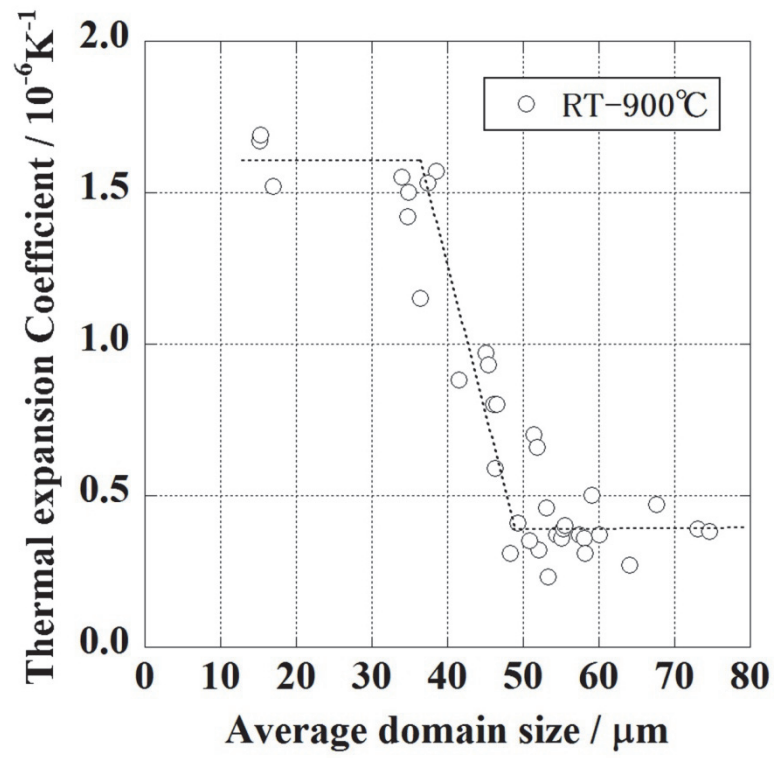


Fig. 3-8 Effect of domain size on CTE

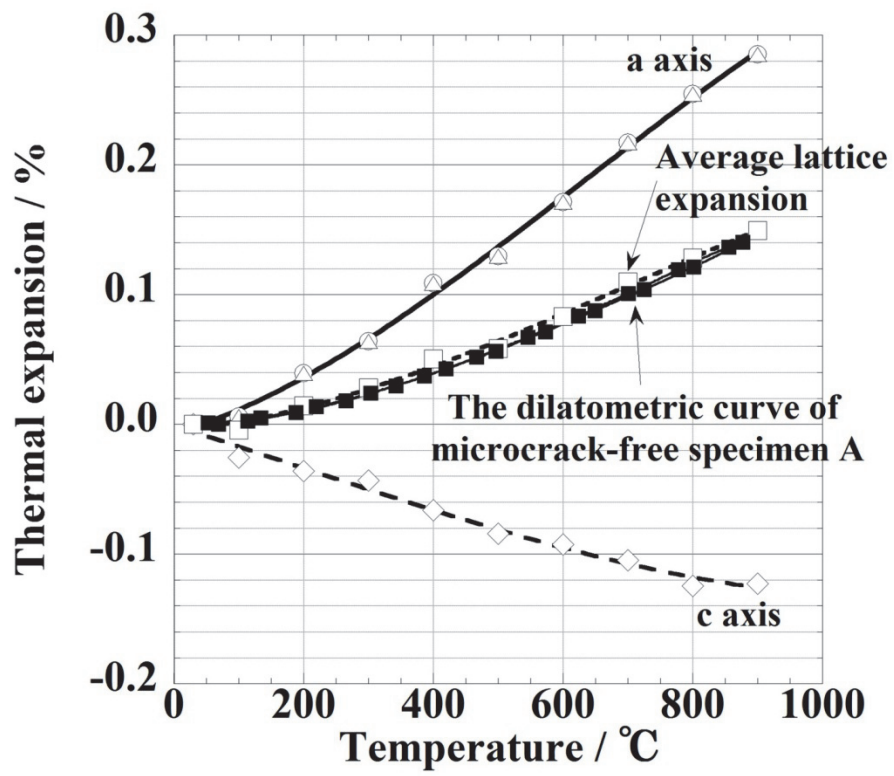


Fig. 3-9 Thermal expansion of the crystal axes of cordierite

Figure 3-9 shows the thermal expansion of sintered cordierite ceramics measured via high-temperature X-ray diffraction. There are many reports^{27, 29-33} about the lattice thermal expansions of cordierite including both hexagonal and orthorhombic crystals (α - and β -type, respectively). The sintered cordierite ceramics obtained in this study were hexagonal crystals, as confirmed by the X-ray diffraction patterns, which agreed well with the X-ray diffraction data reported for the hexagonal crystal (JCPDS 13-0294). Therefore, the lattice expansions shown in Fig. 3-9 were determined using the diffraction data for the hexagonal crystal (JCPDS 13-0294). The lattice CTE of each crystal axis in sintered cordierite ceramics are shown in Table 3-2 along with those from previous studies^{27, 29, 32} in which the thermal expansion was measured to above 900 °C. The lattice CTE that we determined for sintered compact A was slightly different from the results reported by Milberg and Blair,³² even though they reported the same hexagonal crystal. On the other hand, the lattice CTE and mean CTE from our results were in good agreement with the results reported by Mirwald²⁹ and Bruno.²⁷ In this study, the lattice CTEs from our results, $\alpha_a = 3.36 \times 10^{-6} \text{ K}^{-1}$ and $\alpha_c = -1.61 \times 10^{-6} \text{ K}^{-1}$, were used for theoretical calculations.

Table 3-2 The lattice CTE of cordierite ceramics and of previously reports measured at the temperature range between room temperature and 900 °C

Hexagonal			Orthorhombic		
Lattice CTE ($\times 10^{-6} \text{ K}^{-1}$)	A	B	Lattice CTE ($\times 10^{-6} \text{ K}^{-1}$)	C	D
α_a	3.36	2.64	α_a	3.91	2.87
α_a	3.36	2.64	α_b	2.41	3.56
α_c	-1.61	-1.49	α_c	-1.03	-0.92
$\bar{\alpha}$	1.70	1.26	$\bar{\alpha}$	1.76	1.84

(A) This study, (B) Milberg and Blair,³² (C) Mirwald,²⁹ and (D) Bruno et al.²⁷

The observed domains can be regarded as single crystals because the domains were composed of primary grains aligned in the same crystal orientation. Assuming the domains distributed randomly and statistically in the sintered cordierite ceramics, the domain boundaries consist of many combinations of crystal axes. As the simplest approximation, domain boundaries are supposed to be composed of the following nine combinations of crystal axes:

(1) a-a, (2) a-b, (3) a-c, (4) b-a, (5) b-b, (6) b-c, (7) c-a, (8) c-b, (9) c-c

These combinations can be classified into the following three groups according to the CTE values between domains:

Group 1, large CTE: (1) (2) (4) (5)

Group 2, small CTE: (3) (6) (7) (8)

Group 3, negative CTE: (9)

The average CTE of microcrack-free cordierite ceramics can be calculated as a mean value of nine combinations of groups 1, 2, and 3 constituting the domain boundaries as follows:

$$\alpha_1 = \frac{\frac{\alpha_a + \alpha_a}{2} + \frac{\alpha_b + \alpha_b}{2} + \frac{\alpha_c + \alpha_c}{2} + 2 \times \frac{\alpha_a + \alpha_b}{2} + 2 \times \frac{\alpha_a + \alpha_c}{2} + 2 \times \frac{\alpha_b + \alpha_c}{2}}{9}$$

$$= \frac{\alpha_a + \alpha_b + \alpha_c}{3} = 1.7 \times 10^{-6} K^{-1}$$

The calculated result of $1.7 \times 10^{-6} K^{-1}$ from room temperature to 900 °C was in good agreement with the result obtained for sintered polycrystals shown in Fig. 3-8. Also, the calculated average thermal expansion curve in Fig. 3-9 was in good agreement with the thermal expansion curve of the dilatometric curve of microcrack-free specimen A in Fig. 3-4.

By the energy criterion proposed by Cleveland and Bradt,³⁴ the critical grain size at which formation of microcracks initiates was inversely proportional to the square of thermal expansion difference $\Delta\alpha$ and temperature difference ΔT . When the small domains are exposed to stresses caused by the thermal expansion anisotropy, microcracks will not occur during cooling since $\Delta\alpha$ and ΔT are too small for a fracture to initiate. On the other hand, when the large domains are exposed to stresses caused by the expansion anisotropy at cooling, microcracks occur at the domain boundaries having the largest CTE (group 1) first. In contrast, microcracks do not occur yet at the domain boundaries in groups 2 and 3 since the CTEs of these boundaries are small or negative. In this case, the CTE of the ceramics corresponds to an average of group 2 and 3, hereafter designated as α_2 , and is calculated as follows:

$$\alpha_2 = \frac{2 \times \frac{\alpha_a + \alpha_c}{2} + \frac{\alpha_c + \alpha_c}{2} + 2 \times \frac{\alpha_b + \alpha_c}{2}}{5}$$

$$= \frac{\alpha_a + \alpha_b + 3\alpha_c}{5} = 0.4 \times 10^{-6} K^{-1}$$

This value agreed well with the lower limit of the CTE shown in Fig. 3-8. These results indicate that the simple partial microcrack model proposed in this paper is applicable to thermally anisotropic ceramics that have microcracks.

3-4 Conclusions

Dense cordierite ceramics were prepared from sol mixtures, and the domain structures could be easily observed by optical polarizing microscopy and quantified by digital image analysis. After examining the relationship between CTE and the average domain size of the cordierite, the following conclusions were obtained:

- 1 Dense sintered compacts of single-phased cordierite can be prepared from nanosized particles of Mg(OH)₂, alumina sol, and silica sol.
- 2 In sintered cordierite compacts, large domain structure could be observed by optical polarizing microscopy and the domains were composed of primary submicron grains aligned in the same crystal orientation.
- 3 It could be inferred that the critical domain size at which microcracks began to appear was around 40 μm.
- 4 The lower CTE limit of sintered cordierite ceramics at around $0.4 \times 10^{-6} \text{ K}^{-1}$ was attributed to the appearance of partial microcracking caused by stresses arising from thermal expansion anisotropy and domains larger than 40 μm.

References

- 1 C. Panda, W. M. Mobley, and R. Raj, *J. Am. Ceram. Soc.*, 72 [12] 2361–4 (1989)
- 2 H. Suzuki, K. Ota, and H. Saito, *J. Ceram. Soc. Jpn.*, 95 [2] 163–9 (1987)
- 3 H. Suzuki, K. Ota, and H. Saito, *J. Ceram. Soc. Jpn.*, 95 [2] 170–5 (1987)
- 4 N. Kikuchi, T. Sei, T. Tuchiya, S. Hayashi, and K. Hayamizu, *J. Ceram. Soc. Jpn.*, 101 [7] 824–9 (1993)
- 5 J. Rokoh, H. Imai, and H. Hirashima, *J. Ceram. Soc. Jpn.*, 105 [1] 43–7 (1997)
- 6 K. Sumi, Y. Kobayashi, and E. Kato, *J. Am. Ceram. Soc.*, 81 [4] 1029–32 (1998)
- 7 K. Sumi, Y. Kobayashi, and E. Kato, *J. Ceram. Soc. Jpn.*, 106 [7] 693–7 (1998)
- 8 U. Selvaraj, S. Komarneni, and R. Roy, *J. Am. Ceram. Soc.*, 73 [12] 3663–9 (1990)
- 9 S. J. Lee and W. M. Kriven, *J. Am. Ceram. Soc.*, 81 [10] 2605–12 (1998)
- 10 J. Banjuraizah, H. Mohamad, and Z. A. Ahmad, *Int. J. Appl. Ceram. Technol.*, 8 [3] 637–45 (2011)
- 11 W. R. Buessem, N. R. Thielke, and R. V. Sarakauskas, *Ceram. Age*, 60 [3] 8–40 (1952)
- 12 J. A. Kuszyk and R. C. Bradt, *J. Am. Ceram. Soc.*, 56 [8] 420–3 (1973)
- 13 K. Hamano, Y. Ohya, and Z. Nakagawa, *Yogyo-Kyokai-Shi*, 91 [2] 94–101 (1983)
- 14 Y. Ohya, K. Hamano, and Z. Nakagawa, *Yogyo-Kyokai-Shi*, 92 [5] 261–7 (1984)
- 15 D. F. Qian, Y. Ohya, K. Hamano, and Z. Nakagawa, *Yogyo-Kyokai-Shi*, 93 [6] 315–21

- (1985)
- 16 D. F. Qian, Y. Ohya, Z. Nakagawa, and K. Hamano, *J. Ceram. Soc. Jpn.*, 103 [10] 1022–6 (1995)
- 17 A. Shyam, E. Lara-Curzio, A. Pandey, T. R. Watkins, and K. L. More, *J. Am. Ceram. Soc.*, 95 [5] 1682–91 (2012)
- 18 T. Harada, T. Hamanaka, K. Hamaguch, and S. Asami, *Patent US*, 4, 869,944 (1989)
- 19 G. Bruno, A. M. Efremov, C. P. An, B. R. Wheaton, and D. J. Hughes, *J. Mater. Sci*, 47, 3674–89 (2012)
- 20 G. Bruno and S. Vogel, *J. Am. Ceram. Soc.*, 91 [8] 2646–52 (2008)
- 21 H. Ikawa, T. Watanabe, K. Urabe, and S. Udagawa, *Yogyo-Kyokai-Shi*, 93 [12] 762–7 (1985)
- 22 N. Chawla, X. Deng, and D. R. M. Schnell, *Mater. Sci. Eng. A*, 426 314–22 (2006)
- 23 H. Choe, T. Hsieh, and J. Wolfenstine, *Mater. Sci. Eng. A*, 237 250–5, (1997)
- 24 J. Milhans, S. Ahzi, H. Garmestani, M. A. Khaleel, X. Sun, and B. J. Koepfel, *Mater. Des.*, 30 1667–73(2009)
- 25 A. M. Efremov, *Philos. Mag. A*, 86 [36] 5431–40 (2006)
- 26 G. Bruno, A. M. Efremov, B. R. Wheaton, and J. E. Webb, *Acta Mater.*, 58 6649–55 (2010)
- 27 G. Bruno, A. M. Efremov, B. Clausen, A. M. Balagurov, V. N. Simkin, B. R. Wheaton, J. E. Webb, and D. W. Brown, *Acta Mater.*, 58 1994–2003 (2010)
- 28 P. S. Turner, *J. Res. NBS*, 37 239–50 (1946)
- 29 P. W. Mirwald, *Phys. Chem. Miner.*, 7 268–70 (1981)
- 30 M. Hochella, G. Brown, F. Ross, and G. Gibbs, *Am. Mineral.*, 64 337–51 (1979)
- 31 D. L. Evans, G. R. Fischer, J. E. Geiger, and F.W.Martin, *J. Am. Ceram. Soc.*, 63, 629–34 (1980)
- 32 M. E. Milberg and H. D. Blair, *J. Am. Ceram. Soc.*, 60 372–3 (1977)
- 33 J. D. Lee and J. L. Pentecost, *J. Am. Ceram. Soc.*, 59 183–5 (1976)
- 34 J. J. Cleveland and R. C. Bradt, *J. Am. Ceram. Soc.*, 61 [11–12] 478–81 (1978)

Chapter 4

Effect of Particle Size of Tabular Talc Powders on Crystal Orientation and Sintering of Cordierite Ceramics

4-1 Introduction

Cordierite ($2\text{Al}_2\text{O}_3 \cdot 2\text{MgO} \cdot 5\text{SiO}_2$) is in the hexagonal crystal structure and has large anisotropic coefficients of thermal expansions (CTEs) of $2.5 \times 10^{-6} \text{ K}^{-1}$ and $-0.9 \times 10^{-6} \text{ K}^{-1}$ along the a and b axes, and c axis, respectively. Sintered cordierite ceramics have low CTE of approximately $1.7 \times 10^{-6} \text{ K}^{-1}$ in the range from room temperature to $900 \text{ }^\circ\text{C}$. Hence, they have superior thermal shock resistance. It has been considered to be difficult to produce dense cordierite ceramics from natural raw materials such as kaolin ($\text{Al}_2\text{O}_3 \cdot 2\text{SiO}_2 \cdot 2\text{H}_2\text{O}$) and talc ($3\text{MgO} \cdot 4\text{SiO}_2 \cdot \text{H}_2\text{O}$), since they incongruently melt near the sintering temperature. For these reasons, porous cordierite ceramics have been prepared by extruding the powder mixtures composed mainly of kaolin and talc, and have been utilized for a honeycomb structured catalyst carrier in car exhaust systems and a diesel particulate filter (DPF). It is well known that the porous cordierite prepared from kaolin and talc exhibits extremely low CTE less than $1.0 \times 10^{-6} \text{ K}^{-1}$ along the direction parallel to extruding direction since the c-axis of cordierite crystal having negative CTE aligns parallel to the extruding direction during a sintering reaction and thermal reaction^{1,2}. When cordierite ceramics are prepared from mixtures of kaolinite, talc and alumina, preferable orientation of cordierite crystals occurs, because tabular kaolinite particles preferably orient in the green bodies and the resultant fired body has inherited property from the green body³. Many researchers^{4,5} also reported that structure of tabular kaolinite mainly contribute to the preferable orientation of cordierite crystals. Moreover, several researchers⁶⁻⁹ reported that talc powders react with Al_2O_3 component in the other raw materials to form eutectic melt during thermal reaction, and as a result, tabular frame work of talc particle was destructed during firing. From these reports, exclusively the crystalline structure or the anisotropic tabular shape of tabular kaolinite particles has long been believed to affect the crystal orientation of cordierite.

On the other hand, talc powders also have tabular particle shape and layered structure similar to kaolinite. In this study, cordierite ceramics were prepared from several types of kaolin powders and tabular talc powders having various particle size distributions with nanometer-sized alumina sol. Crystal orientation of talc particles and crystal orientation of resultant cordierite were evaluated using the X-ray diffraction measured on the surface of calcined and sintered compact, respectively. From the relation between two evaluated crystal orientations, effect of crystal orientation of talc powders on the preferable orientation of cordierite crystals was clarified. Using the optimum combination of kaolin and talc powders, we could prepare the dense cordierite ceramics having as high crystal orientation as a cordierite honeycomb structured catalyst carrier.

4-2 Experimental procedure

4-2-1 Materials

Seven types of kaolin powders designated as BR, J, UK, GB, KG, NK and NZ, and talc powder (KCM Corp, Haicheng, China) were individually wet-milled with alumina balls ($\phi = 20\text{mm}$) in water, and then classified via elutriation into prescribed median particle sizes. Table 1 shows the crystalline phase, median particle size, and the chemical composition of 7 types of kaolin powders. Each kaolin powders have only a small amount of alkali and alkali earth metal oxide. Their median particle size determined by a laser diffractometry is also shown in Table 4-1. Five types of talc powders having median particle size between $1.8\ \mu\text{m}$ and $16.1\ \mu\text{m}$ were obtained via elutriation as shown in Table 4-2.

Table4-1 Crystalline phase, median particle size and chemical component of seven types of kaolin powders

	BR	J	UK	GB	KG	NK	NZ
Crystalline phase	Kaolinite	Kaolinite	Kaolinite	Kaolinite	Dickite	Dickite	Halloysite
Median size / μm	0.5	2.7	0.5	1.5	5.7	5.6	0.4
SiO₂	45.54	44.9	47.19	46.46	46.99	45.67	45.66
Al₂O₃	39.54	38.6	37.66	38.39	37.71	39.82	38.86
Fe₂O₃	0.18	0.57	0.47	0.52	0.49	0.04	0.18
TiO₂	<0.01	1.6	0.02	0.01	0.24	0.2	0.08
CaO	0.01	0.11	0.03	0.01	0.01	0.13	<0.01
MgO	0.03	0.11	0.27	0.23	0.07	0.05	0.02
K₂O	0.1	0.07	0.47	0.01	0.15	0.03	<0.01
Na₂O	0.01	0.01	0.02	0.01	0.05	0.1	<0.01
P₂O₅	0.03	-	0.11	-	-	-	0.07
Ig.Loss	14.55	13.7	13.52	14.33	13.73	13.96	15.1
Total	99.99	99.67	99.76	99.97	99.44	100	99.97

Table4-2 Median particle size and chemical component of elutriated talc powders

Sample name	T2	T3	T5	T9	T16
Median size / μm	1.8	2.7	5.2	9.2	16.1
SiO ₂	62.45	62.45	62.81	62.91	62.54
Al ₂ O ₃	0.27	0.18	0.17	0.13	0.02
Fe ₂ O ₃	0.06	0.06	0.06	0.06	0.05
TiO ₂	<0.01	<0.01	<0.01	<0.01	<0.01
CaO	0.03	0.08	0.05	0.05	0.33
MgO	29.49	30.79	30.94	31.29	31.91
K ₂ O	<0.01	<0.01	<0.01	<0.01	<0.01
Na ₂ O	<0.01	0.01	0.01	<0.01	0.02
P ₂ O ₅	<0.01	<0.01	<0.01	<0.01	0.05
Ig.Loss	7.42	6.32	5.86	5.47	5.04
Total	99.72	99.89	99.9	99.91	99.96

4-2-2 Preparation

Each kaolin powders, talc powders having various particle size distributions and nanometer-sized alumina sol (Nissan Chemical Industries Co. Ltd.) were ultrasonically dispersed in the stoichiometric composition of cordierite ($2\text{MgO} \cdot 2\text{Al}_2\text{O}_3 \cdot 5\text{SiO}_2$), and then the mixtures were stirred and dried under an infrared lamp. Forty mass % of kaolin powders necessary for preparation of the mixtures were replaced with calcined NZ kaolin at 700 °C in order to suppress a crack occurrence in the sintered body during heating. The powder mixtures were uniaxially pressed into a 25 mm-diameter die at the pressure of 98.0 MPa followed by a cold isostatic pressing at the pressure of 196 MPa. The resultant green compacts were heated to 1000 °C in an electric furnace at the rate of 5 °C/min and then heated at the rate of 2.5 °C/min from 1000 °C to 1350 °C. The furnace was maintained at 1350 °C for one hour and then it was left to cool.

4-2-3 Characterization

Particle size distributions of kaolin powder and talc powder were measured with laser diffraction particle sizer (SALD-2200, Shimazu Corp., Japan). Morphology of various talc powders were individually observed by scanning electron microscope (JSM-6335FM, JEOL Corp., Japan) at an acceleration voltage of 2.0 kV. The X-ray diffraction (XRD) measurement was carried out with RINT2500 (Rigaku Corp., Japan) utilizing CuK α X-ray and a graphite monochromator. Crystal orientations of talc particle and resultant cordierite were individually semi-quantified with XRD

profile measured on the surface of calcined and sintered compacts, and represented as the orientation indices I_T and I_C . In this study, the orientation index of talc I_T was defined by the next equation.

$$I_T = \frac{I_{004}}{I_{004} + I_{020}} \times 100$$

where I_{004} and I_{020} are the XRD intensity of 004 and 020 planes, respectively, based on the diffraction data (JCPDS 19-0770). Increasing in the I_T indicates that the c-axis of talc particle is oriented vertical to the uniaxially pressed surface of compacts. Pressed compacts were calcined at 700 °C to decompose the crystalline structure of kaolinite before XRD measurement, since the diffraction peaks 004 and 020 of talc overlap with those of kaolin. The orientation index of cordierite I_C was calculated by next equation as shown by Lachman et al¹.

$$I_C = \frac{I_{110}}{I_{110} + I_{002}} \times 100$$

where I_{110} and I_{002} are the XRD intensities of 110 and 002 planes respectively, based on hexagonal crystal structure (JCPDS 13-0249). Increasing in the I_C indicates that the c-axis of cordierite crystal is oriented parallel to the pressed surface of the sintered specimens. The relative density of the sintered specimens were calculated from the ratio of the bulk density determined by Archimedes' immersion method to the density of 2.507g/cm³ calculated from lattice parameters of hexagonal cordierite. The coefficient of thermal expansion (CTE) anisotropy of the sintered cordierite compacts were measured with thermo dilatometer (TMA8310, Rigaku Corp., Japan) at a heating and cooling rate of 10 °C/min between room temperature and 900 °C.

4-3 Results and Discussions

4-3-1 Crystal orientation of talc powders

Figure 4-1 shows the SEM images of various talc powders. When ball-milled talc powder has the smallest median particle size of 1.8µm (T2), its tabular shape was almost broken down. Above 2.7 µm in a median particle size (T3~T16), talc powders exhibited anisotropic tabular shape. Their anisotropic tabular shape was clearly observed for talc powders having a large median particle size.

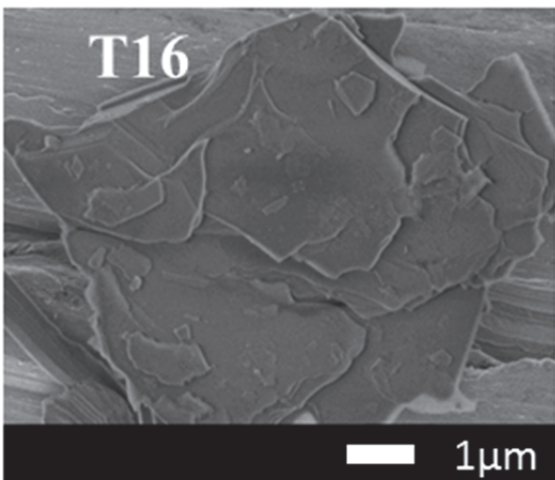
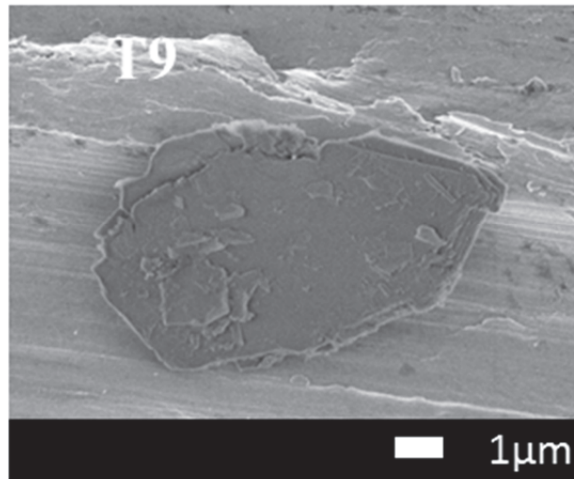
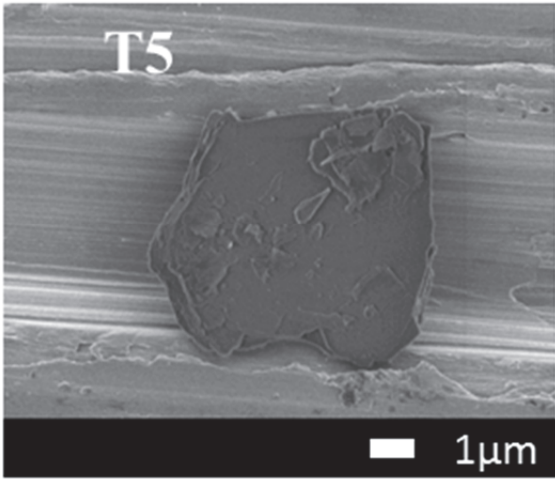
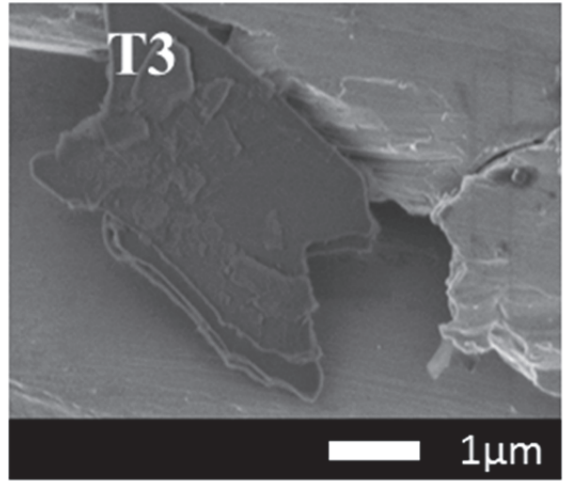
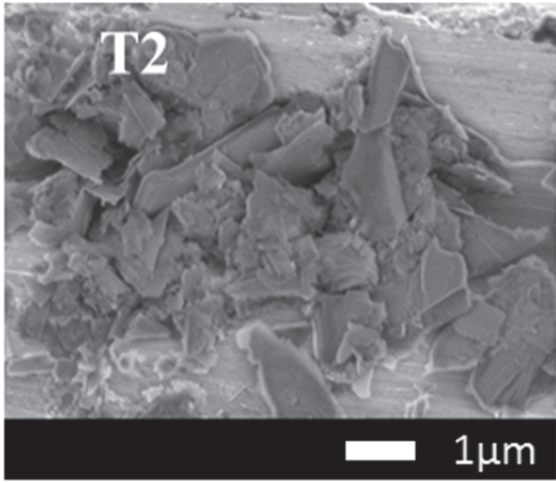


Fig.4-1 SEM images of five types of talc powders

According to the works by Hampel et al.¹⁰ and Chen et al.¹¹, compacts mainly composed of kaolinite powders anisotropically shrank during the firing process, since kaolinite powders having layered crystal structure aligned well in compacts by pressing. Talc also has a layered crystal structure similar to kaolinite: The crystal structure of talc is constructed by a unit layer, consisting of two SiO₄ - tetrahedral layer and one MgO₄(OH)₂ - octahedral layer stacked as sandwich, and these unit layers are combined with each other along the a-b plane by weak Van der Waals force. Additionally, Mg²⁺, Si⁴⁺ and O²⁻ are bonded by ionic force in the directions of *a*- and *b*- axes of talc crystal. Therefore, talc powders have an anisotropic tabular shape also similar to kaolinite, as shown in Fig.4-1. For these reasons, an anisotropic shape of talc powder was thought to be very influential in the sintering anisotropy of compacts. Figure 4-2 shows the effect of particle size of talc powders on the shrinkage anisotropy of the compacts sintered at 1350 °C. The shrinkage anisotropy was defined as the ratio of the vertical shrinkage to horizontal one in this study. In case for using all types of kaolin powders, the shrinkage anisotropy increased with an increase in the median particle size of talc powders. Especially, increase in the shrinkage anisotropy was almost proportional to the median particle size of talc powders up to 2.7 μm. Probably, shrinkage anisotropy depended on the degree of shape anisotropy of tabular talc. Above 2.7 μm in median particle size of talc powders, on the other hand, kaolin also affected the shrinkage anisotropy, since the shrinkage anisotropy increase with a decrease in mean particle size of kaolin powders.

In order to estimate the effect of packing orientation of talc powders, crystal orientation index of talc particle I_T was plotted as a function of the median particle size of talc powders. M. J. Murtagh¹² reported the method estimating quantitatively the degree of anisotropic tabular shape of talc particle from the orientation property of talc particle quantified with the aid of XRD profile measured on glass slides coated with slurry of talc powders. R. R. Wusirika¹³ adopted Murtagh's method¹² utilizing a sample holder packed with talc powders to evaluate a morphological property of talc powder for cordierite ceramics and prepared the cordierite ceramics having extremely low CTE from the mixtures using talc powders having an optimum morphological property (orientation property). In this study, on the other hand, the crystal orientation index I_T was directly measured on the pressed surface of the compact of the mixture. Figure 4-3 shows the orientation index of talc I_T as a function of particle size of talc powders. The I_T rapidly increased with an increase in median particle size of talc powders 1.8 μm to 2.7 μm. Above 2.7 μm, the I_T increased gradually with a further increase in the median particle size independently on the type of kaolin powders. This suggested the difference of the shrinkage anisotropy with a particle size of kaolin powders in Fig.4-2 to be the effect of packing anisotropy of kaolin powders. Talc particles above 2.7 μm exhibited a large anisotropic tabular shape as shown in Fig.4-1, so that c-axes of these particles aligned well in vertical to the pressed surface of compacts in proportional in the particle size.

Figure 4-4 shows the relationship between the shrinkage anisotropy of the sintered compacts and the orientation index of talc I_T . The good linear correlation was obtained between the shrinkage anisotropy of the sintered compacts and the orientation index I_T . The difference in the slope of the

straight line was thought to be an effect of the particle size and morphology of kaolin powders.

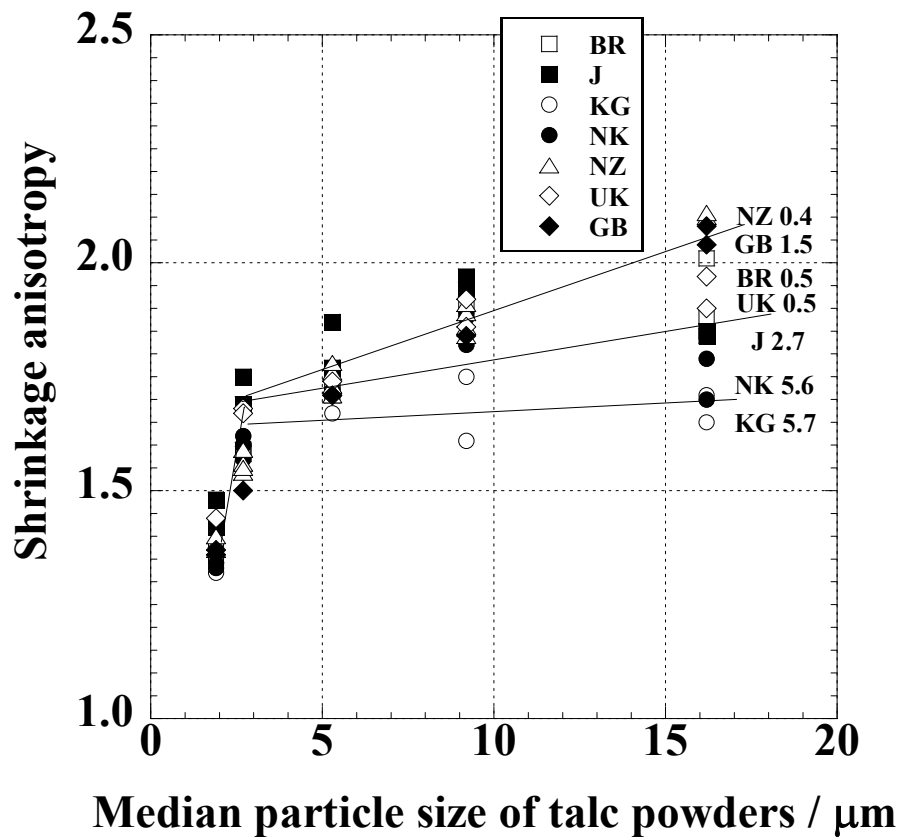


Fig.4-2 Relationship between shrinkage anisotropy and median particle size of talc powders

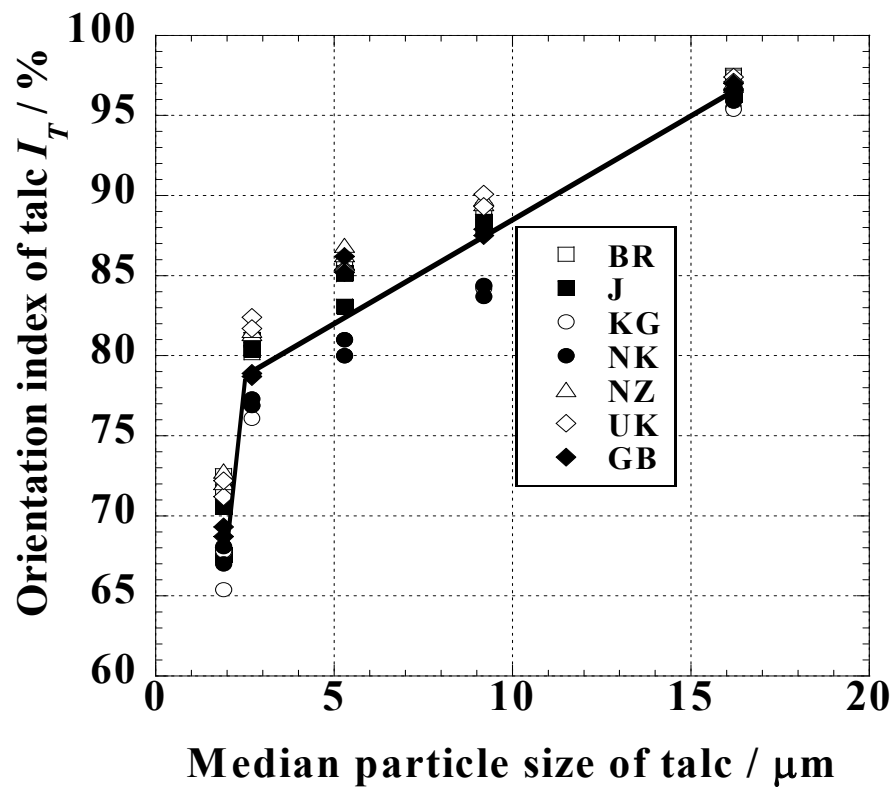


Fig.4-3 Effect of median particle size of talc powders on orientation index of talc

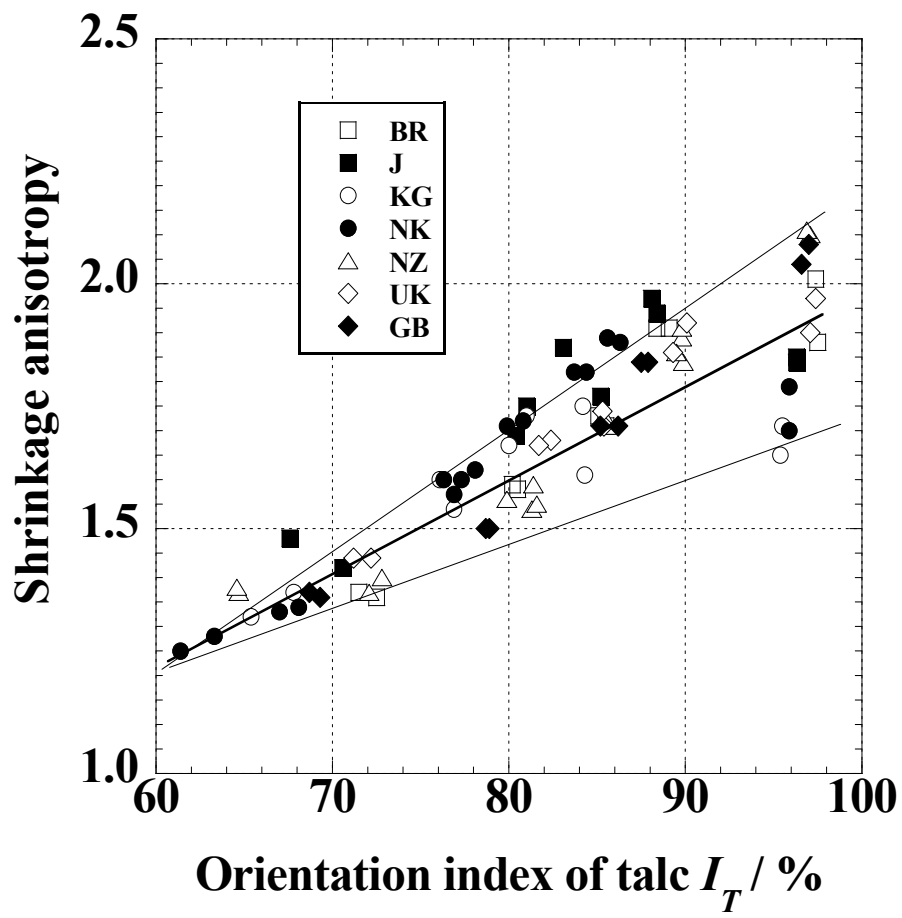


Fig.4-4 Relationship between shrinkage anisotropy and crystal orientation index of talc I_T of sintered specimens

4-3-2 Effect of the particle orientation of talc powders on crystal orientation of cordierite

Figure 4-5 indicates the orientation index of cordierite I_C as a function of the orientation index of talc I_T . The I_C increased with an increase in I_T , and varied depending on the type of kaolin powders for the mixtures. In case for using the kaolin powders J, KG, NK and NZ together with talc powders showing high orientation index I_T about 95%, high crystal orientation indexes I_C about 90% were attained. From these results, crystal orientation of talc powders also contributed to crystal orientation of cordierite, and the c-axis of cordierite crystals was found to align well in vertical to the c-axis of talc particle using talc powders above $2.7\mu\text{m}$. When cordierite ceramics was prepared from the mixtures containing GB kaolin, the I_C showed the lowest value in this experiment, and the reason could not be clarified.

In order to eliminate the effect of crystal orientation of kaolin particles on crystal orientation of cordierite, only calcined NZ kaolin powders was used as a kaolin material for starting mixture and orientation index of talc powder I_T was evaluated using large talc powder having median particle size of $16.1\mu\text{m}$. Figure 4-6 shows XRD patterns measured on the pressed surface of as-pressed compacts with that of talc powder dispersing in resin. Only diffraction peaks of talc were observed on the pressed surface of the as-pressed compact, because crystalline structure of NZ kaolin powder completely decomposed. XRD pattern of talc observed on the surface of as-pressed compact was different from that of talc powder dispersing in resin. The diffraction peak 004 vertical to c-axis of talc was clearly observed on the pressed surface, while the diffraction peak 020 parallel to c-axis of talc was hardly observed. In this case, the orientation index I_T showed 95.6%, corresponding to the samples using talc powders $16.1\mu\text{m}$ as shown in Fig.4-3. XRD patterns of this compact sintered at $1350\text{ }^\circ\text{C}$ is shown in Figure 4-7 along with a pattern of cordierite powder. On the pressed surface of the compacts, high orientation index of cordierite I_C of 89.2 % was obtained and was in good agreement with specimens using J, KG, NK and NZ with the talc powder as shown in Fig.4-5. This result clearly indicates that the preferable crystal orientation of tabular talc particles lead to the preferable orientation of cordierite crystals.

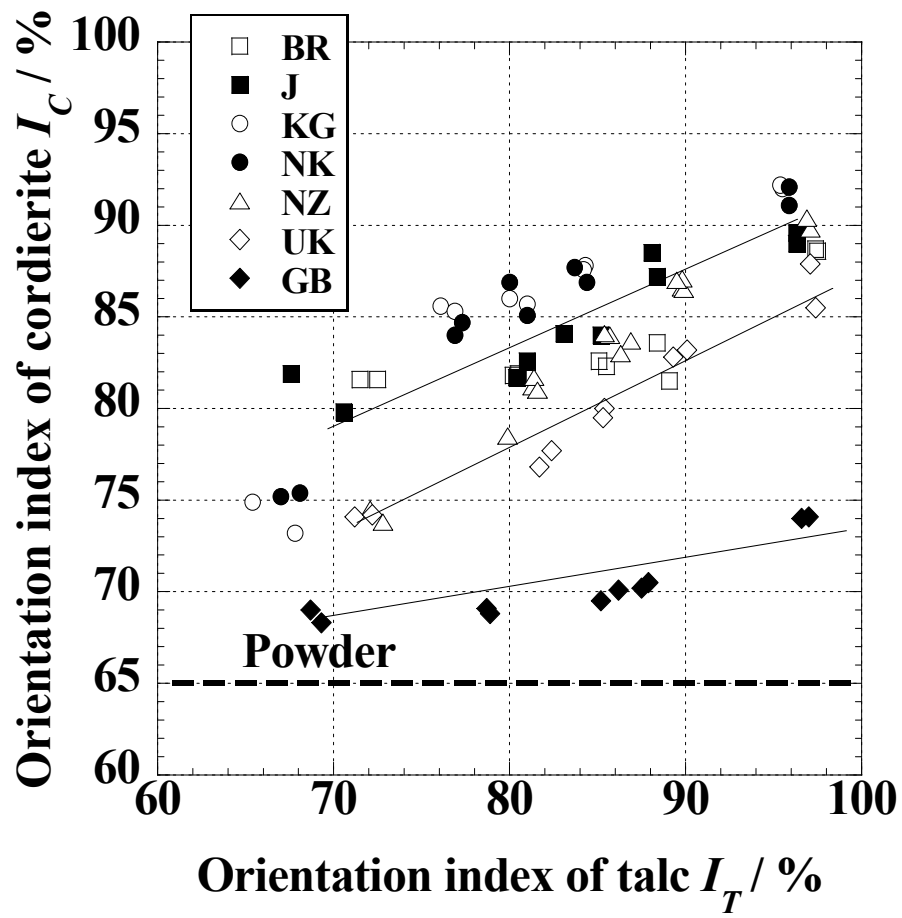


Fig.4-5 Relationship between orientation index I_T of talc powders and orientation index I_C of cordierite crystals

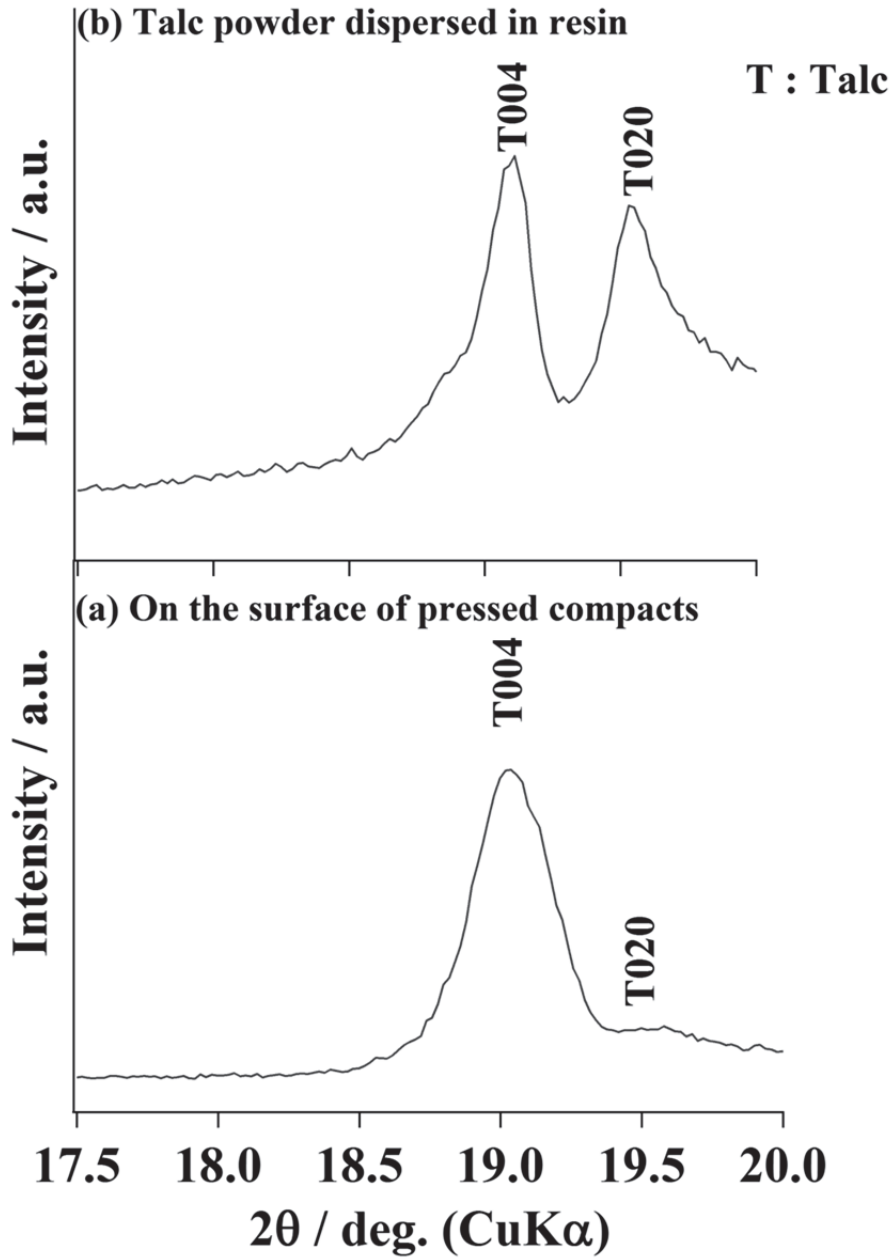


Fig.4-6 XRD patterns of the pressed surface of as-pressed compact from calcined kaolin powder and coarse talc powder (a) and talc powder dispersed in resin (b)

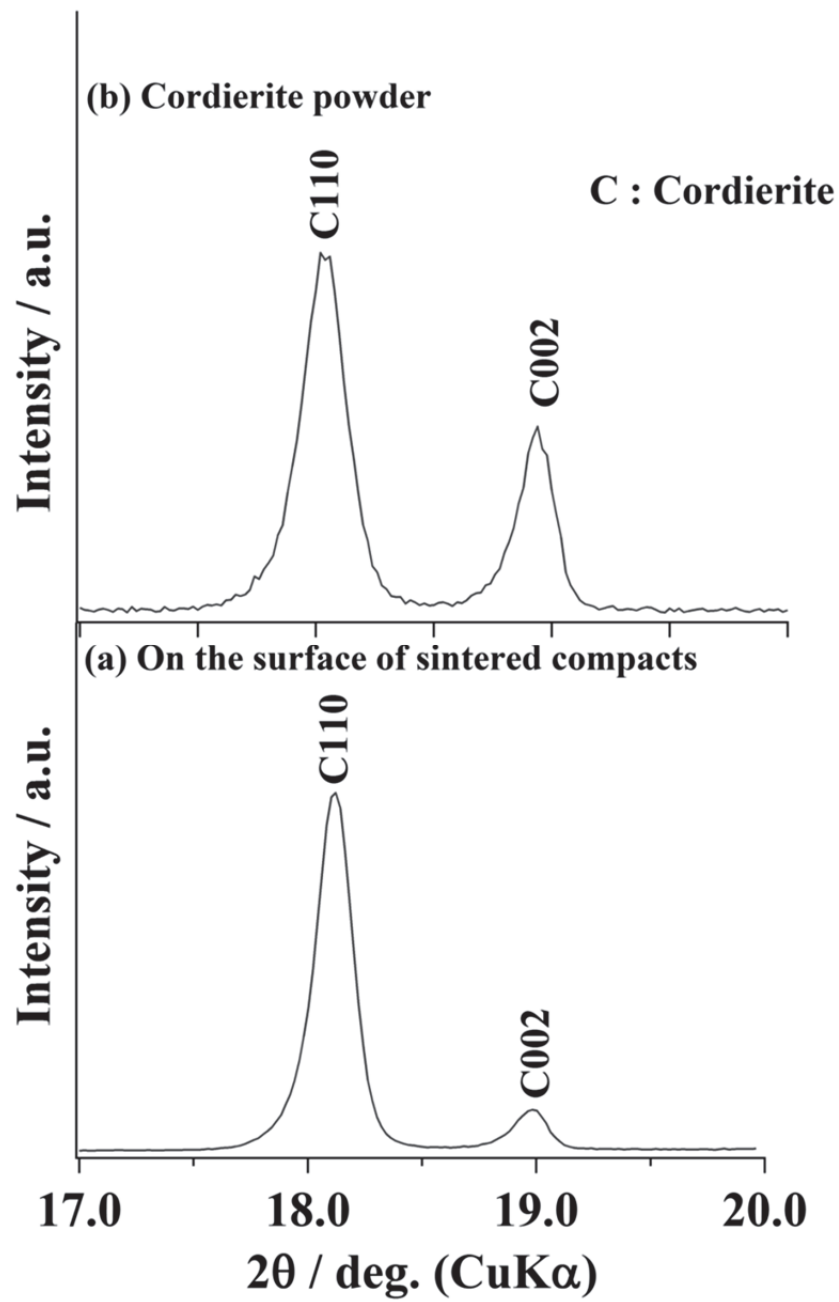


Fig.4-7 XRD patterns of the pressed surface of sintered cordierite compact (a) and cordierite powder (b)

4-3-3 Effect of particle size of talc powders on densification of cordierite ceramics

As well known, sinterabilities of ceramic powder compacts depend on particle size of starting powders. In this section, the effect of particle size of talc powders on the densification of cordierite ceramics were examined by combinations of many kaolin powders and talc powders. Figure 4-8 shows the relative density of the compacts sintered at 1350 °C prepared from several types of kaolin powders and talc powders having various particle size distributions with alumina sol. Relative densities of the sintered compacts decreased with an increase in a median particle size of talc powders. When talc powders below 10 μm were used for the mixtures, the relative density of the sintered compacts depended largely on particle size of kaolin powders. The larger kaolin powders for the mixtures became the lower relative density of the sintered compacts. Higher relative density than 95% was accomplished using fine kaolin powders and fine talc powders for the mixtures.

Figure 4-9 shows the relationship between the relative density and the orientation index of cordierite I_C of the sintered compacts. The dense cordierite ceramics having a higher relative density than 95 % with higher crystal orientation index I_C than 85 % were prepared, when talc powder in the median particle size between 3 and 5μm and UK or KG kaolin (both are dickite) were used for the mixtures.

4-3-4 Anisotropic CTE of sintered cordierite ceramics

When the anisotropic crystal grains were preferably orientated in polycrystalline body, it should have different CTEs in the vertical direction and the parallel direction. Figure 4-10 shows the relationship between the orientation index of cordierite I_C and CTE difference between the directions vertical and parallel to uniaxially pressed surface of specimens heat-treated at 1350 °C. The increase in the I_C means that the c-axis of cordierite crystal having negative CTE aligned more favorably in parallel to the pressed surface. Therefore, the CTE difference increased proportionally with an increase in the I_C . When cordierite grains distribute randomly in a polycrystalline ceramics, CTE should be equal in all directions and CTE difference is zero. When cordierite grains of c-axis perfectly aligned in one plane, CTE in this plane is an average value of α_a and α_c . From the thermal expansion measurement of lattice parameter of cordierite crystal by authors¹⁴, $0.88 \times 10^{-6} \text{K}^{-1}$ could be obtained. On the other hand, CTE in vertical direction corresponds to that of a-axis $3.36 \times 10^{-6} \text{K}^{-1}$. In this case, the maximum difference in CTE was calculated to be $2.4 \times 10^{-6} \text{K}^{-1}$ and was too large to explain the experimental results in Fig.4-10.

We already reported that a thermal expansion coefficient of cordierite was lowered by the occurrence of microcracks between domains larger than 40μm induced by the thermal expansion anisotropy of cordierite crystal axes. In this study, an average thermal expansion coefficient in two directions of many specimens heat-treated at 1350°C was lower than $1.7 \times 10^{-6} / ^\circ\text{C}$ corresponding to the average value of the crystal axes, so that the absolute difference of thermal expansion coefficient was thought to be suppressed by the occurrence of microcracks.

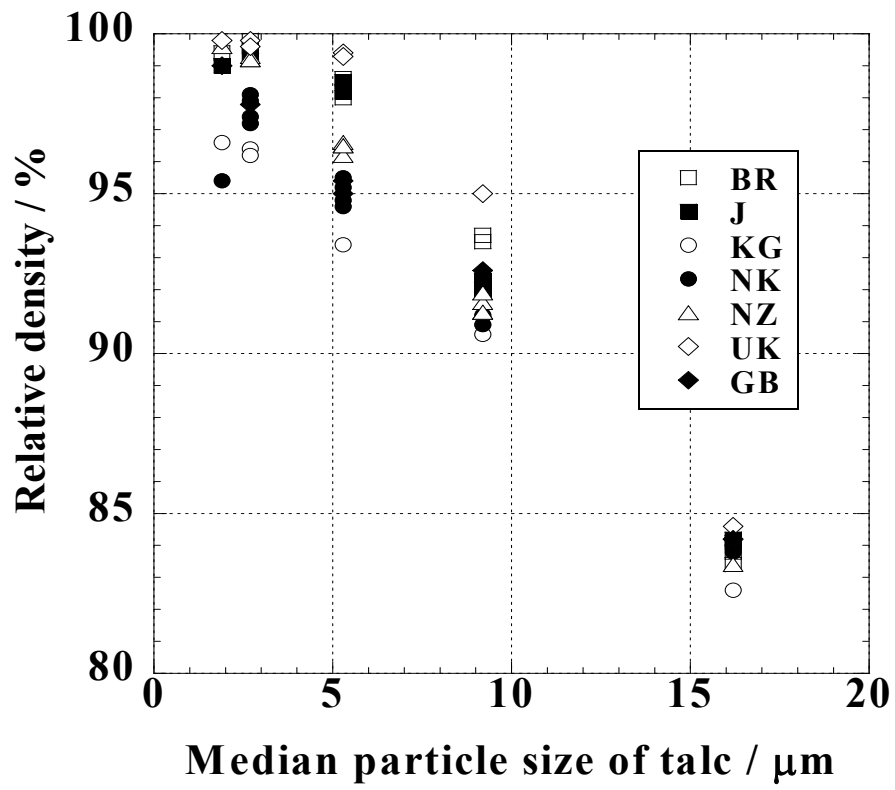


Fig.4-8 Relative density of sintered specimens

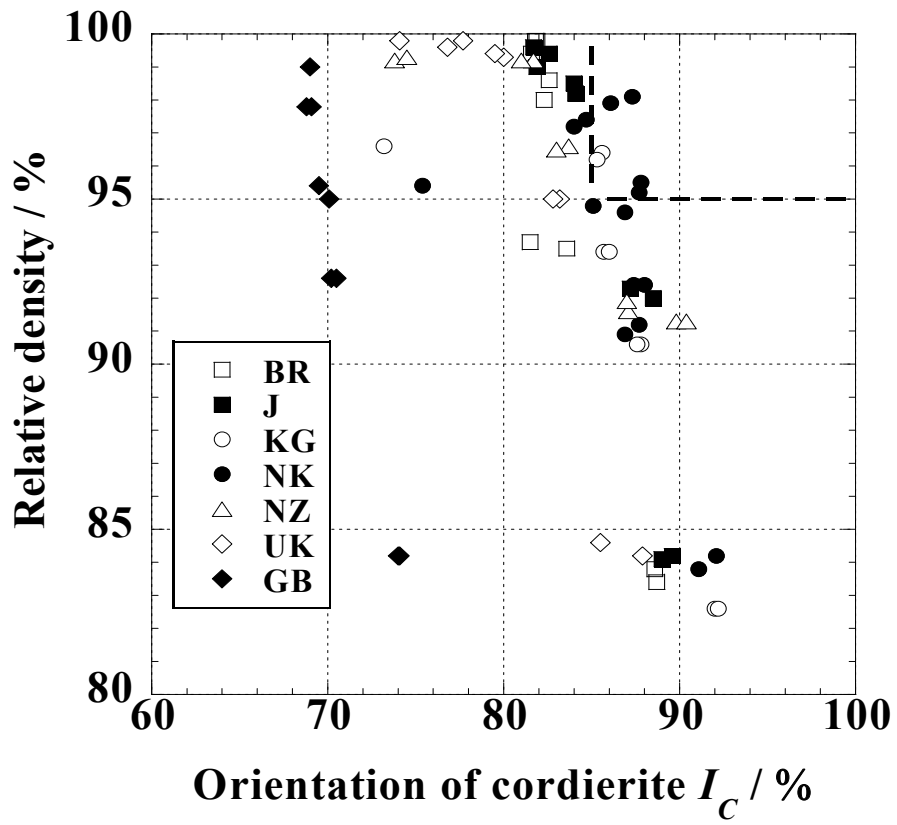


Fig.4-9 Relative density of specimens with various orientation index I_C of cordierite

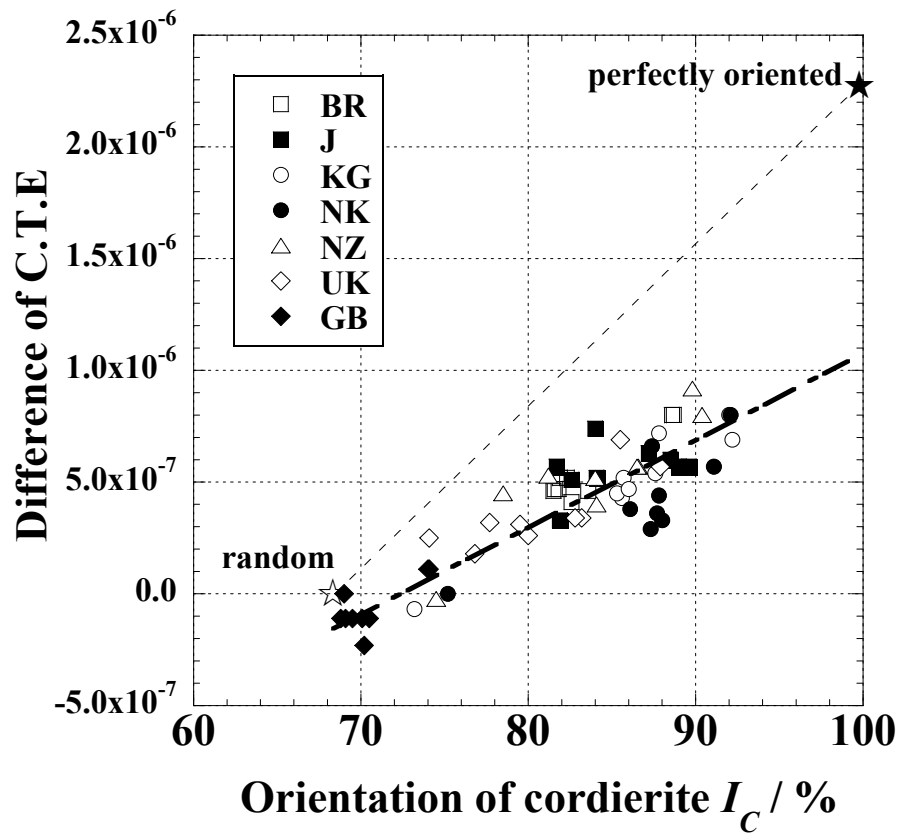


Fig.4-10 Relationship between orientation index of cordierite I_C and CTE difference

4-4 Conclusions

In this study, preferable crystal orientation and sintering characteristics of cordierite ceramics were investigated using several types of kaolin powders and talc powders with various median particle size with alumina sol, and the following conclusions were obtained:

- 1 The c-axis of talc powders in median grain size of above 3 μm was preferably oriented vertical to the pressed surface of the green compact during uniaxially pressing, since the talc powders having median particle size above 3 μm showed a large anisotropic tabular shape.
- 2 The crystal orientation of cordierite increased proportionally with an increase in the crystal orientation of talc powders. Moreover, high crystal orientation was also attained in the case of cordierite ceramics prepared using the combination of calcined kaolin and coarse talc powders. Even if isotropic calcined kaolin was used, resultant cordierite crystals preferably orientated depending on the crystal orientation of talc powders.
- 3 By the combination of fine kaolin powders about 5 μm and talc powders with median particle size between 3 and 5 μm , dense cordierite ceramics having a higher relative density than 95 % were attained with high crystal orientation index I_C of about 85 %, corresponding to the orientation property of a honeycomb structured catalyst carrier of porous cordierite.

References

- 1 I. M. Lachman, *Patent US 3,885,977* (1975)
- 2 I. M. Lachman, R. D. Bagley and R. M. Lewis, *Ceramic Bulletin* Vol. 16, No12 (1981)
- 3 W. O. Williamson, *Proc. Brit. Ceram. Soc.*, No.20 117–32 (1972)
- 4 S.Udagawa and H. Ikawa, *Ceramics* 14 No.11 (1979)
- 5 K. Umehara, *Ceramics* 33 No.7 (1998)
- 6 I. M. Lachman, *Advances in Ceramics*, Vol. 9, Forming of Ceramics, p201–11(1984)
- 7 M. Nakahara, Y. Hashizuka, Y. Kondo and K. Hamano, *J. Ceram. Soc. Jpn*, 102 [1] 18–22 (1994)
- 8 M. Nakahara, Y. Kondo and K. Hamano, *J. Ceram. Soc. Jpn.*, 103 [10] 1051–6 (1995)
- 9 Michael Scheffler and Paolo Colombo, WILEY-VCH, p67–8 (2005)
- 10 B. F. Hampel and I. Cutler, *J. Ame. Ceram. Soc.*, 36 [1] 30–4 (1953)
- 11 C.Y. Chen, G.S. Lan and W.H. Tuan, *Ceram. Int.*, 26 715–20(2006)
- 12 M. J. Murtagh, *Patent US 5,141,686* (1992)
- 13 R. R. Wusirika, *Patent US 7,473,392B2* (2009)
- 14 Y. Kobayashi, M. Katayama, M. Kato and S. Kuramochi, *J. Ame. Ceram. Soc.*, 96[6]1863–8 (2013)

Chapter 5

Crystal orientation of cordierite generated at the interface between $\text{Al}_2\text{O}_3 \cdot 2\text{SiO}_2$ and $3\text{MgO} \cdot 4\text{SiO}_2$

5-1 Introduction

Both kaolinite and talc possess a layered crystal structure with a number of silicates exhibiting large anisotropic tabular particle shapes. It is well known, that when these silicates are used as a starting mixture for the extrusion of cordierite-based ceramics,¹⁻⁵ the *c*-axis of the cordierite crystals is aligned vertically to the *c*-axis of the kaolinite crystals during heat-treatment. Lachman et al.^{1,2} reported that this preferred orientation of cordierite was attributable to the crystal structure and orientation of kaolinite similarly to mullite crystals topotactically generated from kaolinite^{6,7} (the *c*-axis of kaolinite is perpendicular to the *c*-axis of mullite). Subsequently, many researchers^{8,9} have reported that the crystal structure of kaolinite contributes to the preferred orientation of cordierite crystals. We have previously studied the effect of talc powders on the crystal orientation of cordierite, since talc and kaolinite particles have a similar crystal structure and particle shape, and reported that the crystal orientation of cordierite is mostly dependent on the crystal orientation of the talc powders.¹⁰ However, many crystalline phases such as mullite, enstatite, sapphirine, spinel, and cristobalite are transiently generated during heat-treatment of a starting mixture containing silicates.^{2,11-15} Therefore, unlike the example of mullite formation from kaolinite, it is difficult to proclaim that the preferred orientation of cordierite crystals directly correlates with the atomic arrangement of the layered silicate.

In this paper, we studied the crystal orientation of cordierite generated at the interface of $\text{Al}_2\text{O}_3 \cdot 2\text{SiO}_2$ and $3\text{MgO} \cdot 4\text{SiO}_2$ composed of isotropic oxides prepared from calcined amorphous minerals or oxide sols.

5-2 Experimental procedures

5-2-1 Materials

(A) Natural minerals

New Zealand kaolin and talc (KCM Corp, Haicheng, China) were calcined at 700 °C for 5 h, and 1000 °C for 5 h, respectively. Calcined kaolin and calcined talc (hereafter referred to as CK and CT) were individually milled with alumina balls ($\phi = 20$ mm) in water and then were separately elutriated below 1 μm in a particle size.

(B) Oxide sol mixtures

A powder having the same chemical composition as the calcined kaolin was prepared by mixing silica sol (Nissan Chemical Industries, Chiyoda-ku, Tokyo, Japan., SNOWTEX-O) and alumina sol (Nissan Chemical Industries, Chiyoda-ku, Tokyo, Japan., ALUMINASOL 520) in water under

ultrasonic irradiation and then dried in an alumina mortar under an infrared lamp (hereafter referred to as AS). A powder having the same chemical composition as calcined talc was prepared from silica sol and $Mg(OH)_2$ suspensions synthesized from a mixture of magnesium chloride solution and ammonia solution (hereafter referred to as MS) at the same mixing conditions as the AS. These powders were individually heat-treated for one hour and then milled with zirconia beads ($\phi = 3 \text{ mm}$) in ethanol.

5-2-2 Preparation

Calcined kaolin (CK), calcined talc (CT), $Al_2O_3 \cdot 2SiO_2$ powders (AS), and $3MgO \cdot 4SiO_2$ powders (MS) were individually pressed into a $50 \text{ mm} \times 40 \text{ mm} \times 5 \text{ mm}$ die at 98 MPa followed by cold isostatic pressing at 198 MPa. Suspensions of these powders, having a solid concentration of 10 mass%, were also prepared by ultrasonic dispersion in distilled water. The suspensions of CT, CK, MS, and AS were respectively coated onto the surface of CK, CT, AS, and MS compacts by dipping, as shown in Figure 5-1. The thickness of the coating layer was controlled at around 20–30 μm . The coated compacts were heated to a prescribed temperature in an electric furnace at the rate of $5 \text{ }^\circ\text{C min}^{-1}$ and maintained at that temperature for 1 h, and then, the furnace was left to cool.

CK : Calcined kaolin powder
 CT : Calcined talc powder
 AS : $Al_2O_3 \cdot 2SiO_2$ powder
 MS : $3MgO \cdot 4SiO_2$ powder

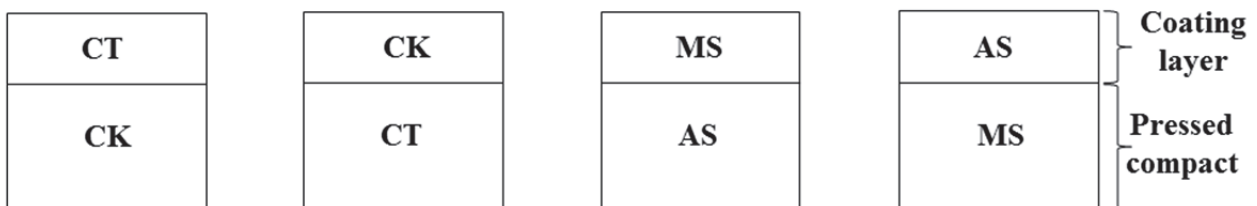


Fig.5-1 Four combinations of compacts and coating layers

5-2-3 Characterization

Scanning electron microscopy (SEM: JSM-6335FM, JEOL Corp., Akishima, Tokyo, Japan) was used for observation of the interface between the pressed compacts and coating layers at an acceleration voltage of 2.0 kV. Crystalline phases were identified by X-ray diffraction (RINT-2500, Rigaku Corp., Japan) utilizing a Cu K α X-ray source and graphite monochromator. X-ray diffraction profiles of the coated surface of specimens were measured directly. An interdiffusion of the elements across the interface between the compact and coating layer was observed with an energy dispersive X-ray analyzer (EDX, JED-2300 JEOL Corp., Akishima, Tokyo, Japan)

5-3 Results and Discussions

5-3-1 Phase composition of powders used for compacts and coating layers

Figure 5-2 shows XRD patterns of calcined kaolin (CK) and talc (CT). Kaolin powder calcined at 700 °C (CK: Fig. 5-2a) was composed of amorphous material with a broad band at around $2\theta = 22^\circ$ and a small amount of cristobalite and quartz, which were originally contained in New Zealand kaolin. On the other hand, Talc powder calcined at 1000 °C (CT: Fig. 5-2b) was composed of enstatite and amorphous silica, with a small amount of corundum resulting from wearing alumina balls during the milling process. Heat-treatment at 500 and 800 dehydrate kaolin and talc, respectively. The layered silicate structures of kaolin and talc were completely destroyed by calcination at 700 °C and 1000 °C, respectively. Figure 5-3 shows XRD patterns of oxide sol mixtures. AS calcined at 800 °C was composed of amorphous material with a small amount of fine γ -alumina decomposed from alumina sol, while MS calcined at 800 °C was composed of only amorphous material without any crystalline structure present. The observed γ -alumina is thought to be fine since a wider diffraction profile of γ -alumina was observed.

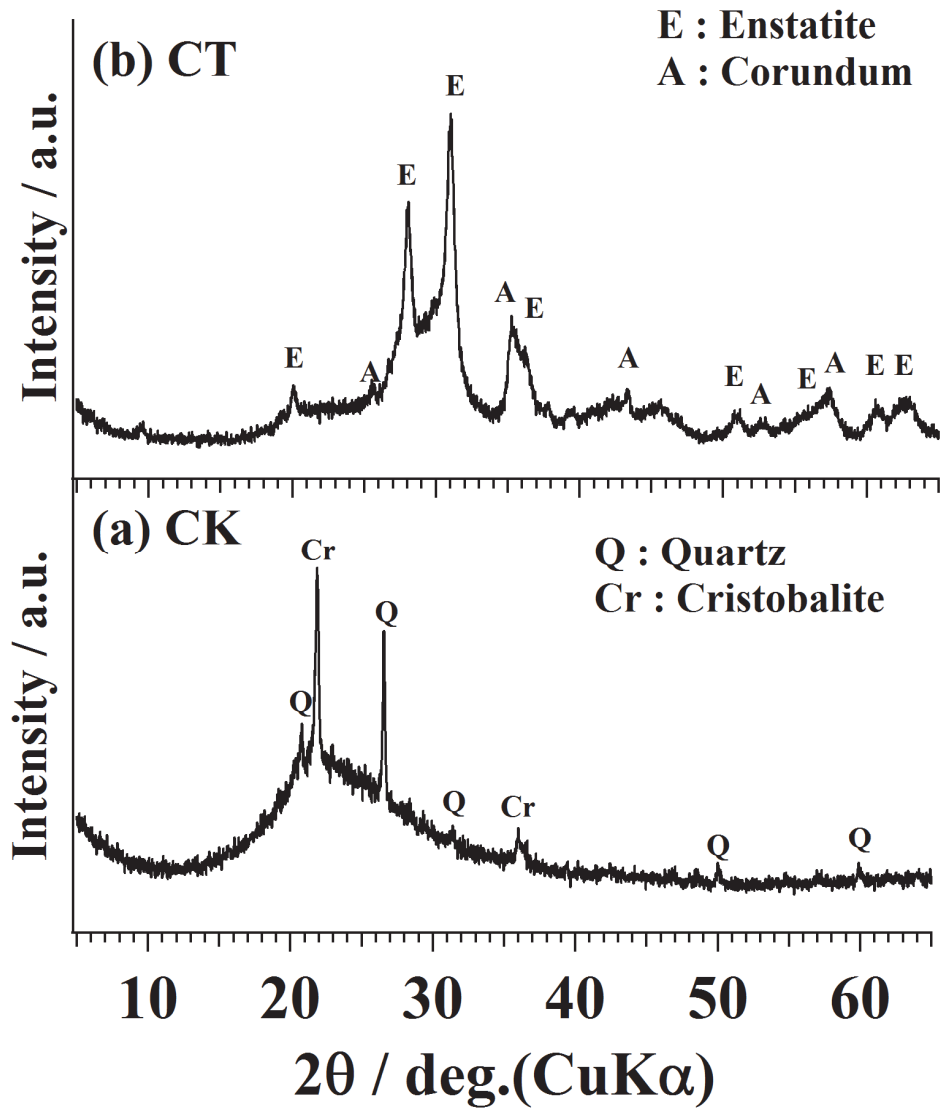


Fig.5-2 XRD patterns of (a) kaolin powders calcined at 700 °C for 5 hour and (b) talc powders calcined at 1000 °C for 5 hour, classified below 1 μm via elutriation

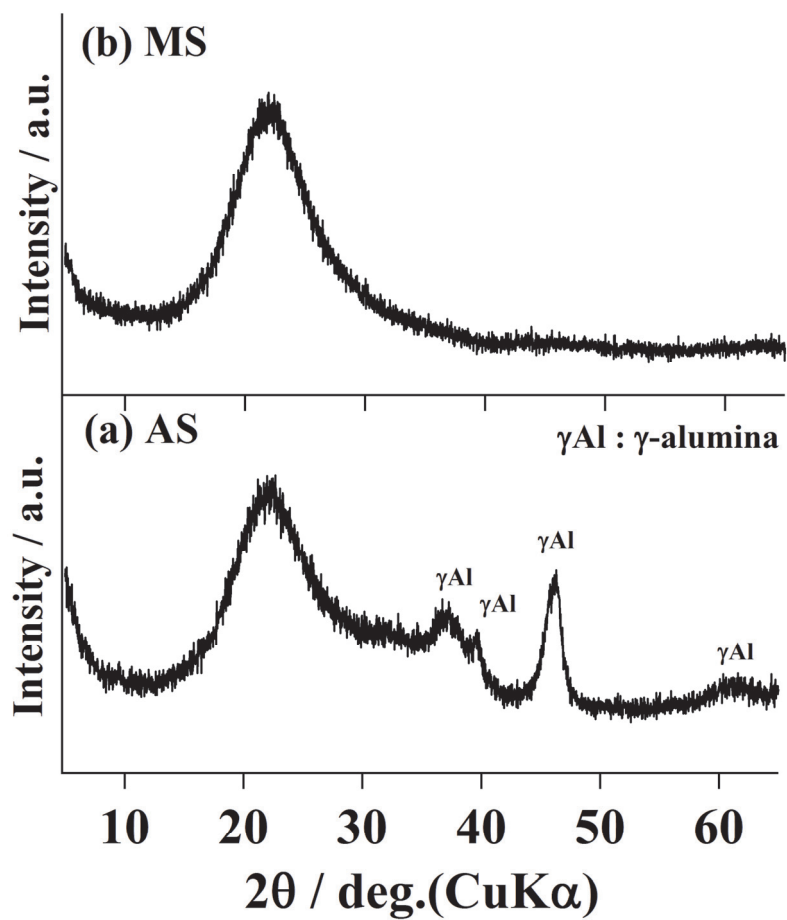
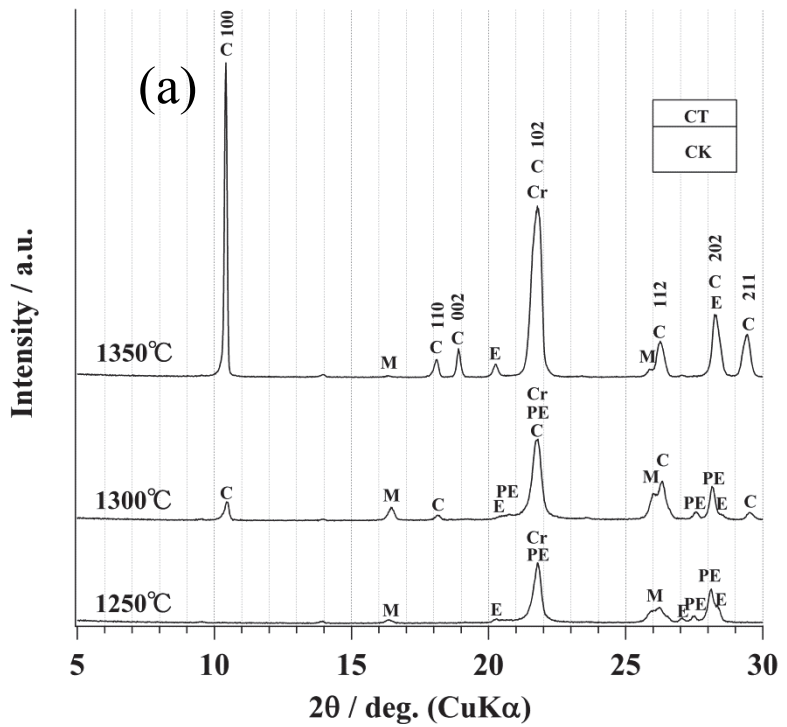
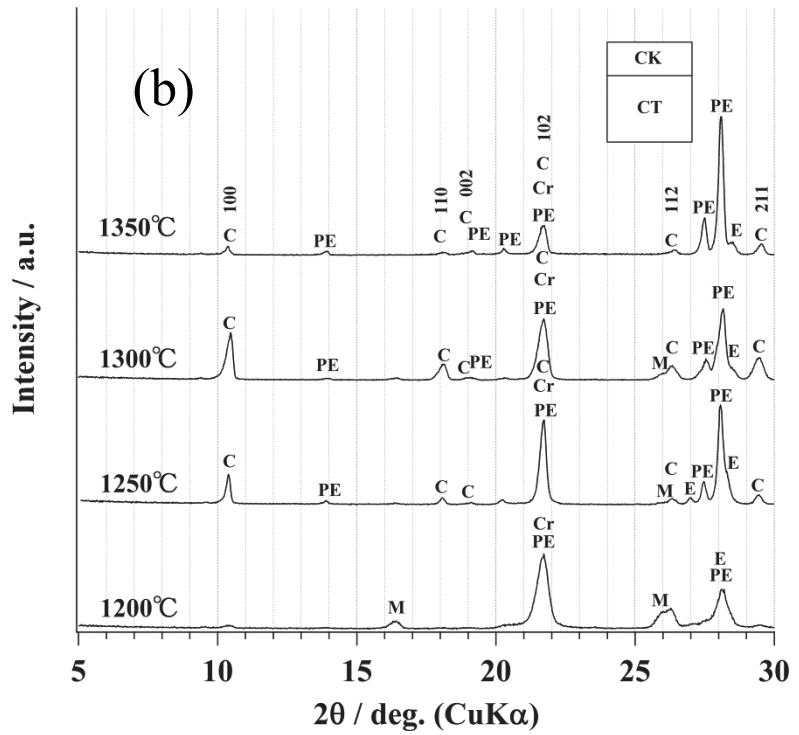


Fig.5-3 XRD patterns of (a) AS powders and (b) MS powders, prepared from oxide sol mixtures calcined at 800 °C for 5 hours

5-3-2 Phase changes of the coated surface of the compact

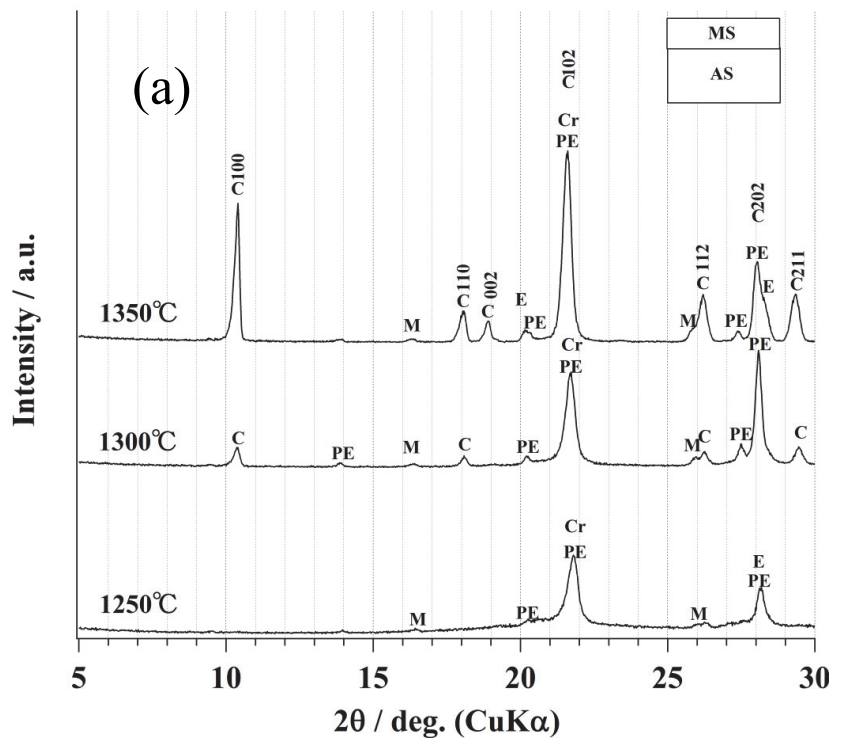
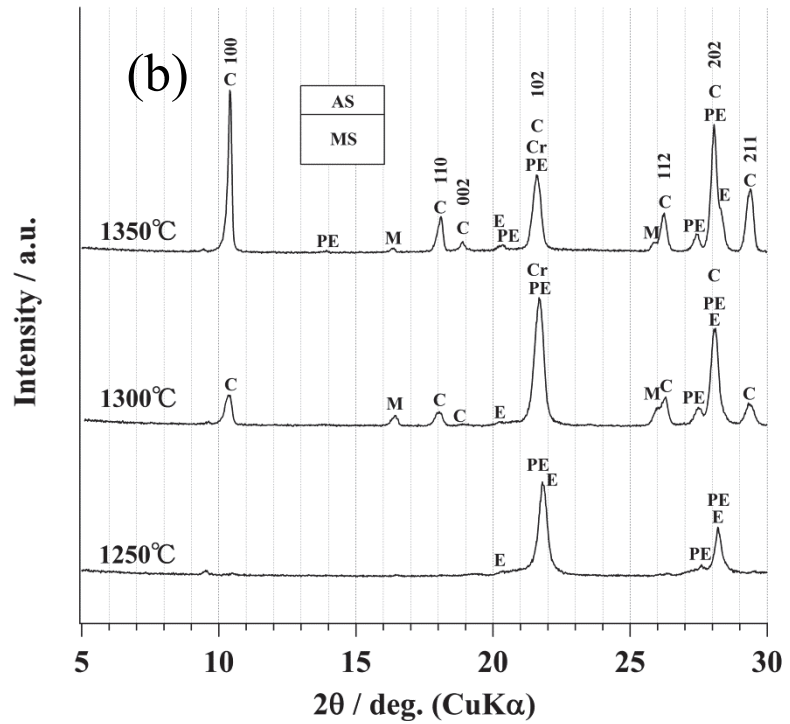
Figure 5-4 (a) shows the XRD patterns of samples prepared from the CK compact with CT coating layer heat-treated between 1250 and 1350 °C for 1 hour. At 1250 °C, mullite (M) and cristobalite (Cr) were observed as decomposed products of kaolin; enstatite (E) and protoenstatite (PE) were also observed as decomposed products of talc. No product formed by thermal reaction between CK and CT was observed. At 1300 °C, diffraction peaks of cordierite, as well as crystals decomposed from talc and kaolin, were observed due to the thermal reaction of CK and CT. Increasing the temperature further to 1350 °C significantly promoted the formation of cordierite crystals. Figure 5-4 (b) shows the XRD patterns of samples prepared from a CT compact with CK coating layer heat-treated between 1200 and 1350 °C for 1 hour. Cordierite X-ray diffraction peaks were observed at 1200 °C, and the peak height increased with increasing temperature up to 1300 °C. At 1350 °C, the diffraction peak height of cordierite suddenly decreased, while the diffraction peaks of protoenstatite increased. The coatings used in this study were thin enough to observe the thermal reaction products between the compact and coating layer.

Figure 5-5 (a) shows the X-ray diffraction patterns of samples prepared from an AS compact with MS coating layer heat-treated between 1250 and 1350 °C for 1 hour. Mullite, enstatite, protoenstatite, and cristobalite were observed at 1250 °C as decomposed products of AS and MS, and X-ray diffraction peaks of cordierite appeared at 1300 °C, increasing in height up to 1350 °C. These observations were similar to the results for specimens prepared from natural raw materials, as shown in Fig. 5-4 (a). Figure 5-5 (b) shows the X-ray diffraction patterns of samples prepared from an MS compact with AS coating layer heat-treated between 1250 and 1350 °C for 1 hour. Phase changes with increasing temperature were very similar to the results shown in Fig. 5-5 (a).



C : Cordierite PE : Protoenstatite E : Enstatite
M : Mullite Cr : Cristobalite

Fig.5-4 shows XRD patterns of the surface of sample combining natural material powders: (a) CK compacts coated with CT, (b) CT compacts coated with CK



C : Cordierite PE : Protoenstatite E : Enstatite
M : Mullite Cr : Cristobalite

Fig.5-5 XRD patterns of the surface of sample combining oxide sol mixture powders: (a) AS compact coated with MS, (b) MS compact coated with AS

5-3-3 Correlation between crystal orientation of cordierite and heat-treatment temperature

In order to discuss the effect of heat-treatment temperature on the crystal orientation of cordierite, XRD patterns between 17.0° and 20.0° for all specimens are shown in Figs. 5-6 (a), 5-6 (b), 5-7 (a), and 7 (b). The compacts with the coating layers were heat-treated at various temperatures for 1 hour. As shown in Fig. 5-6 (a), only the 110 diffraction peaks of cordierite were observed between 1300 and 1335 °C along with a diffraction peak of protoenstatite for the CK compact with CT coating. At 1345 °C, the 002 diffraction peak of cordierite appeared, becoming considerably higher than the 110 diffraction peak with increasing temperature. In the case of the CT compact with CK coating layer, as shown in Fig. 5-6 (b), the 002 diffraction peak was much lower than the 110 diffraction peak between 1250 and 1325 °C. However, a sudden disappearance of the 110 peak was observed at temperatures above 1335 °C. This is thought to be occurred by small amount of impurities contained in kaolin and talc

In the case of the samples derived from sol mixtures, AS and MS, shown in Figs. 5-7 (a) and 5-7 (b), only the 110 diffraction peak of cordierite was observed between 1300 and 1335 °C. This result shows that the absolute preferable crystal orientation of cordierite can be attained only by the interfacial thermal reaction between AS and MS. Above 1345 °C, the 002 diffraction peak appeared along with the 110 diffraction peak, with an intensity ratio, 110/002, decreasing with increasing temperature.

The results shown in Figs. 5-6 and 5-7 suggest that the *c*-axis of the cordierite crystals generated below 1345 °C aligned parallel to the interface of the compact and coating layer. There are many reports¹⁻⁵ on cordierite ceramics prepared from natural raw materials for honeycomb-shaped catalyst carriers in automobile exhaust cleaning systems in which the *c*-axis of the cordierite crystals was found to align preferentially parallel to the *c*-planes of the kaolinite or talc crystals. Therefore, it has long been believed that this preferential crystal orientation of cordierite is brought about by using large anisotropic tabular-shaped layered silicate minerals as starting mixtures for cordierite. The preferential orientation of cordierite crystals has been explained by two mechanisms as follows:

- (1) The large anisotropic tabular shape of kaolinite or talc brings about a preferable orientation of starting particles during the molding process.
- (2) Cordierite crystals appear to have a crystallographic relationship with kaolinite or talc.

In this study, the starting CK, CT, AS, and MS all have a fine and nearly isotropic particle shape. Therefore, layered silicate minerals having a large anisotropic tabular shape, such as kaolinite or talc, are not essential to produce a preferential orientation of cordierite crystals and the interface between the different compositions is an important factor for both nucleation and growth of cordierite.

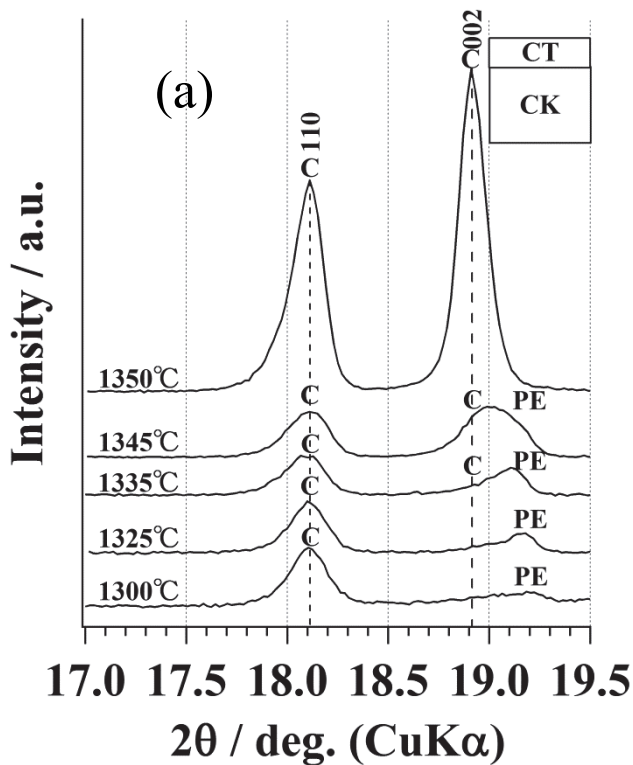
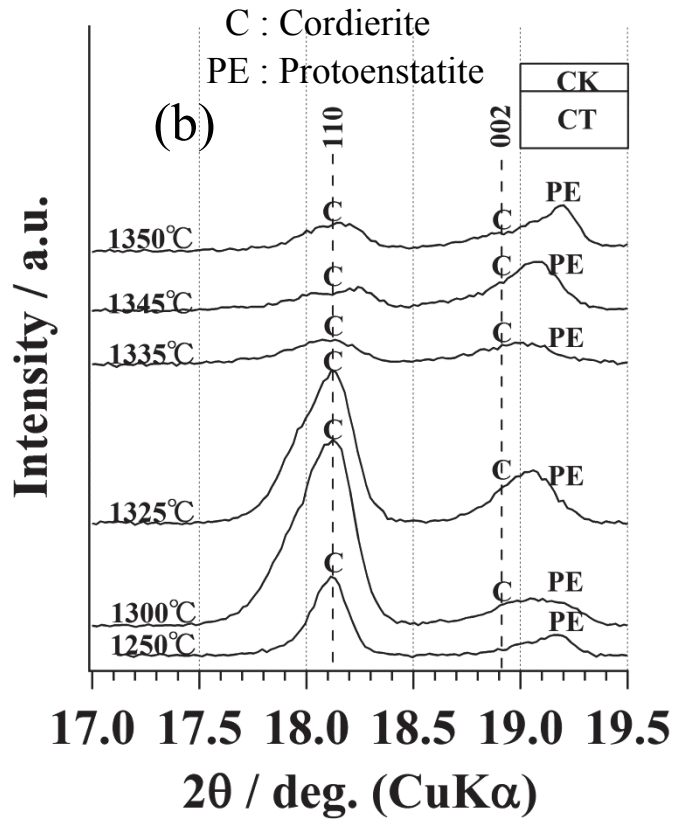


Fig.5-6 XRD patterns of the surface of samples derived from minerals: (a) CK compacts coated with CT and (b) CT compact coated with CK

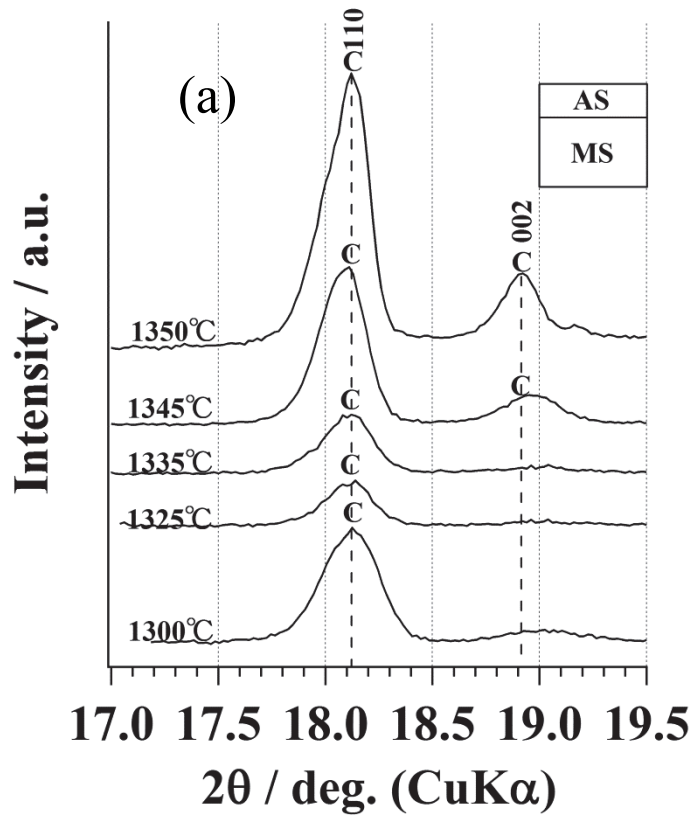
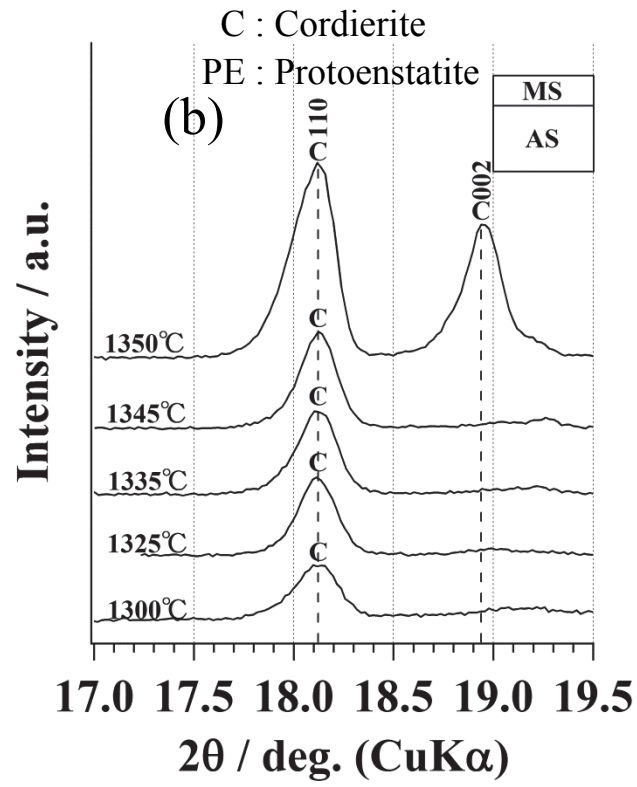


Fig.5-7 XRD patterns of the surface of samples derived from oxide sol mixture (a) AS compact coated with MS and (b) MS compact coated with AS

In order to estimate thermal interdiffusion of Mg^{2+} , Al^{3+} , and Si^{4+} across the interface of the compact and coated layer, cross sections of the CK compact with CT coating layer heat-treated between 1250 and 1350°C for 1 hour were analyzed with EDX in line scanning mode, as shown in Figure 8. Since the concentration of Si^{4+} was similar in CK (or AS) and CT (or MS), a concentration gradient of Si^{4+} across the interface was not observed. The results of the AS compact with MS coating layer were almost identical with those of the CK compact with CT coating layer. Thermal interdiffusion of Mg^{2+} and Al^{3+} across the interface between the CK compact and CT coating layer could not be observed at 1250 °C, so the intermediate compounds composed of three components (MgO , Al_2O_3 , SiO_2) were not detected by X-ray diffraction, as shown in Fig. 5-4 (a). Increasing the temperature up to 1300 °C brought about a concentration gradient of Mg^{2+} and Al^{3+} components across the interface. This result reveals the interdiffusion of Mg^{2+} and Al^{3+} components and the formation of a thin reaction layer at the interface. This thin reaction layer is thought to be composed of cordierite crystals with their c-axis oriented parallel to the interface, as shown in Fig. 5-6 (a). Therefore, a direct formation of cordierite crystals at the contacting interface of different compositions was the most important factor for preferential crystal orientation.

At 1350 °C, Al^{3+} ions migrated from the inner part of the compact and the reaction layer expanded to about 30 μm resulting in a large amount of cordierite crystals generated between the compact and coated layer, which is confirmed by X-ray diffraction, as shown in Fig. 5-4 (a). On the other hand, an Mg^{2+} -rich layer was observed at the surface of the coating layer by line scanning analysis with EDX. This Mg^{2+} -rich part is thought to be enstatite crystal grains decomposed from calcined talc because the coated surface layer is too thick to generate cordierite at the surface. Figure 5-9 shows elemental mappings obtained from area scanning analysis with EDX. Si^{4+} -rich areas were observed for the specimens heat-treated at 1350 °C for 1 hour, which are believed to be cristobalite grains, decomposed from talc powder, from the X-ray diffraction profile in Fig. 5-4 (a). These results indicate that the surface layer was composed of randomly distributed crystals, such as cordierite, enstatite, protoenstatite, and cristobalite, while the inner reaction layer was composed of mainly cordierite crystals.

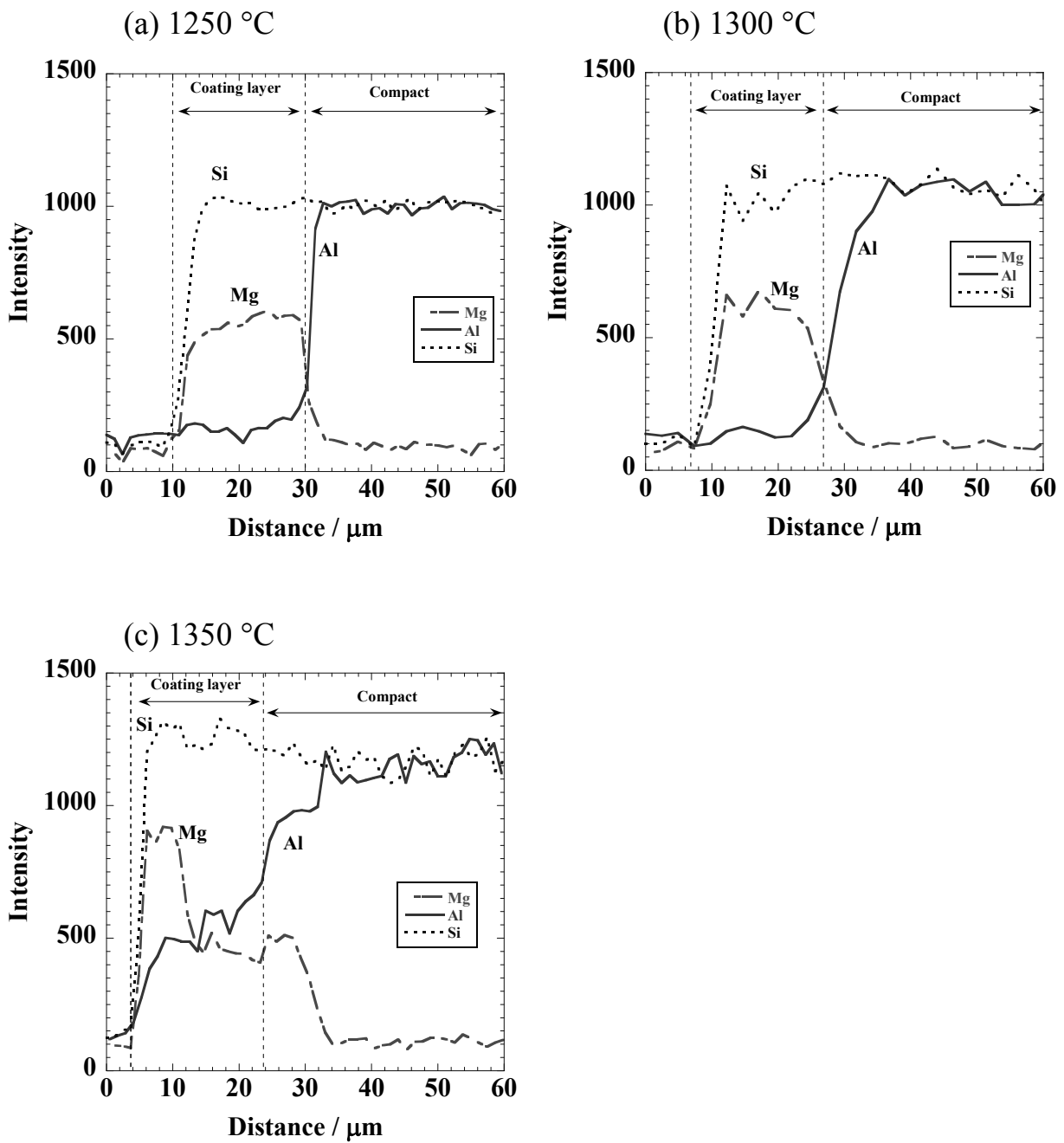


Fig.5-8 Interdiffusion of Mg, Al and Si on CK compact coated with CT coating layer measured with the aid of EDX, (a) heat-treated at 1250 °C, (b) 1300 °C and (c) 1350 °C

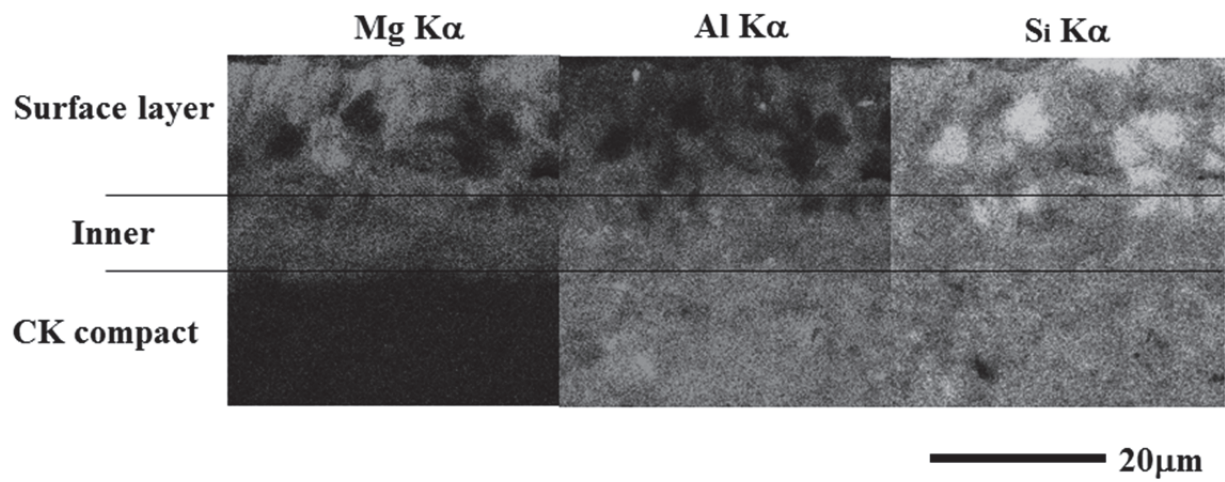


Fig.5-9 Elemental mapping of the cross section of interface between CK compact and coating CT heat-treated at 1350 °C, obtained from area scanning analysis with EDX

Figures 5-6 and 5-7 suggest also that the orientation of cordierite crystals drastically varied above 1345 °C in the cases of all four combinations of CK, CT, AS, and MS. As can be seen in the phase diagram for MgO–Al₂O₃–SiO₂¹⁶, a straight line connecting the points Al₂O₃·2SiO₂ and 3MgO·4SiO₂ almost passes through the lowest eutectic point (MgO: 20.3%, Al₂O₃: 18.3%, SiO₂: 61.4%). Therefore, when the interdiffusion of Mg²⁺ and Al³⁺ progresses above the eutectic temperature of around 1355 °C, a eutectic melt appears near the interface between the CK compact and CT coating layer or between the AS compact and MS coating layer. This melt is thought to be sufficient to bring about the rearrangement of cordierite crystals by dissolution and recrystallization.

In order to confirm the generation of a eutectic liquid at 1350 °C, a CK compact with CT coating was heat-treated at 1350 °C for various holding periods, and then left to cool. The XRD patterns measured on the surface of water-quenched specimens, along with furnace-cooled specimens, are shown in Fig. 5-10. When the temperature was raised to 1350 °C, the surface layer was composed of cristobalite, enstatite, and protoenstatite with glass (present as a liquid at a treating temperature) as shown by a broad halo around 2θ = 25° (Fig. 10 (a)). After 60 min at 1350 °C, a large amount of glass and cordierite appeared (Fig. 5-10 (c)). These results clearly reveal the formation of a eutectic liquid by thermal reaction of Al₂O₃·2SiO₂ and 3MgO·4SiO₂, followed by incongruent melting and recrystallization of cordierite crystals. The recrystallization of cordierite at the surface layer also continued during furnace cooling, as shown in Fig. 5-10 (d).

SEM images of cross-sections of the CK compact with CT coating heat-treated at (a) 1300 °C and (b) 1350 °C, followed by polishing and HF-etching are shown in Fig. 5-11. At 1300 °C, the reaction layer was composed of densely filled fine grains confirmed to be cordierite crystals by the X-ray diffraction pattern. At 1350 °C, large pillared grains aligned parallel to each other were observed near the surface of the coating layer at an angle to the interface and these pillared grains were similarly confirmed to be cordierite crystals by the X-ray diffraction pattern in Fig. 5-6 (a). These large pillared cordierite crystals are thought to be formed by dissolving and recrystallizing the cordierite generated by the solid-state reaction below 1345 °C, assisted by the presence of a eutectic liquid. This morphological transformation from fine grains into longitudinal pillars corresponded to the change in preferential crystal orientation of cordierite as shown in Figs. 5-6 and 5-7.

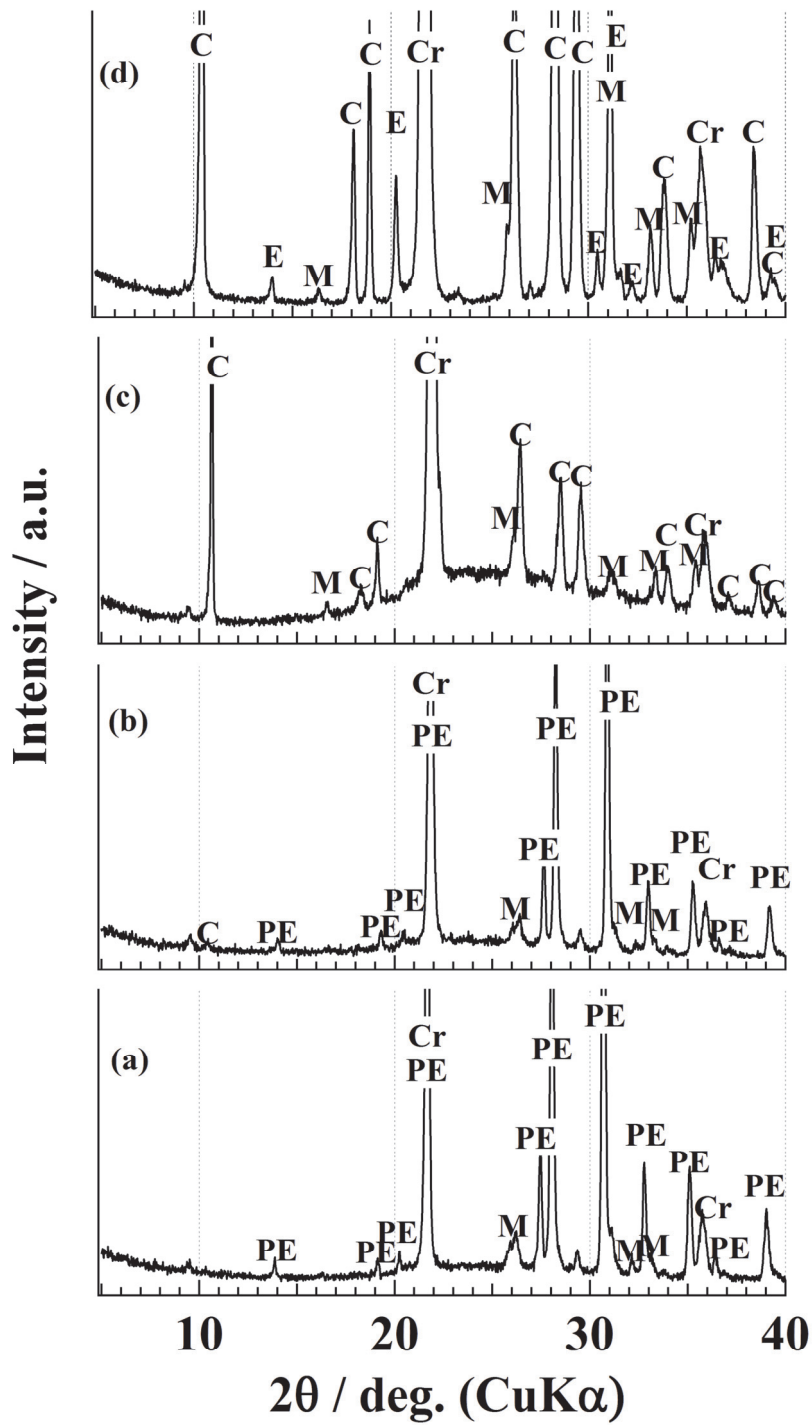


Fig.5-10 XRD patterns of the surfaces of CK compacts coated with CT heat-treated at 1350°C for holding periods (a) 0 min., (b) 20 min., (c) 60 min. and then water-quenched or (d) left to cool down in the furnace

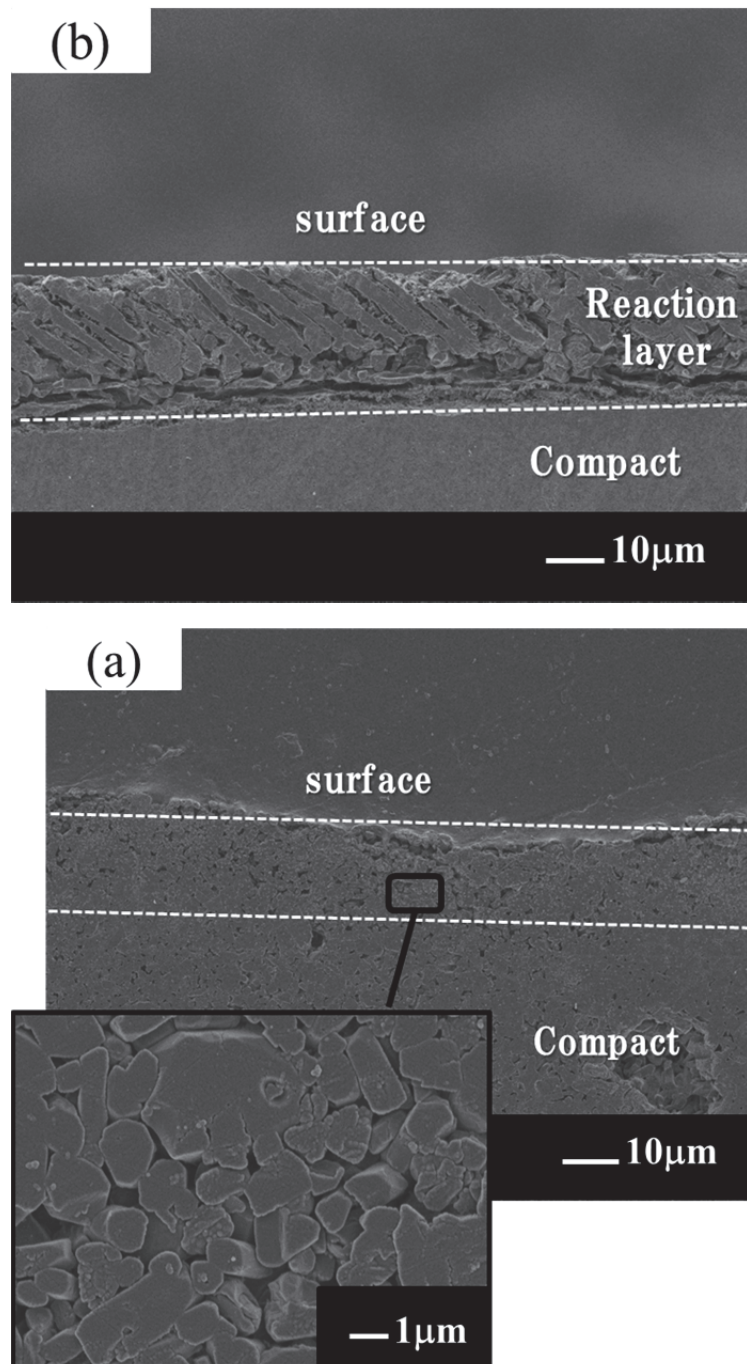


Fig.5-11 SEM images of cross-section of the interface between CK compact and CT coating layer heat-treated at (a) 1300°C and (b) 1350°C followed by polishing and HF-etching

5-4 Conclusions

The thermal reaction and preferential orientation of cordierite crystals at the interface between $\text{Al}_2\text{O}_3 \cdot 2\text{SiO}_2$ and $3\text{MgO} \cdot 4\text{SiO}_2$, derived from fine calcined minerals or oxide sol mixtures, were studied. From the results obtained, the following were concluded:

- 1 For temperatures up to 1250 °C, no crystalline material, comprised of three components (MgO , Al_2O_3 , and SiO_2), was observed, so no thermal reaction between $\text{Al}_2\text{O}_3 \cdot 2\text{SiO}_2$ and $3\text{MgO} \cdot 4\text{SiO}_2$ has occurred.
- 2 Above 1250 °C, the increased diffusion of Al_2O_3 and MgO is sufficient to generate cordierite crystals at the interface of $\text{Al}_2\text{O}_3 \cdot 2\text{SiO}_2$ and $3\text{MgO} \cdot 4\text{SiO}_2$.
- 3 Below 1345 °C, the *c*-axis of the cordierite crystals are preferably oriented parallel to the interface of $\text{Al}_2\text{O}_3 \cdot 2\text{SiO}_2$ and $3\text{MgO} \cdot 4\text{SiO}_2$; this interface is thought to be a very important factor in the nucleation and growth of cordierite crystals.
- 4 Above 1345 °C, the eutectic melt in the $\text{MgO}-\text{Al}_2\text{O}_3-\text{SiO}_2$ system caused cordierite crystals to align parallel to each other, at an angle to the interface, by dissolution and recrystallization.

References

- 1 I.M. Lachman, Patent US 3,885,977 (1975)
- 2 I.M. Lachman and R.D. Bagley, R.M. Lewis, *Am. Ceram. Soc., Ceramic Bulletin*, Vol. 16, No12 (1981)
- 3 B.P. Saha, R. Johnson, I. Ganesh, G.V.N. Rao, S. Bhattacharjee and Y.R. Mahajan, *Mater. Chem. and Phys.*, 67 140–5 (2001)
- 4 M. Nakahara, Y. Kondo, Z. Nakagawa and K. Hamano, *J. Ceram. Soc. Jpn.*, 107 (11) 1118–21 (1999)
- 5 J. Wight, “Cellular Ceramics”, Ed. by M. Scheffler, P. Colombo, WILEY-VCH Verlag GmbH & Co., Weinheim KGaA, 67–8 2005,
- 6 W.O. Williamson, *Proc. Brit. Ceram. Soc.*, 20 117–32 (1972)
- 7 C.Y. Chen, G.S. Lan and W.H. Tuan, *Ceram. Int.*, 26 715–20 (2006)
- 8 S. Udagawa and H. Ikawa, *Jpn. Ceram. Soc. Bull.*, 14(11) 967–6 (1979)
- 9 K. Umehara, *Jpn. Ceram. Soc. Bull.*, 33(7) 530–3 (1998)
- 10 M. Katayama, J. Nakakuki, J.H. Pee and Y. Kobayashi, *J. Ceram. Soc. Jpn.*, 121(11) 934–9 (2013)
- 11 K. Sumi, Y Kobayashi and E. Kato, *J. Am. Ceram., Soc.*, 82(3) 783-785 (1999)
- 12 Y. Kobayashi, K. Simi and E. Kato, *Ceram. Int.*, 26 739–43 (2000)
- 13 Y. Kobayashi, *J. Soc. Powder. Technol. Jpn.*, 38 338–46 (2001)
- 14 R. Johnson, I. Ganesh, B.P. Saha, G.V.N. Rao, S. Bhattacharjee and Y.R. Mahajan, *J. Mater. Sci.*, 38 2953–61 (2003)
- 15 J.R. González-Velasco, R. Ferret, R. López-Fonseca and M.A. Gutiérrez-Ortiz, *Powder Technology*, 153 34–42 (2005)

- 16 E.M. Levin, R.C. Robbins and H.F. McMurdie, "PHASE DIAGRAM FOR CERAMISTS VOLUME I", Am. Ceram. Soc. (1964) pp.246

Chapter 6

Preparation of Dense Mullite Polycrystals by Reaction Sintering of Kaolin Materials and Alumina and their Microstructure

6-1 Introduction

Mullite is the stable intermediate compound in the alumina-silica system and one of the most important oxide ceramics in the ceramics industry. Mullite is also a promising material for advanced ceramics owing to its low thermal expansion, good chemical and thermal stability, and low dielectric constant.¹ Kaolin is another important raw material in the ceramics industry. Nowadays, several pure kaolin materials are commercially available and used in many industrial applications.^{2,3} Heat-treatment of kaolin produces mullite crystals with residual cristobalite or glassy phase.⁴ Therefore, heat-treatment of mixtures of kaolin with alumina should yield single crystalline mullite.^{5,6} However, preparation of dense, single-crystalline mullite ceramics has proved difficult because of the insufficient counter diffusion of Si^{4+} and Al^{3+} , and in many cases, various types of sintering additives were introduced in order to facilitate densification.⁷⁻⁹ These additives as well as intrinsic impurities⁶ in kaolin lead to the formation of a residual glassy phase, and thus damaging thermal and chemical properties, electrical resistance or dielectric constant. Fine mullite powders derived from sol-gel using alkoxides,^{10,11} coprecipitation using alkoxides or inorganic salts,¹² and spray pyrolysis¹³ have recently been used in fabricating dense mullite polycrystals. However, fine powders prepared through such advanced routes using several alkoxides are very expensive and the preparation processes are extremely complicated.

The present study investigates thermal reaction and sinterability of relatively pure kaolin materials mixed with several types of alumina materials. It was found that an optimum combination of kaolin and alumina materials yielded highly-dense and single-crystalline mullite ceramics. The microstructures of these dense mullite ceramics were quantified with the aid of a digital image analysis of photographs observed by scanning electron microscope.

6-2 Experimental Procedure

6-2-1 Starting Materials

New Zealand kaolin (hereafter, referred to 'NZ kaolin') and Green bush kaolin (Green Bush, Australia, hereafter 'GB kaolin') were selected as starting kaolin materials since they have different mineralogical and chemical characteristics. NZ kaolin and GB kaolin were wet-classified to below 1 μm by sedimentation. The refined NZ kaolin (hereafter 'NZ1') consisted of cylindrical halloysite particles with an average diameter of 100 nm, as shown in Fig. 6-1. The refined GB kaolin (hereafter 'GB1') consisted mainly of tabular kaolinite particles. The tabular kaolinite had crystallite size of 16 nm in the direction parallel to the c-axis, estimated by X-ray line broadening.

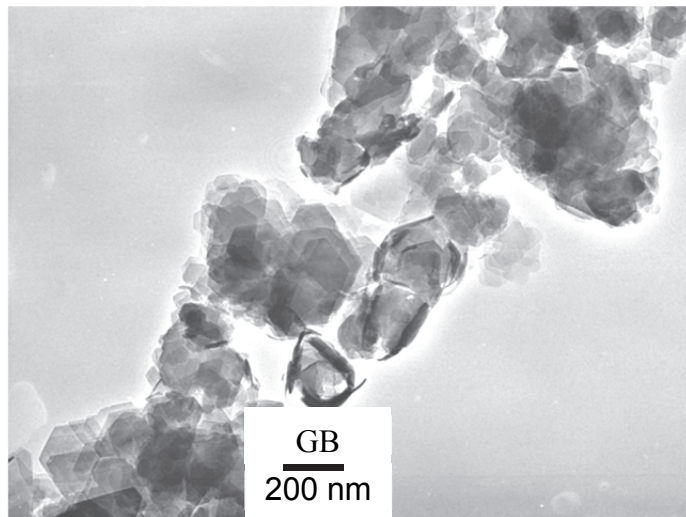
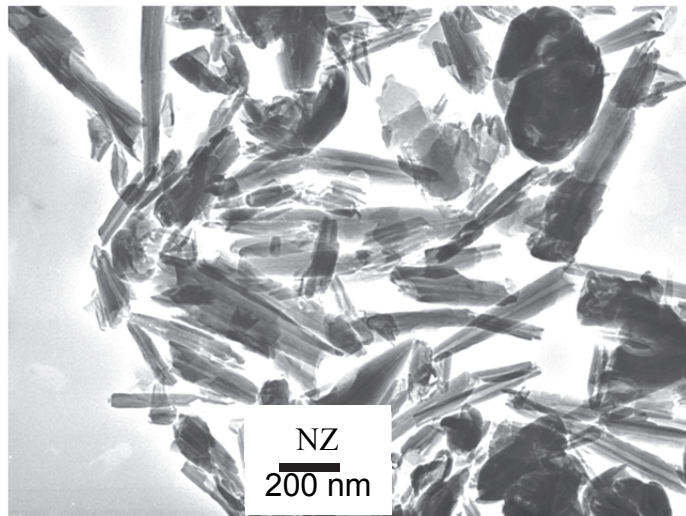


Fig.6-1 TEM observation of kaolin materials

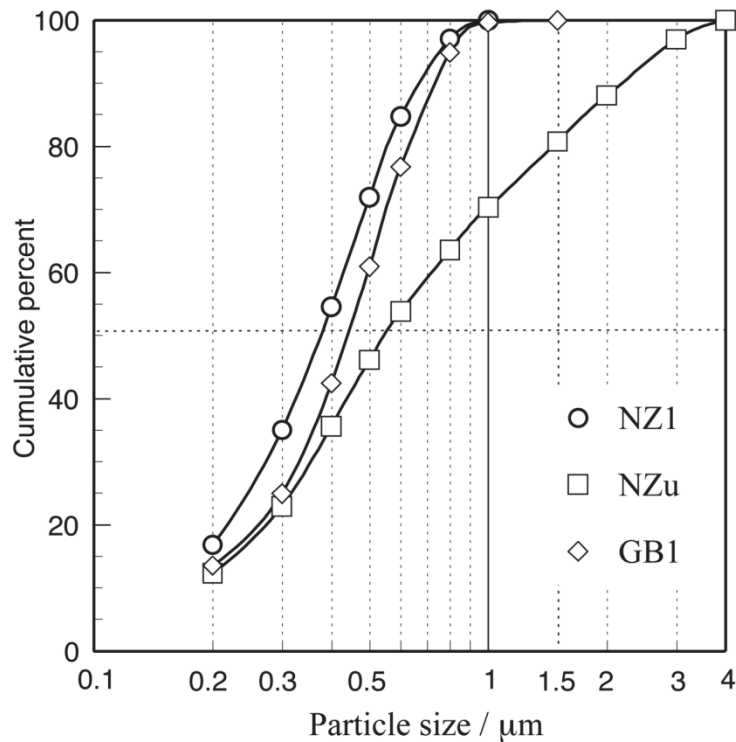


Fig.6-2 Particle size distribution of kaolin materials

Particle size distribution of the refined kaolin materials and the as-received NZ kaolin (hereafter ‘NZu’) are shown in Fig. 6-2. Particle size distribution of the two refined kaolin materials matched each other closely; the mean particle size was about 0.4 μm . NZu contained 30% >1 μm particles, which included about 7 mass% quartz and cristobalite.

Chemical composition of kaolin materials used in this study is shown in Table 1. The $\text{SiO}_2/\text{Al}_2\text{O}_3$ molar ratio of the refined kaolins was 2.02 ~ 2.04, almost coincident with the theoretical composition of kaolinite. X-ray diffraction patterns of the kaolins (Fig. 6-3) reveal that NZ kaolin is composed of dehydrated halloysite with a small amount of quartz and cristobalite, while GB kaolin is composed of pure kaolinite and contains no other crystalline material.

In this study, two types of alumina were used in order to adjust the composition for mullite and thus investigate the thermal reaction with kaolin: i) alumina sol (SN-O, Nissan Chemical Co. Ltd., Japan), composed of boehmite particles dispersed in an aqueous suspension (mean particle size was reported to be 20 nm by a manufacturer) and ii) AES-12 and AL-M41 (Sumitomo Chemical Co. Ltd., Japan), composed of corundum (mean particle size was 0.4 μm and 2.0 μm , respectively). The latter two will hereafter be referred to as A0.4 and A2.0, distinguished based on their mean particle size. Combinations such as A0.4-NZ1 or Sol-GB1 denote mixtures of alumina with kaolin.

Table 6-1 Chemical Compositions of Starting Kaolin Materials

Components	NZu	NZ1	GB1
SiO ₂	48.86	45.72	45.68
Al ₂ O ₃	36.36	38.09	38.36
Fe ₂ O ₃	0.26	0.25	0.51
TiO ₂	0.08	0.08	0.01
CaO	0.01	0.01	0.05
MgO	0.01	0.08	0.27
K ₂ O	0.01	0.01	0.01
Na ₂ O	0.04	0.02	0.01
Ig. Loss	13.97	14.64	14.86
Total	99.60	98.90	99.76
*Molar ratio	2.28	2.04	2.02

* SiO₂ / Al₂O₃

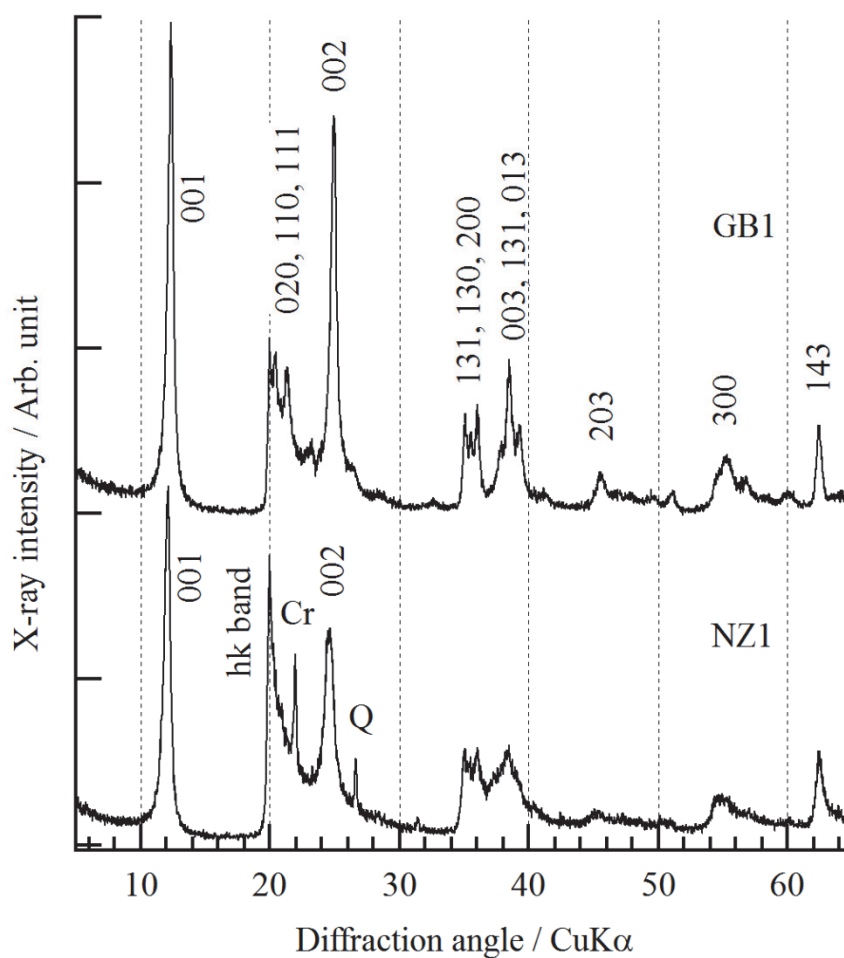


Fig.6-3 X-ray diffraction patterns of refined kaolin materials

6-2-2 Characterization

The morphology of starting materials was observed by transmission electron microscope (TEM; JEOL, JEM-200, Tokyo, Japan). Crystalline phases were identified by means of X-ray diffraction (Rigaku Denki, RAD-B) with CuK α radiation. X-ray intensity was determined by the diffraction peak height and area of crystals shown in Table 2.

Table 6-2 JCPDS Number and Miller Indices Used to Identify Crystals

Crystals	JCPDS Number	Miller index	2 θ / $^{\circ}$ CuK α
Mullite	15-776	110	16.4
Cristobalite	39-1425	101	22.0
γ -alumina	47-1308	-	45.6

Differential thermal analysis (DTA) and thermal gravimetric analysis (TGA) were carried out using a DTA-TGA apparatus (RIGAKU DENKI, TAS-100, Tokyo, JAPAN) at a heating rate of 10°C/min. Bulk density and apparent porosity of sintered specimens were determined by the Archimedes' immersion technique in boiling water. The microstructures of specimens were observed by a scanning electron microscope (SEM; JEOL, JSM-5310, Tokyo, JAPAN) on polished and thermally etched sections.

6-3 Results and Discussion

6-3-1 Thermal changes of kaolin

(1) Thermal Analysis of Kaolin

DTA curves in Fig. 6-4 showed endothermic peaks at around 530°C and exothermic peaks at around 990°C for both kaolins. The endothermic peaks correspond to the weight loss in TG curves. The exothermic peaks correspond to crystallization. The two kaolins exhibited apparently similar thermal reactions.

(2) Phase Changes of Kaolin

X-ray diffraction patterns of NZ1 heat-treated alone at various temperatures are shown in Fig. 6-5. The results of GB1 were almost coincident with those of NZ1. In Fig. 6-6, X-ray peak height of crystals is shown together with the peak area of mullite. Diffraction patterns below 400°C agreed well with those of as-received kaolin materials. Disappearing diffraction peaks of 00 l basal lattice planes above 500°C reveals that the sheet stacking structure of kaolin was disintegrated by dehydroxylation. On the other hand, the h-k diffraction band at around 2 θ = 20° persisted at this

temperature, and was asymmetrical, being steeper on the left. This indicates the presence of a disordered stacking of (AlO₆) octahedral and (SiO₄) tetrahedral sheets.

X-ray diffuse scattering below $2\theta = 10^\circ$ decreased with increasing heat-treatment temperature up to 900°C due to collapsing the micropores generated by dehydroxylation. An Al-Si spinel-type phase or γ -alumina^{4, 14} (hereafter ‘Al-Si spinel’) as well as a small amount of mullite crystals appeared at 1000°C, followed by a decrease in the amorphous materials, as evidenced by the decrease in height of the broad baseline hump at around $2\theta = 22^\circ$ and the slight shift in the hump toward lower diffraction angles.⁴⁾ The chemical composition of the amorphous materials shifted to the silica-rich side since Al₂O₃ was extracted by crystallization of Al-Si spinel as well as mullite. This crystallization at about 1000°C corresponds to the exothermic peaks in the DTA curves in Fig. 6-4. Above 1100°C, the diffraction peak height of mullite increased with decreasing Al-Si spinel, and the broad hump at around $2\theta = 22^\circ$ showed a fixed height between 1000 and 1300°C. In the case of NZ1, Fig. 6-6 reveals that the transformation from Al-Si spinel to mullite started above 1100°C and was virtually completed by about 1300°C. Transformation temperature from Al-Si spinel to mullite for GB1 was lower than that for NZ1 owing to small amounts of impurities, such as MgO and Fe₂O₃, which are thought to act as a network modifier in glass and loosen the network structure of silicate glass. Between 1100 and 1300°C, mullite crystals were extremely small, as evidenced by the broad profile of X-ray diffraction peaks of mullite in Fig. 6-5, and grew until 1650°C. Below the crystallization temperature of cristobalite, a moderate amount of glass (liquid phase at high temperature) was observed. At 1600°C, cristobalite suddenly disappeared with the generation of the liquid phase (glass), as would be predicted based on the eutectic temperature between mullite and silica in the binary phase diagram, reported to be about 1580°C.

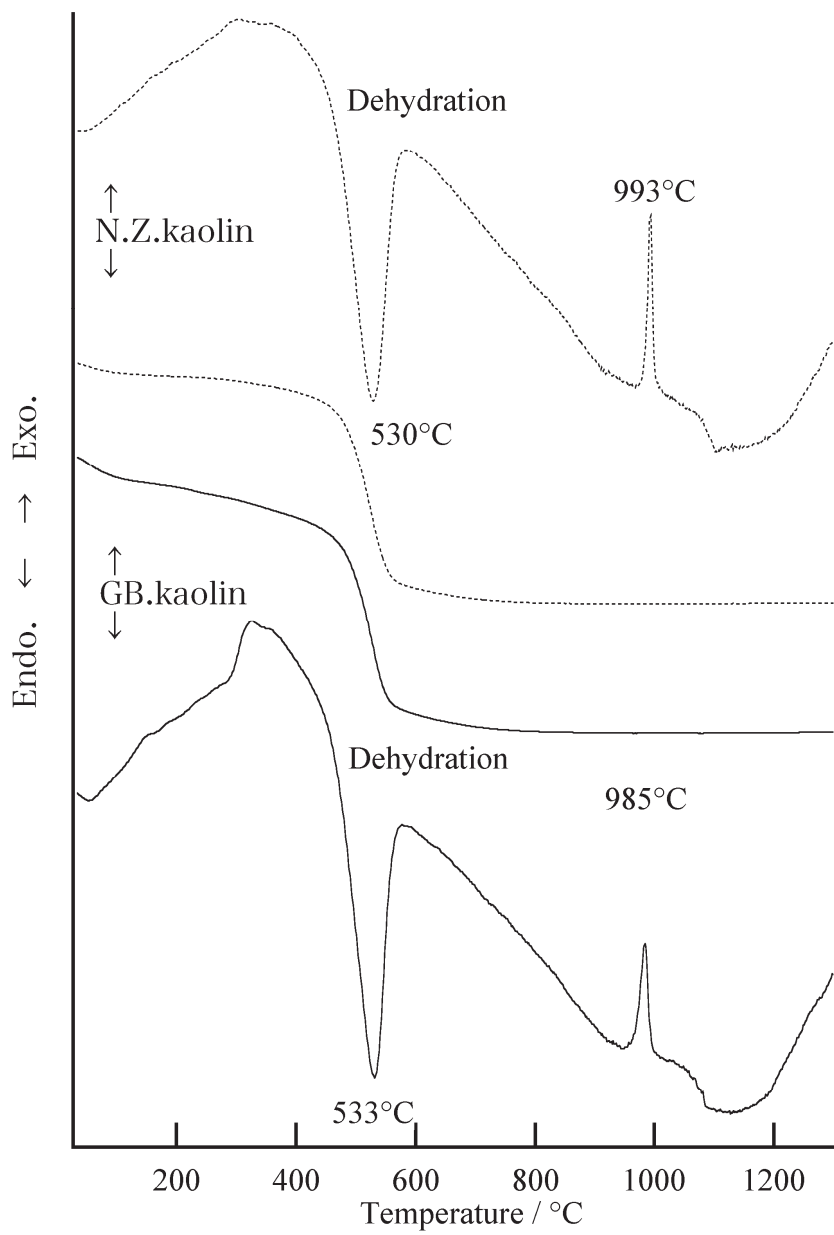


Fig.6-4 DTA-TG curves of kaolin materials

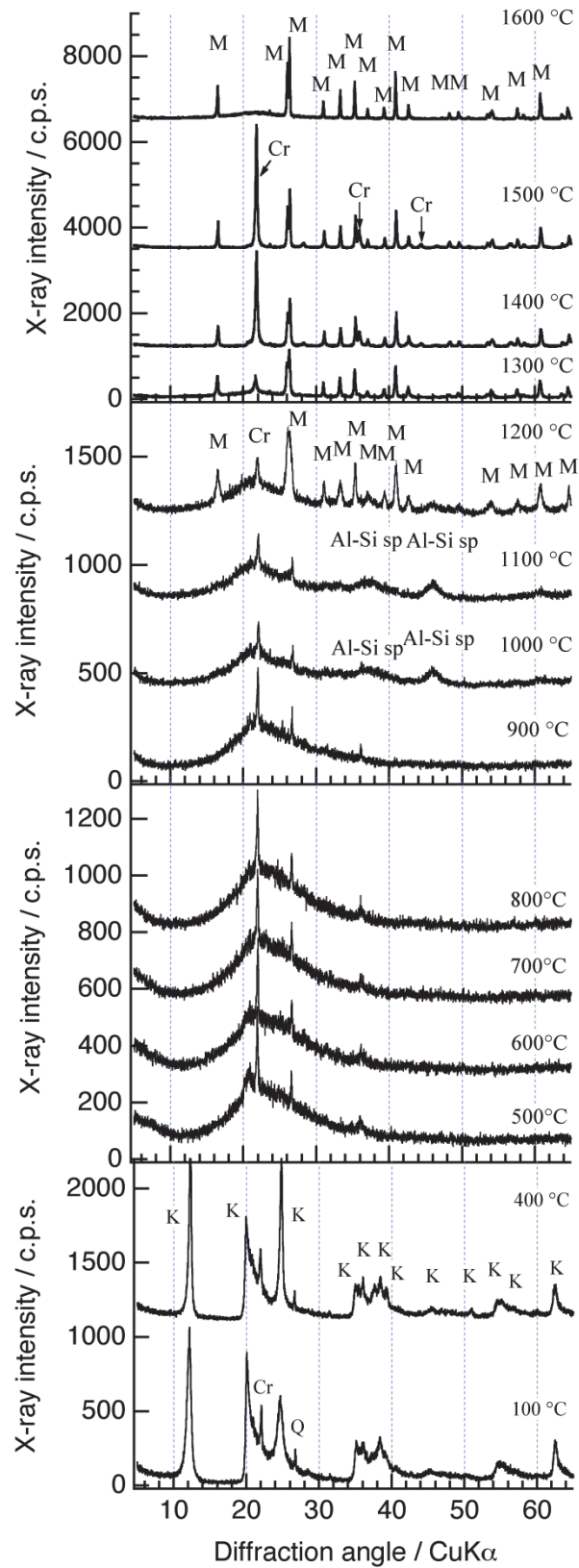


Fig.6-5 X-ray diffraction pattern of refined New Zealand kaolin (NZ1), heat-treated at various temperatures

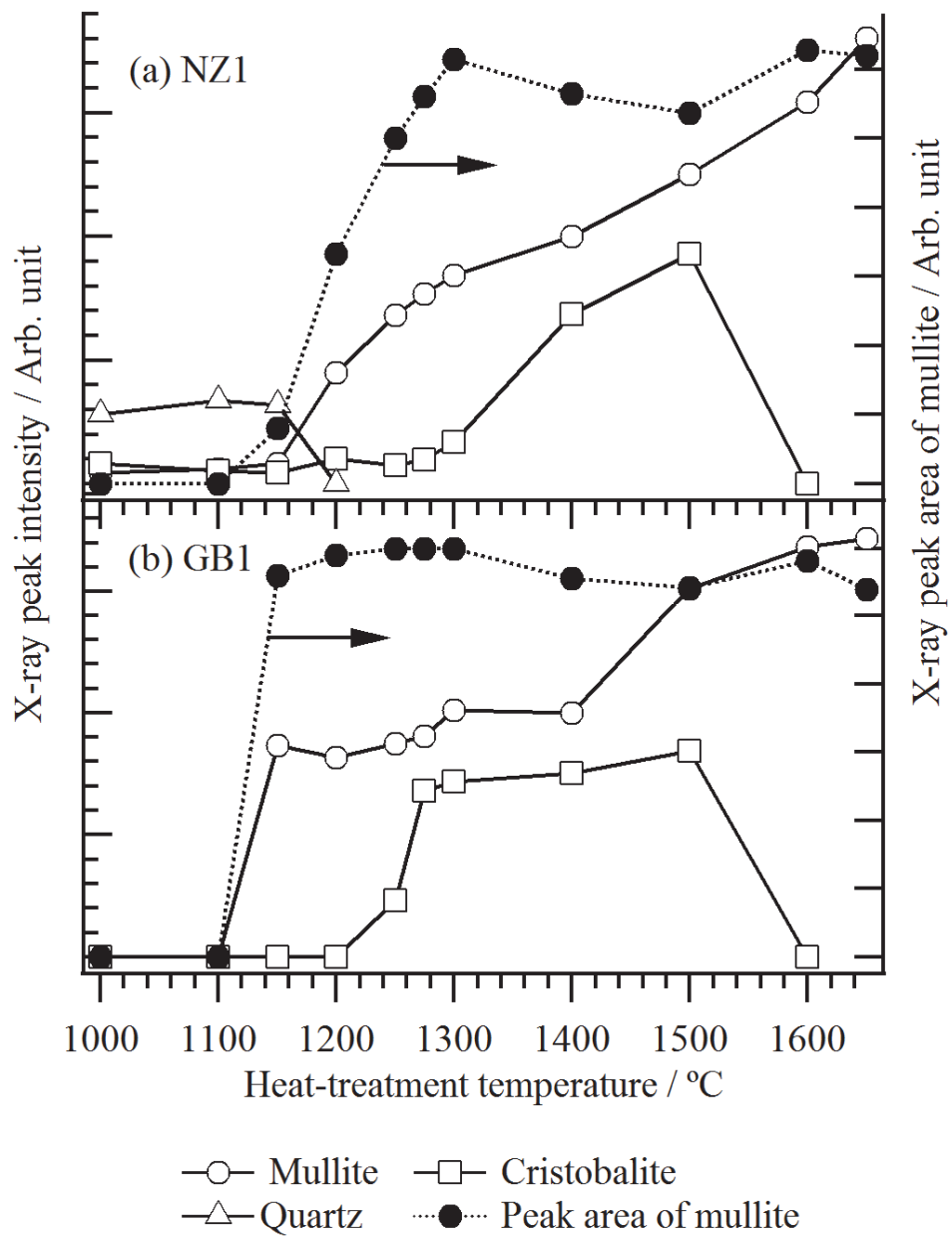


Fig.6-6 Phase changes of refined kaolin materials heat-treated at various temperatures

6-3-2 Thermal reaction of the mixtures

X-ray peak heights of heat-treated mixtures of kaolin and alumina sol are shown in Fig. 6-7. Boehmite included in the alumina sol decomposed into γ -alumina by heat-treatment around 500°C. Since the X-ray diffraction peaks of the resultant γ -alumina coincide with those of Al-Si spinel, they could not be distinguished. Thus, the peak height of the Al-Si spinel and γ -alumina are shown together. Below 1100°C, diffraction patterns of heat-treated mixtures almost coincided with those of pure kaolin, thus, an amorphous material and Al-Si spinel were mainly observed. A large amount of mullite was observed above 1100°C, also in the case of pure kaolin. Mullite content increased with temperature up to 1300°C and 1400°C in the cases of GB1 and NZ1, respectively. Mullite formation temperatures of specimens containing GB1 were somewhat lower than that containing NZ1, corresponding to the results of kaolin alone. No cristobalite was observed in the cases using alumina sol. These results indicated that the residual amorphous phases directly react with the γ -alumina to form mullite crystals in the case of mixtures with nanosized alumina sol.

X-ray peak heights of heat-treated mixtures of kaolin and corundum powder are shown in Fig. 6-8. In the case of the A0.4-GB1 specimen (Fig. 6-8a), fine corundum powder started to react with the residual silica-rich liquid phase at 1200°C. In the case of A0.4-NZ1 (Fig. 6-8b), thermal reactions between the decomposed kaolin and fine alumina started 100°C higher, i.e., at 1300°C. Mullite continuously increased with a further increase in temperature up to 1600°C. In the case of A2.0-NZ1 (Fig. 6-8c), coarse corundum reacted with cristobalite to form mullite above 1400°C. In the case using corundum powders, the mullite formation proceeded in multi-steps, namely, direct crystallization from decomposed kaolin below 1300°C and solid-state reaction of alumina with residual silica-rich amorphous material or cristobalite above 1300°C.

It can be concluded that the reaction between alumina materials and decomposed kaolin is affected by the alumina particle size and impurity included in the kaolin materials, and the thermal reaction between alumina and residual amorphous substances suppressed the crystallization of cristobalite, especially in the cases using nanosized sol and fine-grained corundum, which manifests itself as a difference in phase changes between Figs. 6-7 and 6-8.

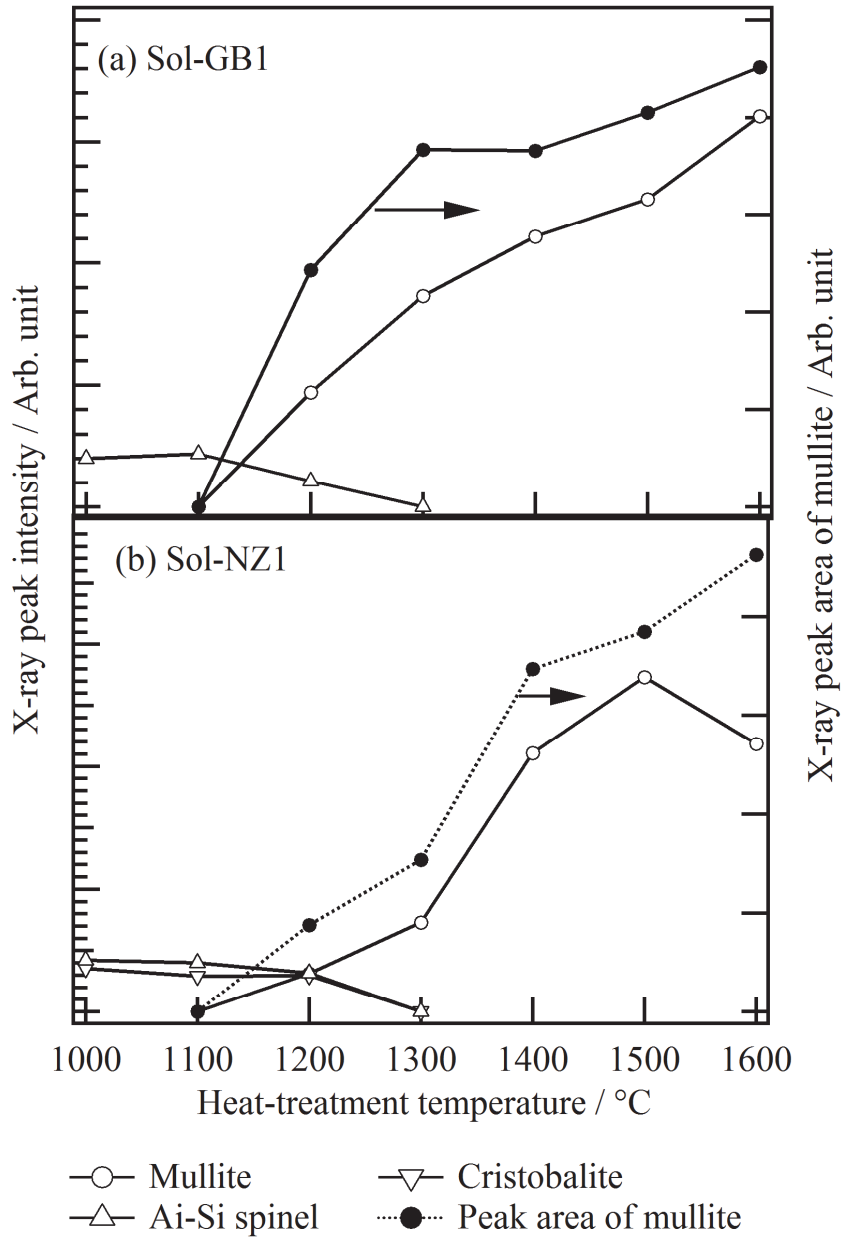


Fig.6-7 Phase changes of kaolin-sol mixtures, heat-treated at various temperatures

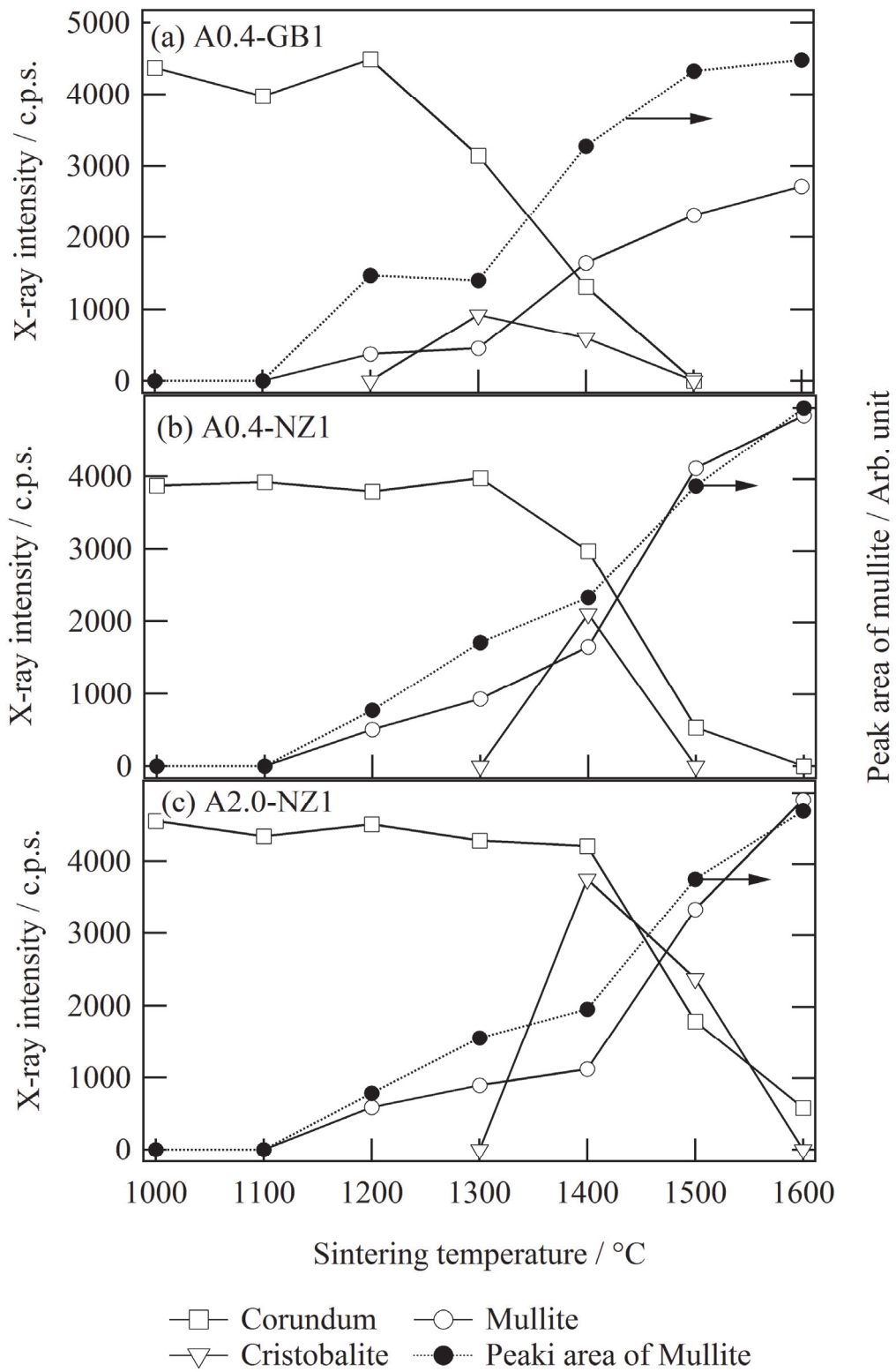


Fig.6-8 Phase changes of kaolin-corundum powders, heat-treated at various temperatures

6-3-3 Densification of the mixtures

Sintering characteristics of powder compacts of kaolin mixed with alumina sol are shown in Fig. 6-9a. Densification appeared to proceed in two steps: i) between 1100 and 1200°C, and ii) between 1300 and 1600°C. Accelerated sintering below 1200°C can be attributed to viscous flow of the liquid phase before crystallization of mullite, as shown in Fig. 6-7. A small amount of impurities, such as MgO and Fe₂O₃, produced a small amount of liquid phase so that the relative sintered density of Sol-GB1 at 1200°C was higher than those of the other specimens. Above 1200°C, the residual liquid phase promoted a final densification up to 1600°C. In the cases of Sol-GB1 and Sol-NZ1, relative densities of above 96% could be obtained by heat-treatment above 1600°C for 1 h. In the case of Sol-NZu, however, relative densities higher than 95% could not be achieved even at 1650°C for 1 h. The insufficient densification is attributed to the presence of quartz and cristobalite particles included in the raw materials acting as inclusions and inhibiting the viscous flow of liquid phase.

Sintering characteristics of powder compacts of kaolin mixed with corundum are shown in Fig. 6-9b. Densification appeared to proceed in a slightly different way, compared with in the case of mixtures with alumina sol. The initial sintering step continued to 100°C higher than in the case of mixtures with alumina sol. Further densification was suppressed by sudden crystallization of cristobalite at 1300°C or 1400°C, which can be linked to the disappearance of the glass phase. At the same time, a gradual decrease in relative density was observed, which can be explained by the dissolution of high-density corundum particles, followed by the formation of low-density mullite crystals. With further heat-treatment above 1500°C, relative density of specimens A0.4-GB1 and A0.4-NZ1 reached a maximum of ~98% at 1650°C. In the cases of A0.4-NZu and A2.0-NZ1, poor sinterability resulted in a lower relative density.

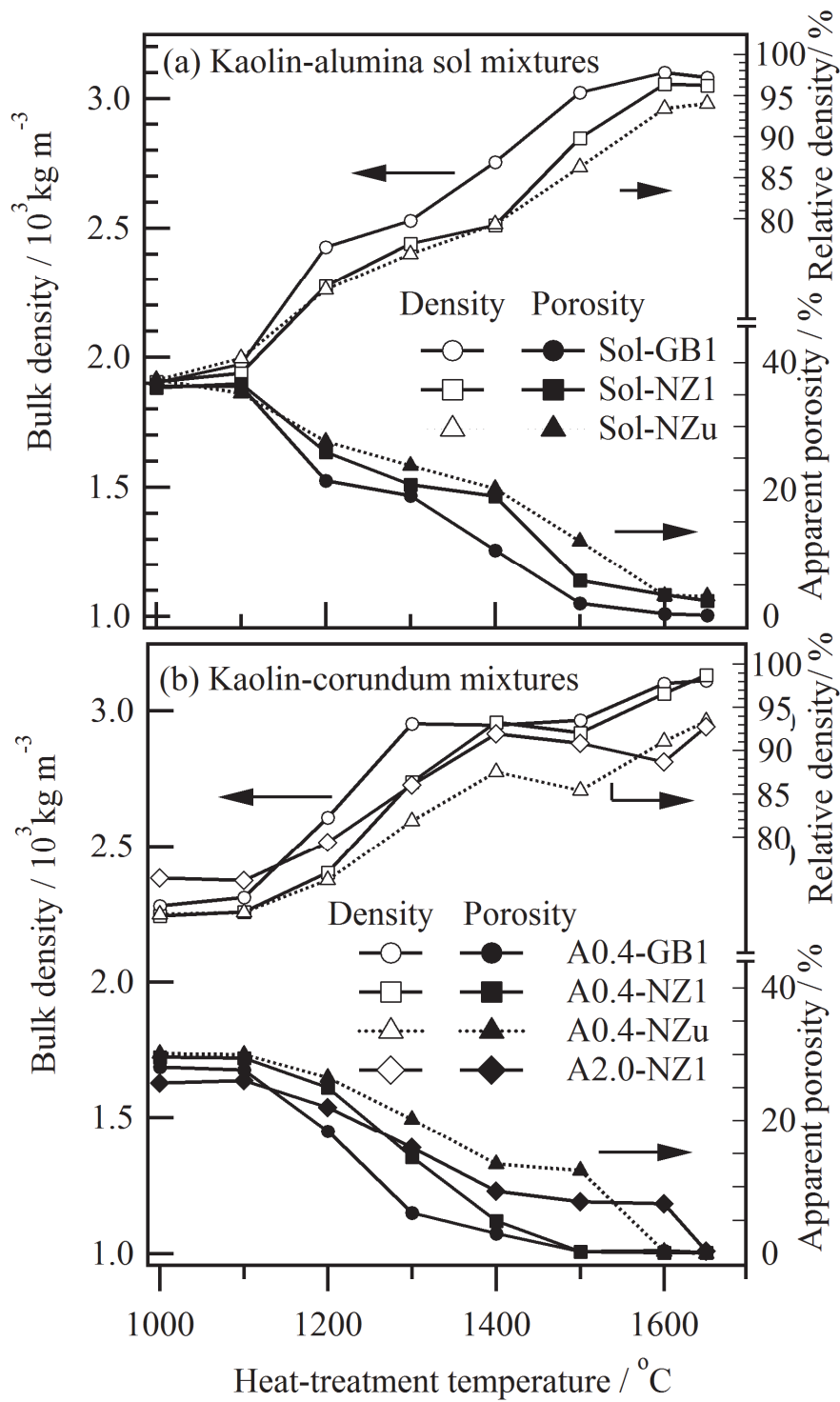


Fig.6-9 Sintering characteristics of kaolin-alumina mixtures

6-3-4 Microstructure of Mullite

Microstructures of mullite ceramics heat-treated at 1650°C for 1 h are shown in Figs. 6-10 and 6-11. In the case of Sol-GB1 (Fig. 6-11a), rod-like mullite crystals coarsened and characteristic crystal facets were observed. The presence of a small amount of glass phase would accelerate crystal growth and the formation of a crystal habit. In the case of Sol-NZ1 (Fig. 6-10b), large mullite crystals were observed, but the secondary glass phase among the mullite grains was less than in the case of Sol-GB1. In Sol-NZu (Fig. 6-10c), small, columnar crystals were observed with many small pores. In these cases, small amounts of impurities generated a residual liquid phase and accelerated grain growth.

In the case of specimens prepared using submicron corundum particles (A0.4), resultant microstructures consisted of smaller grains than those prepared using alumina sol, as shown in Figs. 6-11a, 6-11b and 11-c. A0.4-NZ1 specimens consisted of extremely small, isotropic grains, compared with A0.4-GB1. Prior to this study, kaolin materials have never been successfully used for preparation of dense, fine-grained mullite ceramics.

6-3-5 Quantification of Microstructure

In order to quantify the microstructures of the mullite ceramics, the size and distributions of mullite grains were estimated by the following procedure. Determining the individual grain areas of $S_1, S_2 \dots S_i$, from the digital images originated by scanning electron microscopy, the volumes of the

individual grains were calculated using the equation $V_i = \frac{4}{3} \pi \left(\frac{D_i}{2} \right)^3$, where D_i is the equivalent

diameter of a circle having the same area as S_i , and is equal to $2 \times \sqrt{\frac{S_i}{\pi}}$. From the curves of

cumulative grain volume versus the equivalent diameter, D_i , an equivalent size for 50 volume percent of the cumulative grains was defined as the average grain size D_{50} . Fig.6-12 shows the grain size distributions of mullite specimens prepared from Sol-NZ1 and A0.4-NZ1 having less glass and a higher relative density than 95%. The mullite ceramics prepared from A0.4-NZ1 showed a narrow grain size distribution with D_{50} of 1.0 μm , while that prepared from Sol-NZ1 showed a wide and a bimodal grain size distribution with D_{50} of 2.6 μm . Monodispersed and fine-grained mullite ceramics A0.4-NZ1 prepared by refined kaolin and submicron corundum powder, having relative density of 98% was expected to show superior mechanical properties. The mechanical properties of these mullite ceramics will be reported in the future report.

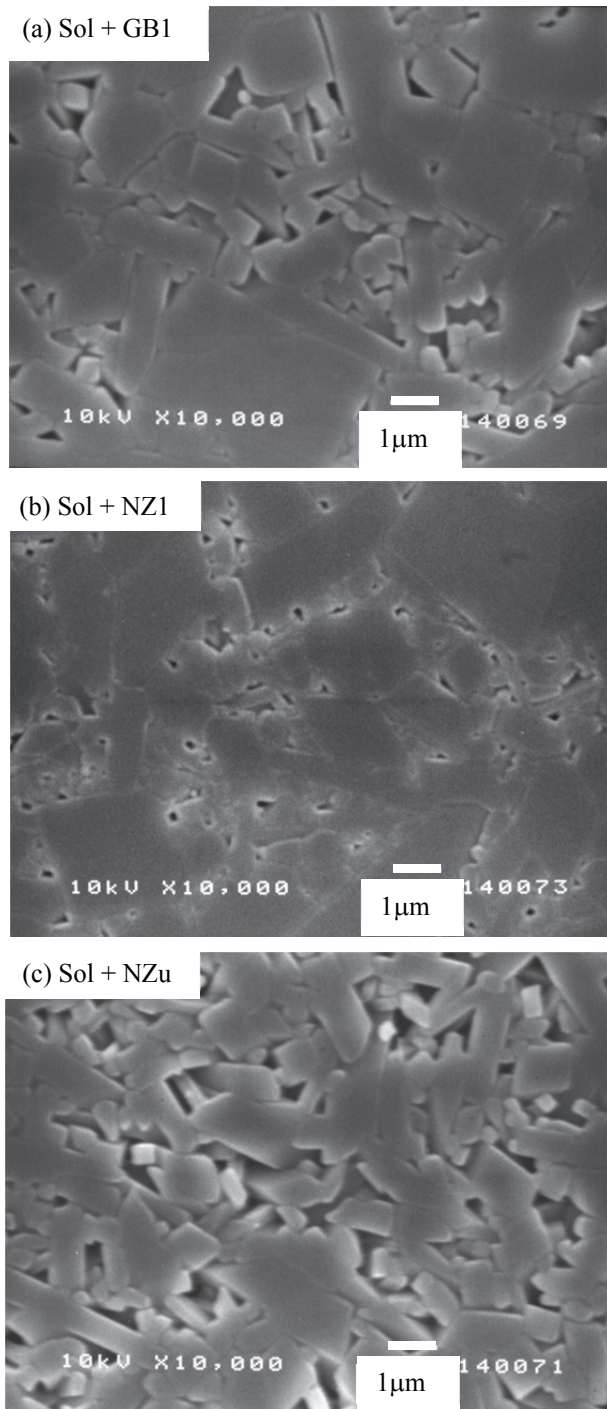


Fig.6-10 Microstructures of mullite ceramics derived from kaolin-sol mixtures, heat-treated at 1650°C. Specimens were polished and thermal-etched at 1600°C for 5 min.

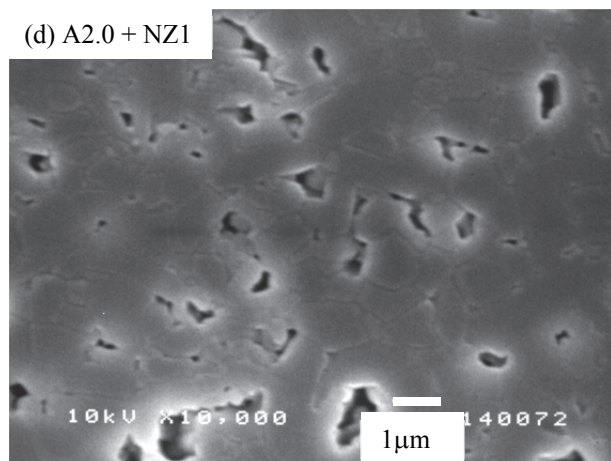
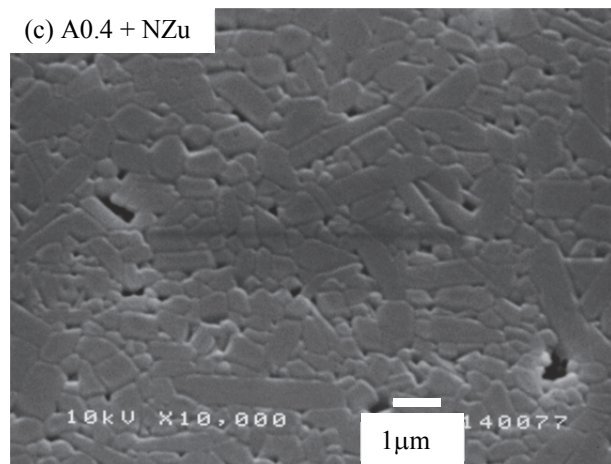
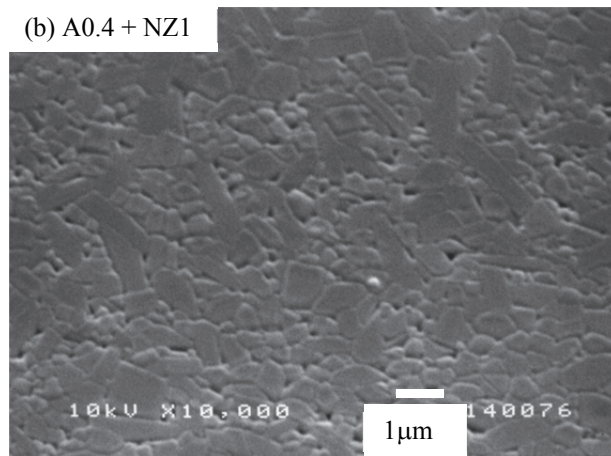
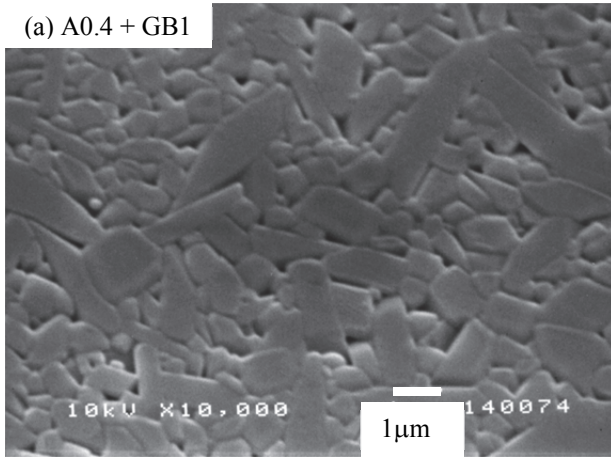


Fig.6-11 Microstructures of mullite ceramics derived from kaolin-corundum mixtures, heat-treated at 1650°C. Specimens were polished and thermal-etched at 1600°C for 5 min.

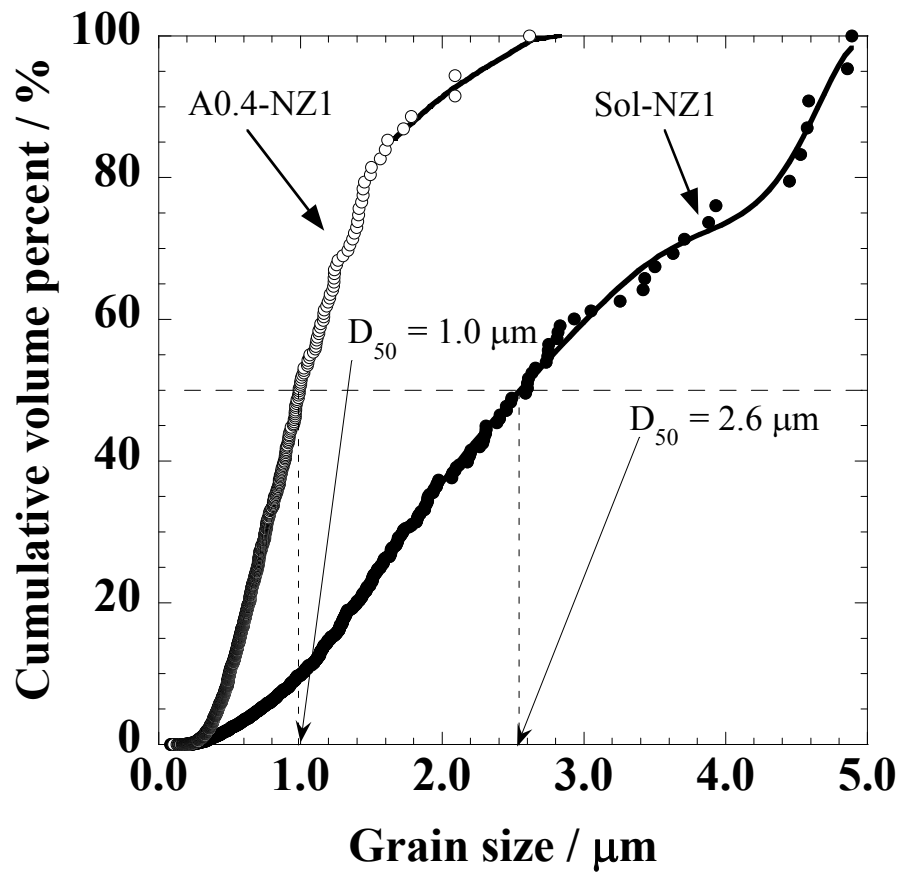


Fig.6-12 Grain size distributions of mullite specimens derived by sintering Sol-NZ1 and A0.4-NZ1

6-4 Conclusion

In this study, the effects of kaolin refinement and alumina particle size on the sintering, phase development and resultant microstructure were investigated in order to prepare dense, single-phase mullite ceramics. The following results were obtained:

- 1 Nanosized alumina sol directly reacted with the amorphous substance decomposed from kaolins to form mullite crystals. On the other hand, when corundum powders were mixed with kaolin materials, the mullite formation proceeded in multi-steps. At the same time, small amount of impurities, such as MgO and Fe₂O₃, promoted a mullite formation independently of alumina particle size.
- 2 Mixtures of a refined kaolin with an alumina sol produced dense mullite ceramics (relative density higher than 96%). Impurities such as Na₂O and MgO, contained in the alumina sol and/or kaolin, formed a small amount of liquid phase (residual glass) and accelerated grain growth of mullite.
- 3 Mixtures of relatively pure kaolin and submicron corundum particles produced dense and single-crystalline mullite ceramics by heat-treatment at 1650°C for 1 h. Resultant mullite ceramics showed relative densities higher than 98% and was composed of mono dispersed and fine mullite grains.

References

- 1 Somiya, S., Davis, R. F. and Pask, J. A. (eds.), Ceramic Transactions Vol. 6, Mullite and Mullite Matrix Composites, Am. Ceram. Soc., 1990, p.1 – 649
- 2 Sumi, K., Kobayashi, Y. and Kato, E., *J. Am. Ceram. Soc.*, 81, [4] 1029–32 (1998)
- 3 Kobayashi, Y. and Inagaki, M., *J. Eur. Ceram. Soc.*, 24 [2] 399–404 (2004)
- 4 Lee, S., Kim, Y., J. and Moon, H., *J. Am. Ceram. Soc.*, 81 [10] 2841–8 (1999)
- 5 Hamano, K., Nakajima, H., Okuda, F. and Konuma, M., *J. Ceram. Soc. Jpn.*, 102 [1] 78–83 (1994)
- 6 Chen, C.Y., Lan, G. S. and Tuan, W. H., *J. Eur. Ceram. Soc.*, 20 [12] 2519–25 (2000)
- 7 Hashimoto, K. and Niwa, K., *J. Ceram. Soc. Jpn.*, 95 [10] 1037–39 (1987)
- 8 Ushifusa, N. and Ogihara, S., *J. Ceram. Soc. Jpn.*, 97 [7] 690–98 (1989)
- 9 Mitamura, T., Kobayashi, H., Ishibashi, N. and Akiba, T., *J. Ceram. Soc. Jpn.*, 99 [5] 351–6 (1991)
- 10 Kumazawa, T., Ohta, S., Nagaoka, T., Yasuoka, M. and Kanzaki, S., *J. Ceram. Soc. Jpn.*, 99 [12] 1228–33 (1991)
- 11 Schneider, H., Merwin, L. and Sebald, A., *J. Mat. Sci.*, 27 805–12 (1992)
- 12 Hamano, K., Sato, T. and Nakagawa, Z., *J. Ceram. Soc. Jpn.*, 94 [8] 818–22 (1986)
- 13 Kumazawa, T., Kanzaki, S., Asami, J. and Tabata, H., *J. Ceram. Soc. Jpn.*, 94 [5] 485–90 (1986)
- 14 MacKenzie, K. J. D., Hartman, J. S. and Okada, K., *J. Am. Ceram. Soc.*, 79 [11] 2980–2 (1996)

Chapter 7

Conclusions

7-1 Quantification of ceramic microstructures with digital images analysis

Microstructure of cordierite ceramics and mullite ceramics respectively were quantified by digital image analysis of binarized photomicrographs, and next conclusions were obtained:

- 1 In sintered cordierite compacts, large domain structure could be observed by optical polarizing microscopy and it was confirmed that the domains were composed of primary submicron grains aligned in the same crystal orientation.
- 2 Also the size and distribution of primary grains of mullite ceramics could be easily quantified with digital image analysis. The results of digital image analysis corresponded well to observation by SEM or OPM.
- 3 The digital image analysis is available to estimate primary and secondary microstructures of ceramics.

7-2 Effect of microstructure on CTE of dense cordierite prepared from sol mixtures

Dense cordierite ceramics were prepared from sol mixtures, and the domain structures could be easily observed by optical polarizing microscopy and quantified by digital image analysis. After examining the relationship between CTE and the average domain size of the cordierite, the following conclusions were obtained:

- 1 Dense sintered compacts of single-phased cordierite can be prepared from nanosized particles of $\text{Mg}(\text{OH})_2$, alumina sol, and silica sol.
- 2 In sintered cordierite compacts, large domain structure could be observed by optical polarizing microscopy and the domains were composed of primary submicron grains aligned in the same crystal orientation.
- 3 It could be inferred that the critical domain size at which microcracks began to appear was around 40 μm .
- 4 The lower CTE limit of sintered cordierite ceramics at around $0.4 \times 10^{-6} \text{ K}^{-1}$ was attributed to the appearance of partial microcracking caused by stresses arising from thermal expansion anisotropy and domains larger than 40 μm .

7-3 Effect of particle size of talc on crystal orientation of cordierite ceramics

Preferable crystal orientation and sintering characteristics of cordierite ceramics were investigated using several types of kaolin powders and talc powders with alumina sol having various median particle size, and the following conclusions were obtained:

- 1 The c-axis of talc powders in median grain size of above 3 μm was preferably oriented vertical to the pressed surface of the green compact during uniaxially pressing, since the talc powders having median particle size above 3 μm showed a large anisotropic tabular

shape.

- 2 The crystal orientation of cordierite increased proportionally with an increase in the crystal orientation of talc powders. Moreover, high crystal orientation was also attained in the case of cordierite ceramics prepared using the combination of calcined kaolin and coarse talc powders. Even if isotropic calcined kaolin was used, resultant cordierite crystals preferably orientated depending on the crystal orientation of talc powders.
- 3 By the combination of fine kaolin powders about 5 μm and talc powders with median particle size between 3 and 5 μm , dense cordierite ceramics having a higher relative density than 95 % were attained with high crystal orientation index I_C of about 85 %, corresponding to the orientation property of a honeycomb structured catalyst carrier of porous cordierite.

7-4 Preferred crystal orientation of cordierite by interdiffusion of $\text{Al}_2\text{O}_3 \cdot 2\text{SiO}_2$ and $3\text{MgO} \cdot 4\text{SiO}_2$

The thermal reaction and preferential orientation of cordierite crystals at the interface between $\text{Al}_2\text{O}_3 \cdot 2\text{SiO}_2$ and $3\text{MgO} \cdot 4\text{SiO}_2$, derived from fine calcined minerals or oxide sol mixtures, were studied. From the results obtained, the following were concluded:

- 1 For temperatures up to 1250 $^\circ\text{C}$, no crystalline material, comprised of three components (MgO , Al_2O_3 , and SiO_2), was observed, so no thermal reaction between $\text{Al}_2\text{O}_3 \cdot 2\text{SiO}_2$ and $3\text{MgO} \cdot 4\text{SiO}_2$ has occurred.
- 2 Above 1250 $^\circ\text{C}$, the increased diffusion of Al_2O_3 and MgO is sufficient to generate cordierite crystals at the interface of $\text{Al}_2\text{O}_3 \cdot 2\text{SiO}_2$ and $3\text{MgO} \cdot 4\text{SiO}_2$.
- 3 Below 1345 $^\circ\text{C}$, the c -axis of the cordierite crystals are preferably oriented parallel to the interface of $\text{Al}_2\text{O}_3 \cdot 2\text{SiO}_2$ and $3\text{MgO} \cdot 4\text{SiO}_2$; this interface is thought to be a very important factor in the nucleation and growth of cordierite crystals.
- 4 Above 1345 $^\circ\text{C}$, the eutectic melt in the $\text{MgO}-\text{Al}_2\text{O}_3-\text{SiO}_2$ system caused cordierite crystals to align parallel to each other, at an angle to the interface, by dissolution and recrystallization.

7-5 Preparation of dense mullite ceramics and their microstructure

The effects of kaolin refinement and alumina particle size on the sintering, phase development and resultant microstructure were investigated in order to prepare dense, single-phase mullite ceramics. The following results were obtained:

- 1 Nanosized alumina sol directly reacted with the amorphous substance decomposed from kaolins to form mullite crystals. On the other hand, when corundum powders were mixed with kaolin materials, the mullite formation proceeded in multi-steps. At the same time, small amount of impurities, such as MgO and Fe_2O_3 , promoted a mullite formation independently of alumina particle size.

- 2 Mixtures of a refined kaolin with an alumina sol produced dense mullite ceramics (relative density higher than 96%). Impurities such as Na_2O and MgO , contained in the alumina sol and/or kaolin, formed a small amount of liquid phase (residual glass) and accelerated grain growth of mullite.
- 3 Mixtures of relatively pure kaolin and submicron corundum particles produced dense and single-crystalline mullite ceramics by heat-treatment at 1650°C for 1 h. Resultant mullite ceramics showed relative densities higher than 98% and was composed of mono dispersed and fine mullite grains.

List of Publications

- 1 Yuichi Kobayashi, Masaki Katayama, Makiko Kato, and Shingo Kuramochi,
“Effect of Microstructure on the Thermal Expansion Coefficient of Sintered Cordierite
Prepared from Sol Mixtures,”
Journal of the American Ceramic Society, 96 [6] 1863–8(2013)
- 2 Masaki Katayama, Jun Nakakuki, Jae-Hwan Pee, and Yuichi Kobayashi,
“Effect of particle size of tabular talc powders on crystal orientation and sintering of
cordierite ceramics,”
Journal of the Ceramic Society of Japan, 121 [11] 934–9(2013)
- 3 Masaki Katayama, Jae-Hwan Pee, and Yuichi Kobayashi,
“Crystal orientation of cordierite generated at the interface between $\text{Al}_2\text{O}_3 \cdot 2\text{SiO}_2$ and
 $3\text{MgO} \cdot 4\text{SiO}_2$,”
Journal of the Ceramic Society of Japan (掲載可)
- 4 Masaki Katayama, Yasuharu Kawai, Yo-hei Mizuno, Kohdai Mizuno, Masayuki Aoyama,
and Yuichi Kobayashi,
“Preparation of dense mullite polycrystals by reaction sintering of kaolin materials and
alumina and their microstructure,”
Journal of the Ceramic Society of Japan (掲載可)

Others

- 1 Yuichi Kobayashi, Masaki Katayama, and Mika Kato,
“Ultra-low Thermal expansion property of Lithium Aluminosilicate,”
Research paper, Research Institute for Industrial Technology, Aichi Institute of
Technology, Vol.13 33– 8(2011)
- 2 Yuichi Kobayashi, Masaki Katayama, Aya Kabeya, Mai Ito, and Mihoko Adachi,
“Preparation of Highly Porous Aluminosilicate Ceramics and Their Properties,”
Research paper, Research Institute for Industrial Technology, Aichi Institute of
Technology, Vol.14 41– 6(2012)
- 3 Yuichi Kobayashi, Masaki Katayama, and Hiroshi Takata,
“Preparation of Dense Cordierite Ceramics by Sol-Mixing Method and Their Thermal
Expansion Property,”
Research paper, Research Institute for Industrial Technology, Aichi Institute of
Technology, Vol.15 47– 50(2013)
- 4 Jae-Hwan Pee, Yuichi Kobayashi, Masaki Katayama, Geun-Hee Kim, and Yoo-Jin Kim,
“Preparation of Lightweight Porcelains Using Various Type of Pore-Forming Additives
and their Mechanical Properties,”
Journal of the Ceramic Society of Japan, (掲載可)

Presentations at international conferences and seminars

- 1 Masaki Katayama, Jun Nakakuki, and Yuichi Kobayashi,
“Crystal orientation and sintering of cordierite ceramics prepared from natural raw materials,”
The 12th International Conference on Ceramic Processing Science, August 4-7, 2013,
Portland, Oregon, USA

- 2 Masaki Katayama, Jae-Hwan Pee, and Yuichi Kobayashi,
“Effect of particle size of talc powders on domain structure of cordierite ceramics,”
The 30th Japan-Korea International Seminar on Ceramics, November 20-23, 2013,
Kitakyushu, Hukuoka, Japan

Acknowledgment

The present study was accomplished in Graduate School of Engineering, Aichi Institute of Technology in the period from 2011 to 2014. The author has been given their great help from laboratory's staffs and many student members.

The author would like to show my greatest appreciation to *Professor Yuichi Kobayashi* who gave me an opportunity of investigation of ceramic science and provided valuable advices, discussion and consultation.

The author is greatly indebted to *Professor Masanori Hirano*, *Professor Tsuyoshi Nakajima* and *Professor Yoshimi Ohzawa* for their kind helps and useful advices for making this thesis.

The author thanks to all the student members of ceramics laboratory, where he had a very fulfilling time.

The author thanks especially to his parents for longstanding their support.

February 2014

Masaki Katayama